City Research Online

City, University of London Institutional Repository

Citation: Pagani, Alfonso (2016). Strong-form governing equations and solutions for variable kinematic beam theories with practical applications. (Unpublished Doctoral thesis, City, University of London)

This is the accepted version of the paper.

This version of the publication may differ from the final published version.

Permanent repository link: https://openaccess.city.ac.uk/id/eprint/15963/

Link to published version:

Copyright: City Research Online aims to make research outputs of City, University of London available to a wider audience. Copyright and Moral Rights remain with the author(s) and/or copyright holders. URLs from City Research Online may be freely distributed and linked to.

Reuse: Copies of full items can be used for personal research or study, educational, or not-for-profit purposes without prior permission or charge. Provided that the authors, title and full bibliographic details are credited, a hyperlink and/or URL is given for the original metadata page and the content is not changed in any way.

City Research Online: http://openaccess.city.ac.uk/ publications@city.ac.uk

Strong-form governing equations and solutions for variable kinematic beam theories with practical applications

Alfonso Pagani

School of Mathematics, Computer Sciences and Engineering
City University London

This dissertation is submitted for the degree of
Doctor of Philosophy

Supervisors:
J.R. Banerjee
E. Carrera

July 2016

È neciessaria chosa che piegando la molla ch'era dritta, che dalla parte del suo colmo ella si rarifichi, e dalla parte del cavo ella si condensi. La qual mutatione fa a uso di piramide, onde si dimostra che in mezo d'essa molla non si a mai mutatione.

Leonardo da Vinci about bending of beam
Codex Madrid I, Folio 84, 1493

Acknowledgements

Writing a thesis is not an easy task and it never contains only the work of a single person. I am grateful to a long list of people and colleagues. First of all, I am deeply thankful to my academic tutors, who really gave substance to my work. Professor Banerjee and Professor Carrera encouraged me along my whole path and were always instrumental in the development of my research and my personality. I am also grateful to Dr. Marco Boscolo, former researcher at City University London, who helped me with the extension of DSM to CUF-based refined beam theories. Professor Ferreira from Universidade do Porto played an important role in my work, and he gave me great ideas in the development of the RBFs method. I cannot, but help mentioning my colleagues of the MUL2 team in Torino: Marco, Matteo, Enrico, Mirella, Stefano, Tommaso, Andrea, Alberto and many others who work hard constantly and were always available for discussion and help. Finally, the biggest thank probably goes to my family and Teresa, who patiently assisted and sustained me.

Abstract

Due to the work of pioneering scientists of the past centuries, the three-dimensional theory of elasticity is now a well-established, mature science. Nevertheless, analytical solutions for three-dimensional elastic bodies are generally available only for a few particular cases which represent rather coarse simplifications of reality. Against this background, the recent development of advanced techniques and progresses in theories of structures and symbolic computation have made it possible to obtain exact and quasi-exact resolution of the strong-form governing equations of beam, plate and shell structures.

In this thesis, attention is primarily focused on strong-form solutions of refined beam theories. In particular, higher-order beam models are developed within the framework of the Carrera Unified Formulation (CUF), according to which the three-dimensional displacement field can be expressed as an arbitrary expansion of the generalized displacements.

The governing differential equations for static, free vibration and linearized buckling analysis of beams and beam-columns made of both isotropic and anisotropic materials are obtained by applying the principle of virtual work. Subsequently, by imposing appropriate boundary conditions, closed-form analytical solutions are provided wherever possible in the case of structures with uncoupled axial and in-plane displacements. The solutions are also provided for a wider range of structures by employing collocation schemes that make use of radial basis functions. Such method may be seriously affected by numerical errors, thus, a robust and efficient method is also proposed in this thesis by formulating a frequency-dependant dynamic stiffness matrix and using the Wittrick-Williams algorithm as solution technique.

The theories developed in this thesis are validated by using some selected results from the literature. The analyses suggest that CUF furnishes a reliable method to implement refined theories capable of providing almost three-dimensional elasticity solution and that the dynamic stiffness method is extremely powerful and versatile when applied in conjunction with CUF.

Contents

List of Figures **xi**

List of Tables **xiii**

Nomenclature **xv**

1 Introduction **1**

1.1 One-dimensional structural theories 1

1.2 Numerical methods 4

1.3 Thesis objectives and outline 5

2 Kinematics of beams **9**

2.1 Classical beam theories 9

2.2 Higher-order models 12

2.2.1 Generalized beam theory 13

2.2.2 Warping functions 15

2.2.3 3D Solutions based on the Saint-Venant model and the proper generalized decomposition 16

2.3 Asymptotic methods 17

3 Carrera Unified Formulation **19**

3.1 Preliminaries 19

3.2 Unified formulation of beams 21

3.2.1 Taylor expansion (TE) 22

3.2.2 Lagrange expansion (LE) 23

4 Governing differential equations **25**

4.1 Principle of virtual work 25

4.1.1 Virtual variation of the strain energy 26

4.1.2 Virtual variation of the work done by axial pre-stress 28
4.1.3 Virtual variation of external work 29
4.1.4 Virtual variation of inertial work 31
4.2 Strong-form equations of unified beam theory 32
4.2.1 Static analysis 32
4.2.2 Free vibration analysis 35
4.2.3 Buckling analysis 36
4.2.4 Free vibration of axially loaded beams 37

5 Closed-form analytical solution 41
5.1 Displacement field and loading 41
5.2 Governing differential equations in explicit algebraic form 42
5.2.1 Static analysis 42
5.2.2 Free vibration analysis 44
5.3 Limitations of the method 45

6 Radial Basis Functions 47
6.1 Collocation of the unknowns 47
6.2 Formulation of the eigenvalue problem with radial basis functions 49

7 Dynamic Stiffness Method 53
7.1 L-matrix form of the governing differential equations 54
7.1.1 Free vibration analysis 55
7.1.2 Free vibration analysis of axially loaded beams 57
7.1.3 Buckling analysis 58
7.2 Solution of the differential equations 60
7.3 Dynamic stiffness matrix 62
7.4 The Wittrick-Williams algorithm 65
7.5 Eigenvalues and eigenmodes calculation 66

8 Numerical Results 67
8.1 Static analysis 67
8.1.1 Composite beams subjected to sinusoidal pressure load 67
8.2 Free vibration analysis 77
8.2.1 Metallic, rectangular cross-section beams 77
8.2.2 Thin-walled cylinder 81
8.2.3 Four- and two-layer composite beams 84

8.2.4 Cross-ply laminated composite plates 85
8.2.5 Symmetric 32-layer composite plate 89
8.3 Free vibration of beam-columns 91
8.3.1 Semi-circular cross-section beam 91
8.4 Buckling analysis 96
8.4.1 Metallic rectangular cross-section column 96
8.4.2 Thin-walled symmetric and non-symmetric cross-sections 98
8.4.3 Cross-ply laminated beams 100

9 Summary of Principal Contributions 105
9.1 Work summary 105
9.2 Main contributions 107

10 Conclusions and scope for future work 109
10.1 Conclusions 109
10.2 Scope for future work 110

Appendix A Material coefficients 113

Appendix B Solution of a system of second order differential equations 117

Appendix C Forward and backward Gauss elimination 121

Appendix D A list of publications arising from the research 125

Bibliography 127

Index 141

List of Figures

1.1 Leonardo's description of beam bending [1]. 1

2.1 Adopted coordinate system. 9
2.2 Differences between Euler-Bernoulli and Timoshenko beam theories. . . . 10
2.3 Homogeneous condition of transverse stress components at the unloaded edges of the beam. 11
2.4 Rigid torsion of the beam cross-section. 13
2.5 GBT approximation, global, $()_g$, and local, $()_L$, reference systems. 14

3.1 Coordinate system and fiber orientation angle. 21
3.2 Cross-section L-elements in natural geometry. 23
3.3 Two assembled L9 elements in actual geometry. 24

4.1 Components of a surface loading; lateral surfaces and normal vectors of the beam. 29
4.2 Components of a line loading. 31
4.3 Generalized forces applied at the ends of the beam. 32

7.1 Expansion of the matrix $\mathbf{L}^{\tau s}$ for a given expansion order and TE. 56
7.2 Boundary conditions of the beam element and sign conventions. 62
7.3 Assembly of dynamic stiffness matrices. 65

8.1 Simply supported composite beam of two-layer square cross-section subjected to sinusoidal pressure load. 68
8.2 Distribution of normalized axial displacement $\bar{u}_y$ along $\bar{z}$ and at $(x,y) = (0,0)$; simply-supported composite beam under sinusoidal surface loading. 70
8.3 Distribution of normalized transverse displacement $\bar{u}_z$ along $\bar{z}$ and at $(x,y) = (0,L/2)$; simply-supported composite beam under sinusoidal surface loading. 70
8.4 Distribution of normalized axial stress, $\bar{\sigma}_{yy}$, along $\bar{z}$ and at $(x,y) = (0,L/2)$; simply-supported composite beam under sinusoidal surface loading. 71

8.5 Distribution of normalized axial stress, $\bar{\sigma}_{zz}$, along $\bar{z}$ and at $(x,y) = (0,L/2)$; simply-supported composite beam under sinusoidal surface loading. 72
8.6 Distribution of normalized axial stress, $\bar{\sigma}_{yz}$, along $\bar{z}$ and at $(x,y) = (0,0)$; simply-supported composite beam under sinusoidal surface loading. 75
8.7 Solid rectangular cross-section. 77
8.8 First (a), second (b) and third (c) bending modes for a SS square beam ($L/b = 10$); DSM $N = 4$ TE model. 79
8.9 First bending (a), second bending (b), first torsional (c) and second torsional (d) modes for a CF square cross-section beam ($L/b = 10$); DSM $N = 5$ TE model. 80
8.10 Cross-section of the thin-walled cylinder. 81
8.11 Percentage error between the RBFs and exact DSM solutions for various expansion orders and boundary conditions; Thin-walled cylinder. 83
8.12 First flexural (a), second flexural (b), first shell-like (c), second shell-like (d), first torsional (e) and second torsional (f) modes for a CC thin-walled cylinder; DSM $N = 5$ TE model. 84
8.13 Effect of ply orientation angle on first flexural natural frequencies of two-layer CF beams; DSM $N = 4$ TE model versus [144]. 86
8.14 Effect of material anisotropy on the first flexural natural frequencies of angle-ply and cross-ply CF beams; DSM $N = 4$ TE model versus [144]. . . 86
8.15 First four modes of the SS-F-SS-F cross-ply plate with $a/h = 5, N = 6$. . . 88
8.16 First four modes of the SS-F-SS-F cross-ply plate with $a/h = 10, N = 6$. . . 88
8.17 Experimental setup for the measurement of the natural frequencies, symmetric 32-layer plate. 90
8.18 First five modes of the FFFF symmetric 32-layer thin plate, $N = 6$. 90
8.19 Semi-circular cross-section. 91
8.20 Uncoupled (a, b, c) and coupled (d, e, f) modal shapes for the unloaded ($P = 0$) SS semi-circular beam; DSM-TE $N = 6$ model. 95
8.21 First non-dimensional critical buckling load ($P^*_{cr} = \frac{P_{cr}L^2}{\pi^2 EI}$) versus length-to-height ratio, L/h, for the rectangular metallic beam. 97
8.22 Cross-section of the C-shaped beam. 98
8.23 Second flexural-torsional buckling mode of the C-shaped section beam by the seventh-order ($N = 7$) CUF model. 99
8.24 Cross-section of the box beam. 99

List of Tables

3.1 McLaurin's polynomials. 22

8.1 Maximum non-dimensional transverse displacement, $\bar{u}_z(0, L/2, -h/2)$, of the simply-supported composite beam under sinusoidal surface loading. . . 69

8.2 Non-dimensional axial displacement, $\bar{u}_y(0, 0, -h/2)$, of the simply-supported composite beam under sinusoidal surface loading. 72

8.3 Non-dimensional axial stress, $\bar{\sigma}_{yy}$, at various z coordinates and $(x, y) = (0, L/2)$; simply-supported composite beam under sinusoidal surface loading. 73

8.4 Non-dimensional transverse normal stress, $\bar{\sigma}_{zz}$, at $(x, y, z) = (0, L/2, h/2)$; simply-supported composite beam under sinusoidal surface loading. 74

8.5 Non-dimensional transverse shear stress, $\bar{\sigma}_{yz}$, at $(x, y, z) = (0, 0, -h/4)$; simply-supported composite beam under sinusoidal surface loading. 74

8.6 First to fourth non-dimensional bending frequencies $\omega^* = \frac{\omega L^2}{b}\sqrt{\frac{\rho}{E}}$ for the SS square beam; $L/b = 10$. 78

8.7 Comparison between TE and LE CUF models; non-dimensional natural frequencies $\omega^* = \frac{\omega L^2}{b}\sqrt{\frac{\rho}{E}}$ for the SS square beam ($L/b = 10$). 79

8.8 Non-dimensional natural periods $\omega^* = \frac{\omega L^2}{b}\sqrt{\frac{\rho}{E}}$ for the CF square beam; $L/b = 10$. 80

8.9 Natural frequencies (Hz) of the thin-walled cylinder for different boundary conditions; Comparison of RBFs and DSM solutions. 82

8.10 Non-dimensional natural frequencies, $\omega^* = \frac{\omega L^2}{b}\sqrt{\frac{\rho}{E_{11}}}$, of a CC $[+45/-45/+45/-45]$ antisymmetric angle-ply beam. 85

8.11 Non-dimensional natural frequencies, $\omega^* = \omega\frac{a}{h}\sqrt{\frac{\rho}{E_2}}$, for the cross-ply SS-F-SS-F plate. 87

8.12 Natural frequencies (Hz) of the FFFF symmetric 32-layer composite thin plate. 89

8.13 Natural frequencies (Hz) for the unloaded ($P = 0$) semi-circular cross-section beam. 92

8.14 Natural frequencies (Hz) for the semi-circular cross-section beam undergoing a compression load ($P = 1790$ N). 93
8.15 Natural frequencies (Hz) for the semi-circular cross-section beam undergoing a traction load ($P = -1790$ N). 94
8.16 First three non-dimensional buckling loads ($P^*_{cr} = \frac{P_{cr}L^2}{\pi^2 EI}$) of the metallic beam, $L/h = 20$. 96
8.17 First non-dimensional buckling load ($P^*_{cr} = \frac{P_{cr}L^2}{\pi^2 EI}$) of the metallic beam for different length-to-height ratios L/h. 97
8.18 Flexural-torsional buckling loads [N] for the axially compressed C-section beam. 98
8.19 Critical buckling loads [MPa] for various length-to-side ratio, L/a, of the SS square box beam. 100
8.20 First four buckling loads [MPa] of the SS square box beam for $L/a = 100$. . 101
8.21 Effect of length-to-height ratio, L/h , on the non-dimensional critical buckling loads ($P^*_{cr} = \frac{P_{cr}L^2}{E_2 bh^3}$) of symmetric and anti-symmetric cross-ply SS laminated beams. 102
8.22 Critical buckling loads [N] of the 8-layer cross-ply rectangular beam for different boundary conditions. 103

Nomenclature

Roman Symbols

$\mathbf{B}^{\tau s}$	3×6 fundamental nucleus of the matrix containing the coefficients of the natural boundary conditions
$\tilde{\mathbf{C}}$	Matrix of the material coefficients
c	RBFs shape parameter
$\mathbf{D}$	Linear differential operator
F_τ	Cross-sectional expansion functions
$\mathbf{K}^{\tau s}$	3×3 fundamental nucleus of the differential stiffness matrix
$\mathbf{K}^{\tau s}_{\sigma^0_{yy}}$	3×3 fundamental nucleus of the differential, geometrical stiffness matrix
$\mathbf{K}^{\tau s i j}$	3×3 fundamental nucleus of the algebraic stiffness matrix due to RBFs collocation
$\mathscr{K}$	Dynamic stiffness matrix
L4	Bi-linear Lagrange polynomial expansion
L9	Quadratic Lagrange polynomial expansion
L16	Cubic Lagrange polynomial expansion
L	Length of the beam
L_{ext}	Work of the external loadings
L_{ine}	Work of the inertial loadings
L_{int}	Strain energy work
$L_{\sigma^0_{yy}}$	Work of the axial pre-stress

$\mathbf{l}^k$	Line load vector on the k-th subdomain
$\mathbf{L}^{\tau s}$	3×9 fundamental nucleus of the matrix containing the coefficients of the ordinary differential equations
M	Number of terms of the expansion
m	Number of half-waves along the beam axis
$\mathbf{M}^{\tau s}$	3×3 fundamental nucleus of the mass matrix
$\mathbf{M}^{\tau sij}$	3×3 fundamental nucleus of the mass matrix due to RBFs collocation
N	Expansion order of TE models
n	Number of centres for RBFs collocation
$\mathbf{\Pi}^{\tau s}$	3×3 fundamental nucleus of the differential matrix of the natural boundary conditions
$\mathbf{\Pi}^{\tau s}_{\sigma^0_{yy}}$	3×3 fundamental nucleus of the differential matrix of the geometrical boundary conditions
$\mathbf{\Pi}^{\tau sij}$	3×3 fundamental nucleus of the algebraic matrix of the natural boundary conditions due to RBFs collocation
$\mathbf{p}^k$	Pressure load vector on the k-th subdomain
$\mathbf{p}^{\tau}_k$	3×1 fundamental nucleus of the loading vector
$\mathbf{P}_s$	Generalized loads at the end of the beam
$\mathbf{q}_{si}$	Vector of the collocated unknowns
$\mathbf{u}$	Displacement vector
$\mathbf{u}_\tau$	Generalized displacement vector
$\mathbf{U}_\tau$	Vector of the displacements amplitudes
V	Beam volume

Greek Symbols

δ	Virtual variation
$\boldsymbol{\varepsilon}$	Strain vector

ϕ_i	Radial basis function
ω	Angular frequency
Ω	Beam cross-section
$\boldsymbol{\sigma}$	Stress vector
σ_{yy}^0	Axial pre-stress

Superscripts and subscripts

i	Collocation index of the variable
j	Collocation index of the variation
s	Expansion index of the variable
τ	Expansion index of the variation

Acronyms / Abbreviations

BLWT	Beam Layer-Wise Theory
CLPT	Classical Lamination Plate Theory
CUF	Carrera Unified Formulation
DOFs	Degrees of Freedom
DSM	Dynamic Stiffness Method
DSV	De Saint-Venant
EBBM	Euler-Bernoulli Beam Model
ESCBP	Exact Solution for the Cylindrical Bending of Plates
FEM	Finite Element Method
FSDT	First order Shear Deformation Theory
GBT	Generalized Beam Theory
HSDT	Higher order Shear Deformation Theory
LE	Lagrange Expansion

LTSDT	Layer-wise Trigonometric Shear Deformation Theory
ODEs	Ordinary Differential Equations
PVW	Principle of Virtual Work
RBFs	Radial Basis Functions
PGD	Proper Generalized Decomposition
TBM	Timoshenko Beam Model
TE	Taylor Expansion
VABS	Variational Asymptotic Beam Sectional Analysis
VAM	Variational Asymptotic Method

Chapter 1

Introduction

1.1 One-dimensional structural theories

Beam models have been developed and exploited extensively over the last several decades for structural analysis of slender bodies, such as columns, arches, helicopter and turbine blades, aircraft wings and bridges amongst others. These models reduce the three-dimensional (3D) problem into a set of one-dimensional (1D) variables, which depend only on the beam-axis coordinate. Clearly, 1D structural theories, or beam theories, are simpler and computationally more efficient than 2D (plate/shell) theories or 3D (solid) elasticity solutions. This simple feature makes beams still very appealing for static and dynamic analyses of structures.

Over the years, many beam models have been developed using different approaches. The main contributions made to the development of the beam theories are outlined in this chapter by referring to different categories depending on the levels of complexity involved. Each category is then described in detail in the subsequent chapters of this thesis.

The first known description of the mechanical behavior of a beam under bending was given by Leonardo da Vinci. In his Madrid Codex [1], Leonardo correctly described the bending behavior of a slender beam, as shown in Fig. 1.1. He hypothesized the well-known linear distribution of the axial strain on the cross-section.

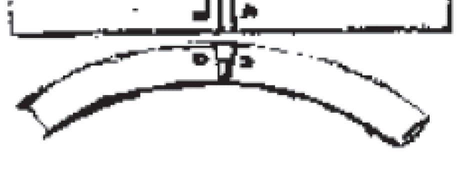

Figure 1.1 Leonardo's description of beam bending [1].

The classical, oldest and most frequently employed beam models are those by Bernoulli [2] and Euler [3], hereafter referred to as Euler-Bermoulli Beam Model (EBBM), de Saint Venant [4] (DSV) and Timoshenko Beam Model [5, 6] (TBM). These theories share many important features but they also have some important differences. A comprehensive comparison of EBBM and TBM can be found in [7] and in Chapter 2 of this thesis. In essence, TBM enhances EBBM and DSV by considering the rotatory inertia and shear deformation effects. However, TBM considers only a uniform shear distribution through the cross-section of the beam. It is well-known that a more appropriate distribution should at least be parabolic in order to accommodate the zero stress boundary conditions on the free edges of the beam. Shear correction factors related to the cross-sectional geometry are commonly employed as remedies to compensate for the zero shear condition at the boundaries. While EBBM and DSV are reliable tools for the analysis of homogenous, compact, isotropic slender beam structures under bending, TBM can be employed for moderately thick orthotropic or isotropic beams.

Classical beam theories represent a computationally cheap and, to some extent, reliable tool for many structural mechanics problems. These models are essentially based on a linear axial, out-of-plane displacement field and a constant transverse, in-plane displacement field. In other words, these models can predict linear axial strain distributions and rigid transverse displacements. Although this simplified displacement field requires no more than five degrees of freedom (DOFs), it also precludes the possibility of detecting many important effects, such as out-of-plane warping, in-plane distortions, torsion, coupling effects, or some other local effects. These additional phenomena usually occur due to small slenderness ratios, thin walls, geometrical and mechanical asymmetries, and the anisotropy of the material.

Many methods have been proposed to overcome the above limitations of classical beam theories so as to allow the application of 1D models to any geometry or boundary conditions, without jeopardizing their computational efficiency when compared to 2D and 3D models. Several examples of these models can be found in well known books on the theory of elasticity, for example, the book by Novozhilov [8]. A possible and modern grouping of all these methodologies to build higher-order beam models could be made as follows:

- The introduction of shear correction factors.
- Inclusion of warping functions.
- Saint-Venant based 3D solutions and the implementation of the Proper Generalized Decomposition (PGD) method.
- The Variational Asymptotic Beam Sectional Analysis (VABS) based on the Variational Asymptotic Method (VAM).

- The Generalized Beam Theory (GBT).
- The Carrera Unified Formulation (CUF).

As previously mentioned, some of the preliminary approaches were based on the introduction of shear correction factors to improve the global response of classical beam theories, see Timoshenko [5, 6, 9], Sokolnikoff [10] and Cowper [11].

The introduction of warping functions to improve the displacement field of beams is another well-known strategy that followed. Warping functions were first introduced in the framework of the Saint-Venant torsion problem [10, 12, 13]. Some of the earliest contributions to this approach were those made by Umanskij [14], Vlasov [15] and Benscoter [16].

The Saint-Venant solution has been the theoretical basis of many advanced beam models. For instance, 3D elasticity equations were reduced to beam-like structures by Ladevéze and his co-workers [17]. Using this approach, a beam model can be built as the sum of a Saint-Venant part and a residual part and then applied to thick beams and thin-walled sections.

The PGD for structural mechanics was first introduced by Ladevéze [18]. It is a useful tool to reduce the numerical complexity of a 3D problem. Bognet *et al.* [19, 20] extended PGD to plate/shell problems, whereas Vidal *et al.* [21] extended PGD to beams.

The asymptotic method, on the other hand, represents a significant tool to develop structural models. In the beam model scenario, the works by Berdichevsky *et al.* [22, 23] were among the earliest contributions that exploited the VAM. Such initiatives introduced an alternative approach to construct refined beam theories in which a characteristic parameter (e.g. the cross-sectional thickness of a beam) is exploited to build an asymptotic series. The terms that exhibit the same order of magnitude as the parameter are retained. Some valuable contributions on asymptotic methods related to VABS models can be found in [24].

Side by side to the above development, the GBT was essentially derived from Schardt's work [25–27]. The GBT enhances classical theories by exploiting a piece-wise description of thin-walled sections. It has been employed extensively and extended, in various forms, by Silvetre and Camotim [28]. Many other higher-order theories, based on enhanced displacement fields over the beam cross-section, have been introduced to include non-classical effects. Some considerations on higher-order beam theories were made by Washizu [29]. Other refined beam models can be found in the review carried out by Kapania and Raciti [30, 31], which focused on static bending, vibration, wave propagations, buckling and post-buckling problems. Refined beam models have been also exploited extensively for aeroelastic applications. Some of the most important contributions are those by Librescu and Song [32] and Qin and Librescu [33].

One of the most recent contributions to beam theories has been developed within the framework of the CUF [34]. The main novelty of CUF models is that the order of the theory is a free parameter, or can be an input of the analysis and it can be chosen using a convergence study. CUF can also be considered as a tool to evaluate the accuracy of any structural model in a unified manner. For a comprehensive review of CUF literature, the readers are referred to [35].

1.2 Numerical methods

In the majority of the literature on 1D-CUF, the Finite Element Method (FEM) has been used to handle arbitrary complex geometries and loading conditions. Closed form solutions of the structural problems discussed in this thesis can be solved in an exact sense only for a limited class of problems. For example, by assuming the beam kinematics such as the ones which satisfy the simply supported boundary conditions and by limiting the analysis to metallic or cross-ply laminated composite structures, exact solution can be achieved. In this way the axial and in-plane displacement fields can be decoupled and the governing equations can be solved analytically.

To obtain quasi type closed-form solutions with arbitrary boundary conditions for eigenvalue problems, the Dynamic Stiffness Method (DSM) can be used. DSM has been quite extensively developed for beam elements by Banerjee [36–40], Banerjee *et al.* [41], and Williams and Wittrick [42]. Plate elements based on DSM were originally formulated by Wittrick [43] and Wittrick and Williams [44]. Recently, DSM has been applied to Mindlin plate assemblies by Boscolo and Banerjee in [45, 46] and to a higher order shear deformation theory for composite plates by Fazzolari *et al.* [47, 48]. In these papers, some background information on the use of DSM can be found.

The DSM is appealing in elastodynamic analysis because, unlike the FEM, it provides the exact solution of the equations of motion of a structure once the initial assumptions on the displacements field have been made. This essentially means that, unlike the FEM and other approximate methods, the model accuracy is not unduly compromised when a small number of elements are used in the analysis. For instance, one single structural element can be used in the DSM to compute any number of natural frequencies to any desired accuracy. Of course, the accuracy of the DSM will be as good as the accuracy of the governing differential equations of the structural element in free vibration. In fact, the exact Dynamic Stiffness (DS) matrix stems from the solution of the governing differential equations.

It should be noted that the DSM leads to a nonlinear, transcendental eigenvalue problem and an iterative procedure may be needed for solution (see [49]). Thus, the availability of further numerical methodologies to be used for the approximate solution of the strong form governing equations can be of interest. As an example, the use of alternative methods to FEM and DSM for the analysis of structures, such as the meshless methods based on collocation theory with Radial Basis Functions (RBFs), is attractive due to the absence of a mesh and the considerable ease of the collocation techniques. In recent years, RBFs method showed excellent accuracy in the interpolation of data and functions. The RBFs method was first used by Hardy [50, 51] for the interpolation of geographical scattered data and later used by Kansa [52, 53] for the solution of partial differential equations. Afterward, Ferreira successfully applied RBFs to the analysis of beams and plates [54, 55]. RBFs method is appealing because it results either in an algebraic system or in a linear eigenvalue problem depending on the case. However, numerical instabilities may be encountered in this method and they are discussed later in the present work.

In this thesis and in Pagani *et al.* [56–59], DSM has been extended to 1D-CUF models for both metallic and generically laminated composite structures. Also, RBFs method is explored as an alternative method for the solution of strong form governing equations for CUF beams (see [60]).

1.3 Thesis objectives and outline

The present work aims at providing differential governing equations in strong form (as opposed to weak form, which represents an integral form of these equations) of 1D refined CUF structural models and their subsequent solutions by various closed-form and numerical methods. A wide range of problems are considered, including static analysis, free vibration analysis, free vibration of axially loaded beams, and linearized buckling analysis of beam-columns. The main novelties of this research are: (i) the explicit expressions of the strong form governing equations of CUF beam theories, especially the equations of motion of axially-loaded beam-columns; (ii) the extension of DSM and RBFs to free vibration and buckling analysis of refined CUF beam theories; and (iii) the exact closed-form benchmark solutions for various structural problems, including analytical layer-wise solutions of laminated beams and plates. The general lay-out of the thesis is as follows:

- Brief bibliographic surveys on classical and refined beam modelling techniques and related solution methods are given in this introductory chapter.

- Chapter 2 discusses in detail the kinematics of slender structures. Starting from the classical assumptions, refined beam models are formulated as the natural consequences of the additions of terms within the displacement field. Various state-of-the-art approaches are also discussed, including GBT, VAM and asymptotic models.

- In Chapter 3, higher-order beam models are formulated in a unified manner by employing the CUF. Within the framework of CUF, the beam kinematics are written as the generic expansion of the generalized displacements using arbitrary cross-sectional functions. Depending on the choice of the kind and the order of the cross-sectional functions, various beam theories can be formulated. In this thesis, two classes of 1D CUF models are considered. These are namely, the Taylor Expansion (TE) class and the Lagrange Expansion (LE) class.

- The strong form governing equations of the generic, refined beam model are developed in Chapter 4. By using the Principle of Virtual Work (PVW) as variational statement, various problems are addressed by either including or excluding the virtual works due to inertial loadings, external loadings and pre-stress along with the virtual work of the strain energy. According to CUF, the governing equations are written in terms of the fundamental nuclei. These nuclei, given the theory order, can be automatically expanded to obtain the equations of the desired theory.

- In Chapter 5, closed-form analytical solutions are provided by imposing simply supported boundary conditions and limiting the analysis to metallic or cross-ply laminates. Attention is focused on the static and free vibration problems, although the procedure can be extended to other problems.

- The material and boundary condition limitations are overcome in Chapter 6, where a collocation method is formulated by using RBFs to approximate the displacement functions and the corresponding derivatives.

- In Chapter 7 the governing equations are rearranged and the transcendental dynamic stiffness matrix is formulated. By using an iterative procedure, namely the Wittrick and Williams algorithm [49], the non-linear eigenvalue problem is solved.

- Some selective results are discussed in Chapter 8. The attention is mainly focused on the efficiency of both TE and LE models as well as on the accuracy of the proposed numerical methodologies when applied to the analysis of solid and thin-walled cross-section beams. Both metallic and composite beams and plates are addressed.

- The conclusions are finally drawn in Chapters 9 and 10.

Some appendices are provided for clarity and completeness.

- In Appendix A, the material coefficients and the constitutive relations are discussed in detail.
- Appendix B briefly recalls the resolution technique for a generic system of second order differential equations, which is useful in the DSM formulation.
- An innovative forward/backward Gauss elimination algorithm is devised in Appendix C.
- Finally, a list of publications arising from the research is provided in Appendix D.

Chapter 2

Kinematics of beams

This chapter provides details of some of the most important beam models that have been developed in the last few years and, in most cases, are still being developed. For the sake of brevity, only the main features of each formulation are given and described in order to highlight their advantages and disadvantages. The right-handed Cartesian coordinate system shown in Fig. 2.1 is adopted throughout this thesis.

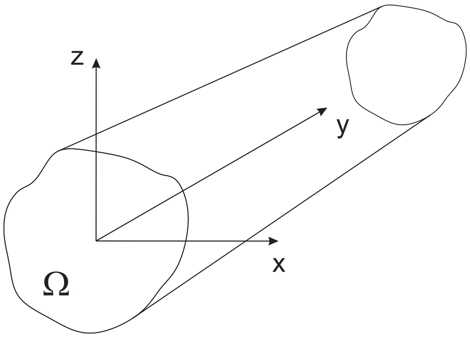

Figure 2.1 Adopted coordinate system.

2.1 Classical beam theories

Consider a beam structure under bending in the plane *xy* (see Fig. 2.2). The kinematic field of EBBM (Euler-Bernoulli Beam Model) can be written as:

$$\begin{aligned} u_x &= u_{x1} \\ u_y &= u_{y1} - x\,\frac{\partial u_{x1}}{\partial y} \end{aligned} \tag{2.1}$$

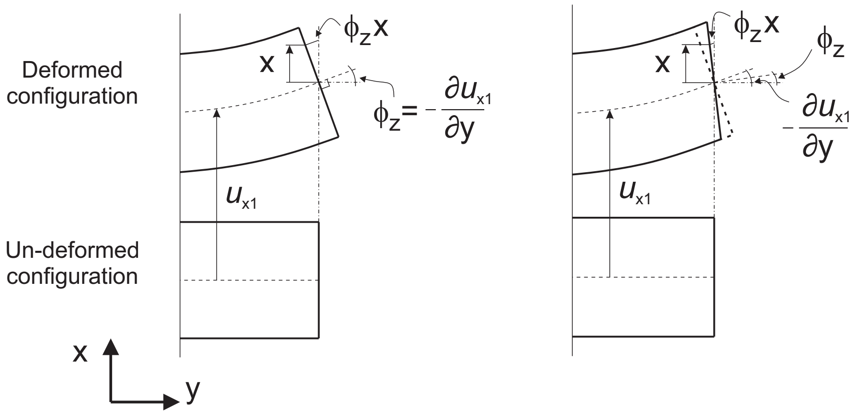

(a) EBBM (b) TBM

Figure 2.2 Differences between Euler-Bernoulli and Timoshenko beam theories.

where u_x and u_y are the displacement components of a point belonging to the beam domain along x and y, respectively. u_{x1} and u_{y1} are the displacements of the beam axis, whereas $-\frac{\partial u_{x1}}{\partial y}$ is the rotation of the cross-section about the z-axis (i.e. ϕ_z) as shown in Fig. 2.2a. According to EBBM, the deformed cross-section remains plane and orthogonal to the beam axis. EBBM neglects the cross-sectional shear deformation. Shear stresses play a very important role in many problems (e.g. short beams, composite structures) and their omission can lead to incorrect results. One may like to generalize Eq. (2.1) and overcome the EBBM assumption of the orthogonality of the cross-section. The improved displacement field leads to the TBM (Timoshenko Beam Model),

$$\begin{aligned} u_x &= u_{x1} \\ u_y &= u_{y1} + x\,\phi_z \end{aligned} \tag{2.2}$$

TBM constitutes an improvement over EBBM since the cross-section does not necessarily remain perpendicular to the beam axis after deformation and one degree of freedom (i.e. the unknown rotation ϕ_z) is added to the original displacement field (see Fig. 2.2b). Nevertheless, the main problem of TBM is that the homogeneous conditions of the transverse stress components at the top/bottom surfaces of the beam are not fulfilled. It is well-known, in fact, that TBM is based on a uniform shear distribution through the thickness of the cross-section of the beam and a more appropriate distribution should at least be parabolic in order to accommodate for the stress-free boundary conditions on the free edges of the beam (see Fig. 2.3).

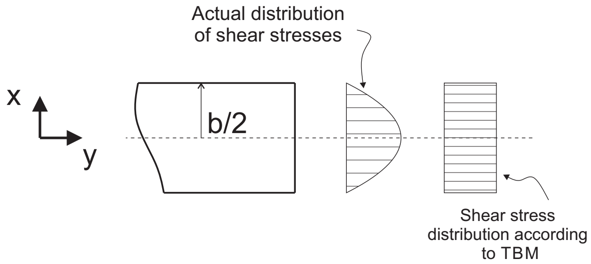

Figure 2.3 Homogeneous condition of transverse stress components at the unloaded edges of the beam.

One of the earlier attempts to improve the accuracy of TBM was the adoption of shear correction factors. Shear correction factors have been introduced over the years to enhance classical beam theories by several authors, see for example [5, 6, 9–11]. Shear correction factors can be defined in various ways, and they depend on the problem characteristics to a great extent. Two examples of shear correction factor definitions are given here. Cowper [11] considered the mean deflection of the cross-section (W), the mean angle of rotation of the cross-section around the neutral axis (Φ) and the total transverse shear force acting on the cross-section (Q), using the following integrals.

$$W = \frac{1}{\Omega}\int\int u_x \, dx\, dz \tag{2.3}$$

$$\Phi = \frac{1}{I}\int\int x u_y \, dx\, dz \tag{2.4}$$

$$Q = \int\int \sigma_{xy} \, dx\, dz \tag{2.5}$$

where Ω is equal to the cross-section area, and I is the second moment of area of the cross-section. The shear correction factor, K^C, is then calculated by exploiting the following equation:

$$\frac{\partial W}{\partial y} - \Phi = \frac{Q}{K^C A G} \tag{2.6}$$

where G is the shear modulus of beam material.

Gruttmann and Wagner [61] adopted the following definition of shear correction or shape factor, which was earlier introduced in [62, 63]:

$$\int\int (\sigma_{yx}^2 + \sigma_{yz}^2)\, dx\, dz = \frac{F_x^2}{K_x^G A} + \frac{F_z^2}{K_z^G A} \tag{2.7}$$

In Eq. (2.7) the shear correction factors, K_x^G and K_z^G, are respectively obtained by imposing F_z and F_x to be equal to zero.

The shear correction factor can be seen as a nonphysical, but artificial way to overcome classical beam modelling inconsistency. As shown by Carrera *et al.* [64], refined beam models based on higher-order displacement fields do not require shear correction factors.

2.2 Higher-order models

For a complete removal of the inconsistency in Timoshenko's beam theory and an improvement of the accuracy of classical beam theories, one may have to assume an arbitrary number of terms in the displacement field [29]. However, the number and the characteristics of these *higher-order* terms should be chosen properly. For example, in order to overcome the inconsistency of TBM, one can require Eq. (2.2) to have null transverse strain components ($\gamma_{xy} = \frac{\partial u_x}{\partial y} + \frac{\partial u_y}{\partial x}$) at $x = \pm\frac{b}{2}$ of Fig. 2.3. This leads to a third-order displacement field as follows, which provides the basis for the well-known Vlasov-Reddy beam theory [15, 65],

$$\begin{aligned} u_x &= u_{x1} \\ u_y &= u_{y1} + f_1(x)\,\phi_z + g_1(x)\,\frac{\partial u_{x1}}{\partial y} \end{aligned} \tag{2.8}$$

where $f_1(x)$ and $g_1(x)$ are cubic functions of the x coordinate. It should be noted that, even though the model based on Eq. (2.8) has the same number of degrees of freedom as the TBM, it clearly overcomes classical beam theory limitations by postulating a quadratic distribution of transverse stresses on the cross-section of the beam.

However, the above theories are not able to include any kinematics resulting from the application of torsional moments. The simplest way to include torsion consists of considering a rigid rotation of the cross-section around the y-axis (i.e. ϕ_y), see Fig. 2.4. The resulting displacement model is:

$$\begin{aligned} u_x &= z\,\phi_y \\ u_z &= -x\,\phi_y \end{aligned} \tag{2.9}$$

where u_z is the displacement component along the z-axis. According to Eq. (2.9), a linear distribution of transverse displacement components is needed to detect the rigid rotation of the cross-section about the beam axis. Beam models that include second-order shear strain capabilities and torsional components can be obtained by summing all the contributions discussed above. By considering the deformations also in the yz-plane, one has

$$\begin{aligned} u_x &= u_{x1} + z\,\phi_y \\ u_y &= u_{y1} + f_1(x)\,\phi_z + f_2(z)\,\phi_x + g_1(x)\,\left(\frac{\partial u_{x1}}{\partial y} + z\frac{\phi_y}{\partial y}\right) + g_2(z)\,\left(\frac{\partial u_{z1}}{\partial y} - x\frac{\phi_y}{\partial y}\right) \\ u_z &= u_{z1} - x\,\phi_y \end{aligned} \tag{2.10}$$

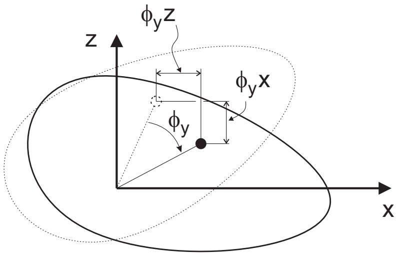

Figure 2.4 Rigid torsion of the beam cross-section.

where $f_1(x)$, $g_1(x)$, $f_2(z)$, and $g_2(z)$ are all cubic functions. For example, in the case of a rectangular cross-section, the cubic functions from Vlasov's theory [15] are

$$\begin{aligned} f_1(x) &= x - \frac{4}{3b^2}x^3, \quad g_1(x) = -\frac{4}{3b^2}x^3 \\ f_2(z) &= z - \frac{4}{3h^2}z^3, \quad g_2(z) = -\frac{4}{3h^2}z^3 \end{aligned} \tag{2.11}$$

where b and h are the dimensions of the rectangular cross-section along the x- and z-axis, respectively.

The aforementioned beam model, although an advancement, cannot account for many other *higher-order effects*, such as the second-order in-plane deformations of the cross-section and out-of-plane warping. Many refined beam theories have been proposed over the last decades to overcome these limitations of classical beam modelling and they are briefly discussed in the following sections. As a general guideline, one can state that the richer the kinematic field, the more accurate the 1D model turns out to be [29]. However, a richer displacement field clearly leads to a higher number of equations to be solved. Furthermore, the choice of the additional expansion terms is obviously problem dependent. The most accurate beam models that have been developed in the last few years are now briefly discussed.

2.2.1 Generalized beam theory

The assumption of rigid cross-section introduced by the classical models does not allow the correct detection of the cross-sectional warping, which is a fundamental consideration in the characterization of thin-walled beams. The Generalized Beam Theory (GBT) represents a family of models introduced to overcome this problem and to accurately describe the mechanical behaviour of thin-walled members. GBT originated from the pioneering works of Schardt [25, 26] and Schardt and Heinz [66]. First-order beam models based on GBT

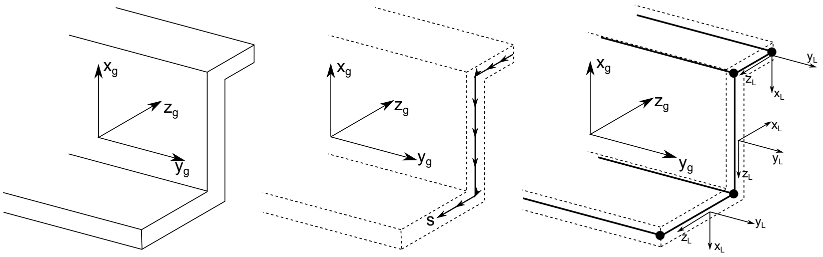

Figure 2.5 GBT approximation, global, $()_g$, and local, $()_L$, reference systems.

were proposed by Davies and Leach [67], while refined second-order models were given simultaneously by the same authors in [68]. An extension of GBT to orthotropic materials was proposed by Silvestre and Camotim [28] and Silvestre [69]. The GBT approach, as shown in [28], assumes that the displacement field of a prismatic thin-walled beam (see Fig. 2.5) is a product of two functions as shown below

$$\mathbf{u}(x_g, y_g, z_g) = \mathbf{u}(s)\,\psi(y_g) \tag{2.12}$$

where $\mathbf{u}(s)$ is the mid-wall displacement vector, which depends on the curvilinear coordinate s going around the cross-section (see Fig. 2.5), and $\psi(y_g)$ is an amplitude function defined along the beam axis y. Figure 2.5 also shows how, according to GBT, the beam can be assumed to be composed of a number of panels (see [28]). In its simplest form, GBT states that, for each panel:

- The Kirchhoff's hypotheses are satisfied ($\gamma_{xy} = 0$, $\gamma_{xz} = 0$ and $\varepsilon_{xx} = 0$).
- The only membrane (m) strain considered is the longitudinal one, i.e. $\varepsilon_{yy}^{m} \neq 0$. On the other hand, all the flexural (f) strains are taken into account, i.e. $\varepsilon_{yy}^{f} \neq 0$, $\varepsilon_{zz}^{f} \neq 0$ and $\gamma_{yz}^{f} \neq 0$.

The mid-wall deflection curve can be considered as a piece-wise segment defined by using a number of nodes (see Fig.2.5). If the generalized displacements $\mathbf{u}(s)$ are assumed to have a linear behaviour, the GBT kinematics becomes

$$\mathbf{u}(x_g, y_g, z_g) = \mathbf{u}_k F_k(s)\,\psi(y_g) \tag{2.13}$$

where $F_k(s)$ is a linear function that is equal to 1 in the k-th node and 0 in the other nodes, and $\mathbf{u}_k$ is the displacement vector in the k-th node. Moreover, GBT introduces a number of geometrical relations that allow the transverse displacements, u_x and u_z, to be expressed in terms of the longitudinal displacement, u_y.

The GBT has been widely used in the analysis of thin-walled structures over the past twenty years. This type of model has been used to solve several structural problems and a few examples are reviewed next. The GBT was applied to dynamic problems in the works by Bebiano [70, 71], in which the global and local modes were investigated. Also, the elastic stability of thin-walled structures has been investigated extensively using the GBT. Schardt [72, 27] used the GBT model to perform the buckling analysis of thin-walled structures. The same approach was used by Goncalves and Camotim [73] to investigate the local and the global buckling of isotropic structures. Other investigators who used the GBT models in buckling analysis are Dinis *et al.* [74], Silvestre [75] and Basaglia *et al.* [76] amongst others. An experimental verification of the GBT for the buckling analysis was provided by Leach and Davies [77]. The capabilities of GBT in the analysis of thin-walled structures and its low computational costs make GBT particularly useful for non-linear analyses. Goncalves and Camotim [78] introduced a non-linear formulation based on GBT to investigate the post-buckling behaviour of thin-walled structures, in which plasticity and inelastic effects were included. Other non-linear beam models based on GBT were presented by Basaglia *et al.* [79] and Abambres *et al.* [80, 81].

2.2.2 Warping functions

The so-called warping function was originally introduced with the Saint-Venant torsion problem, which has been formulated in many textbooks and papers over the years [10, 12, 13] as a standard procedure in the theory of elasticity. According to the Saint-Venant free warping problem, the warping function is the solution of Laplace's equation subjected to Neumann boundary conditions [82].

The most well-known theories that account for higher-order phenomena through the use of the warping function are those by Vlasov [15] and Benscoter [16]. In these theories, non-uniform warping in thin-walled profiles is taken into account by including, in the displacement field, the following longitudinal warping displacement, u_y^{wrp}:

$$u_y^{\mathrm{wrp}}(x,y,z) = \Gamma(x,z)\,\mu(y) \tag{2.14}$$

where y is the longitudinal axis of the beam, x and z are the coordinates of the cross-section, μ is the warping parameter, and Γ is the Saint-Venant warping function, which depends on the geometry of the cross-section. In the case of a shear-bending problem on the xy-plane, the warping function is a cubic function of the x-coordinate [83] and μ does not necessarily depend on the cross-sectional strain γ_{xy} . On the other hand, in the case of torsion, the warping parameter μ is the derivative of the rotation angle [15] or it can be an independent function [16].

The application of the Vlasov beam model to thin-walled beams with a closed cross-section leads to unsatisfactory results, since the mid-plane shear strains in the walls cannot be neglected. One of the earliest investigators to formulate the warping function for closed profiles was Umanskij [14]. From then on, many researchers have developed advanced beam theories based on the use of the Saint-Venant warping function. Some recent important contributions are summarized as follows. El Fatmi [84–86] developed a non-uniform warping theory that accounts for three independent warping parameters and related warping functions. Prokic [87–89] formulated a new warping function that is able to account for both closed and open cross-sections. Sapountzakis and his co-workers developed a boundary element method that includes the warping DOF (Degree of Freedom) for non-uniform torsional dynamic [90, 91] and static [92–94] analyses. Wackerfub and Gruttmann [95] developed a Finite Element (Finite Element) based on the Hu-Washizu variational formulation and focussing on the construction of ‘locally-defined’ warping functions. In [82, 96], the unknown warping function has been approximated using an isoparametric concept. Prandtl’s membrane analogy and the Saint Venant torsion theory have been used in [97], on the basis of the Vlasov theory, to obtain an approximate Saint Venant warping function for a prismatic thin-walled beam. In [98], the warping functions have been determined iteratively using equilibrium equations along the beam. Yoon and Lee [99] formulated the entire warping displacement field as a combination of the three basic warping functions (one free warping function and two interface warping functions).

2.2.3 3D Solutions based on the Saint-Venant model and the proper generalized decomposition

Ladevéze and Simmonds [17, 13] and Ladevéze *et al.* [100] built models for 3D solutions of beam problems by adding enrichment terms to the Saint Venant solution. In such a framework, the displacement field can be written as

$$u(x,y,z) = u_{SV}(x,y,z) + u_{NSV}(x,y,z) \tag{2.15}$$

where u_{SV} and u_{NSV} are the Saint-Venant and residual parts of the displacement field, respectively. The u_{NSV} term, also known as the decaying term, takes into account various non-classical effects, e.g. the end-effects. Such solutions are exact since they do not add any further assumptions to the 3D elasticity equations. However, these solutions are problem dependent.

Another important contribution to the solution of the 3D elasticity problem is the Proper Generalized Decomposition (PGD), which was introduced by Ladevéze [18]. Given a 3D problem, PGD decomposes it as the summation of N 1D and/or 2D functions (noting that y is the axial coordinate of the beam) as follows

$$u(x,y,z) \approx \sum_{i=1}^{N} U_i^x(x) \cdot U_i^y(y) \cdot U_i^z(z) \tag{2.16}$$

or,

$$u(x,y,z) \approx \sum_{i=1}^{N} U_i^{xz}(x,z) \cdot U_i^y(y) \tag{2.17}$$

where U are the 2D or 1D unknown functions. This decomposition allows one to solve the 3D problem with 2D or 1D complexity. Bognet *et al.* [19, 20] applied PGD to plate/shell problems, while Vidal *et al.* [21] extended PGD to beams.

2.3 Asymptotic methods

So far, refined beam theories derived from axiomatic methods have been discussed. Axiomatic theories are developed on the basis of a number of hypotheses that cannot be always mathematically proved [101]. Moreover, another important drawback of axiomatic methods is the lack of information about the accuracy of the approximated theory with respect to the exact 3D solution. In other words, it is not usually possible to evaluate a-priori the accuracy of an axiomatic theory. The difficulty due to this lack of information has to be overcome by engineers who have to evaluate the validity of a theory on the basis of their knowledge and experience.

The asymptotic method is generally seen as a step towards the development of approximate theories with known accuracy with respect to the 3D exact solution (see [102]), which, in the case of beams, is a good method that can approximate the 3D energy though 1D terms with known accuracy.

The Variational Asymptotic Method (VAM) is an interesting proposition that was originally introduced by Berdichevsky [22] in modelling beams. VAM exploits small parameters of a beam structure, such as the thickness of the cross-section, h. The unknown functions (e.g. warping) are then expanded in terms of h as

$$f = f_0 + f_1\, h + O(h^2) \tag{2.18}$$

The strain energy is then obtained according to this expansion and only the terms of a certain order with respect to h are retained. The unknown functions, which are asymptotically correct up to a chosen order of h, are then obtained by minimizing the strain energy. The solution to this variational problem can then be found in closed-form for certain cross-sectional geometries and materials only. In order to overcome the limitations of VAM and to be able to deal with anisotropic and non-homogenous materials, as well as arbitrary cross-sections, the Variational Asymptotic Beam Sectional Analysis (VABS) has been developed [24, 103–106]. Essentially, VABS exploits the FE approach over the beam cross-section to solve the variational problem.

In general, the development of asymptotic theories is more difficult than the development of axiomatic ones. The main advantage of these theories is that they contain all of the terms whose effectiveness is of the same order of magnitude. Moreover, these theories are exact as h, or any other small parameter that is exploited to build the expansion, tends to zero.

Chapter 3

Carrera Unified Formulation

Whether axiomatic or asymptotic, the accuracy of a structural theory depends very much on the problem to be analysed. One may merge or amalgamate together the beam theories discussed in the previous chapter in order to address a particular problem. For example, a beam model able of addressing shear, twisting and warping can be formulated by combining Eqs. (2.10) and (2.14). Unfortunately, the resulting model may not be suitable for a different problem, e.g., it may not be able to detect in-plane deformations on the beam cross-section.

In this chapter, the Carrera Unified Formulation (CUF) is introduced. In essence, CUF, by employing a index notation, allows the unification of all the theories of structures in one single formula. Subsequently, in the next part of the thesis, CUF will be used in conjunction with variational principles to derive the governing equations for any-order beam model in a concise and general manner.

3.1 Preliminaries

The rectangular Cartesian coordinate system adopted in this thesis has already been shown in Fig. 2.1, together with a schematic beam structure. The cross-section of the beam, which lies on the xz-plane, is denoted by Ω, whereas the limits of y are $0 \leq y \leq L$. Consider the transposed displacement vector, which can be expressed as

$$\mathbf{u}(x,y,z;t) = \left\{ \begin{array}{ccc} u_x & u_y & u_z \end{array} \right\}^T \tag{3.1}$$

The time variable (t) is implied, but omitted in the remaining part of this chapter for clarity purposes. The components of stress, $\boldsymbol{\sigma}$, and strain, $\boldsymbol{\varepsilon}$, are expressed in transposed forms as follows:

$$\boldsymbol{\sigma} = \left\{ \begin{array}{cccccc} \sigma_{yy} & \sigma_{xx} & \sigma_{zz} & \sigma_{xz} & \sigma_{yz} & \sigma_{xy} \end{array} \right\}^T$$
$$\boldsymbol{\varepsilon} = \left\{ \begin{array}{cccccc} \varepsilon_{yy} & \varepsilon_{xx} & \varepsilon_{zz} & \varepsilon_{xz} & \varepsilon_{yz} & \varepsilon_{xy} \end{array} \right\}^T \tag{3.2}$$

In the case of small deformations and angles of rotation, the strain-displacement relations are

$$\boldsymbol{\varepsilon} = \mathbf{D}\mathbf{u} \tag{3.3}$$

where **D** is the following linear differential operator matrix

$$\mathbf{D} = \begin{bmatrix} 0 & \frac{\partial}{\partial y} & 0 \\ \frac{\partial}{\partial x} & 0 & 0 \\ 0 & 0 & \frac{\partial}{\partial z} \\ \frac{\partial}{\partial z} & 0 & \frac{\partial}{\partial x} \\ 0 & \frac{\partial}{\partial z} & \frac{\partial}{\partial y} \\ \frac{\partial}{\partial y} & \frac{\partial}{\partial x} & 0 \end{bmatrix} \tag{3.4}$$

Constitutive laws are now exploited to obtain stress components to give

$$\boldsymbol{\sigma} = \tilde{\mathbf{C}}\boldsymbol{\varepsilon} \tag{3.5}$$

In the case of *monoclinic material* (i.e., material with one single plane of symmetry, which is the *xy*-plane in the present analysis) the matrix $\tilde{\mathbf{C}}$ is

$$\tilde{\mathbf{C}} = \begin{bmatrix} \tilde{C}_{33} & \tilde{C}_{23} & \tilde{C}_{13} & 0 & 0 & \tilde{C}_{36} \\ \tilde{C}_{23} & \tilde{C}_{22} & \tilde{C}_{12} & 0 & 0 & \tilde{C}_{26} \\ \tilde{C}_{13} & \tilde{C}_{12} & \tilde{C}_{11} & 0 & 0 & \tilde{C}_{16} \\ 0 & 0 & 0 & \tilde{C}_{44} & \tilde{C}_{45} & 0 \\ 0 & 0 & 0 & \tilde{C}_{45} & \tilde{C}_{55} & 0 \\ \tilde{C}_{36} & \tilde{C}_{26} & \tilde{C}_{16} & 0 & 0 & \tilde{C}_{66} \end{bmatrix} \tag{3.6}$$

Note that the the above matrix describes the constitutive relations of a fibre reinforced lamina with respect to a generic coordinate system (x,y,z) rotated by an angle θ with respect to the material coordinate system $(1,2,3)$, see Fig. 3.1. In fact, a fibre reinforced lamina exhibits an *orthotropic* behaviour with respect to the material coordinate system $(1,2,3)$. Orthotropic materials present three mutually perpendicular planes of elastic symmetry and, thus, they

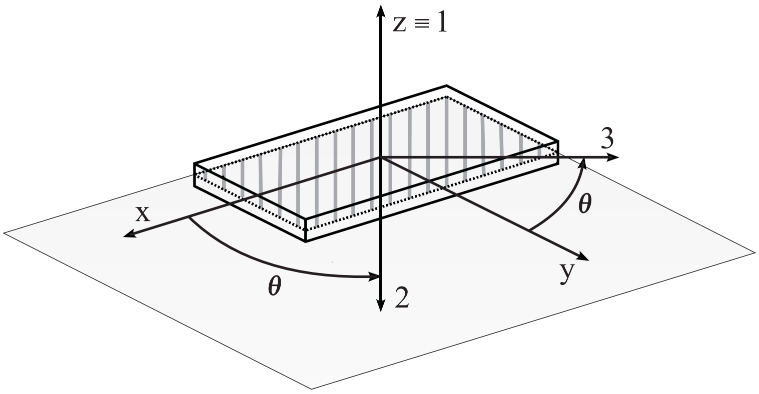

Figure 3.1 Coordinate system and fiber orientation angle.

are fully characterized by nine elastic coefficients. Therefore, the 13 elastic coefficients $\tilde{C}_{ij}$, which are elements of matrix $\tilde{\mathbf{C}}$ in Eq. (3.6), can be expressed as functions of the nine coefficients with respect to the orthotropic axes $(1,2,3)$ and the fibre rotation angle θ. The explicit expressions for the coefficients $\tilde{C}_{ij}$ are given in Appendix A. It should be stressed that models with constant and linear distributions of the in-plane displacement components, u_x and u_z, may require modified material coefficients to overcome the Poisson locking problem, see [107]. The explicit expressions of the reduced material coefficients are not reported here, but the readers are referred to the text by Carrera *et al.* [108], where the details are given together with a more comprehensive analysis of the effect of Poisson locking and its correction.

3.2 Unified formulation of beams

According to Carrera Unified Formulation (CUF), the generic displacement field of a beam model can be expressed in a compact manner as an expansion in terms of arbitrary functions, F_τ,

$$\mathbf{u}(x,y,z) = F_\tau(x,z)\mathbf{u}_\tau(y), \qquad \tau = 1,2,...,M \tag{3.7}$$

where F_τ are the functions of the coordinates x and z on the cross-section; $\mathbf{u}_\tau$ is the vector of the *generalized displacements*; M stands for the number of terms used in the expansion; and the repeated subscript, τ, indicates summation. The choice of F_τ determines the class of the 1D CUF model.

3.2.1 Taylor expansion (TE)

Taylor Expansion (TE) 1D CUF models consists of McLaurin series that use the 2D polynomials $x^i\ z^j$ as the F_τ basis. Table 3.1 shows M and F_τ as functions of the expansion order, N, which represents the maximum order of the polynomials used in the expansion.

N	M	F_τ
0	1	$F_1 = 1$
1	3	$F_2 = x, F_3 = z$
2	6	$F_4 = x^2, F_5 = xz, F_6 = z^2$
3	10	$F_7 = x^3, F_8 = x^2z, F_9 = xz^2, F_{10} = z^3$
$\vdots$	$\vdots$	$\vdots$
N	$\frac{(N+1)(N+2)}{2}$	$F_{(N^2+N+2)/2} = x^N, F_{(N^2+N+4)/2} = x^{N-1}z, \ldots, F_{N(N+3)/2} = xz^{N-1}, F_{(N+1)(N+2)/2} = z^N$

Table 3.1 McLaurin's polynomials.

According to CUF, classical (see Eqs. (2.1) and (2.2)) and higher-order models (e.g., Eqs. (2.10)) consist of particular cases of TE theories. It should be noted that Eqs. (2.1), (2.2), and (2.9) are degenerated cases of the linear ($N = 1$) TE model, which can be expressed as

$$\begin{aligned} u_x &= u_{x_1} + x\, u_{x_2} + z\, u_{x_3} \\ u_y &= u_{y_1} + x\, u_{y_2} + z\, u_{y_3} \\ u_z &= u_{z_1} + x\, u_{z_2} + z\, u_{z_3} \end{aligned} \tag{3.8}$$

where the parameters on the right-hand side (u_{x_1}, u_{y_1}, u_{z_1}, u_{x_2}, etc.) are the unknown generalized displacements of the beam axis as functions of the y-coordinate. Higher-order terms can be taken into account according to Eq. (3.7). For instance, the displacement fields of Eqs. (2.8) and (2.10) can be considered as particular cases of the third-order ($N = 3$) TE model,

$$\begin{aligned} u_x &= u_{x_1} + x\, u_{x_2} + z\, u_{x_3} + x^2\, u_{x_4} + xz\, u_{x_5} + z^2\, u_{x_6} + x^3\, u_{x_7} + x^2z\, u_{x_8} + xz^2\, u_{x_9} + z^3\, u_{x_{10}} \\ u_y &= u_{y_1} + x\, u_{y_2} + z\, u_{y_3} + x^2\, u_{y_4} + xz\, u_{y_5} + z^2\, u_{y_6} + x^3\, u_{y_7} + x^2z\, u_{y_8} + xz^2\, u_{y_9} + z^3\, u_{y_{10}} \\ u_z &= u_{z_1} + x\, u_{z_2} + z\, u_{z_3} + x^2\, u_{z_4} + xz\, u_{z_5} + z^2\, u_{z_6} + x^3\, u_{z_7} + x^2z\, u_{z_8} + xz^2\, u_{z_9} + z^3\, u_{z_{10}} \end{aligned} \tag{3.9}$$

A more comprehensive treatment of the TE CUF models can be found in [108], where details about the derivation of classical models from the linear ($N = 1$) TE model and various numerical simulations to capture the degenerate cases are also given.

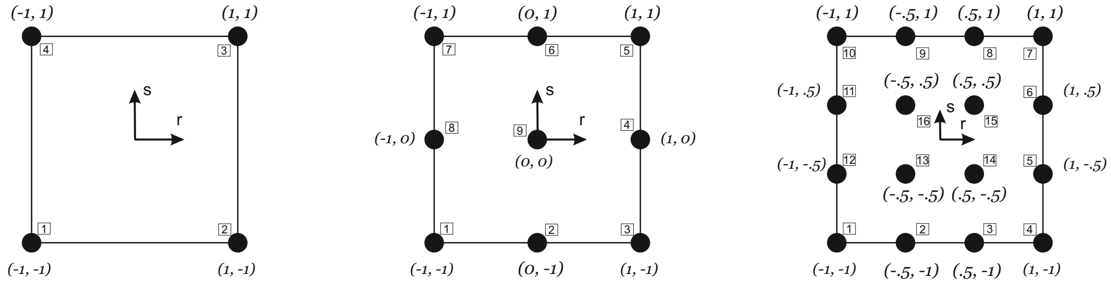

(a) Four-point element, L4 (b) Nine-point element, L9 (c) Sixteen-point element, L16

Figure 3.2 Cross-section L-elements in natural geometry.

3.2.2 Lagrange expansion (LE)

In this work, another CUF class of models has played an important role and it is referred to as the Lagrange Expansion (LE) class. The LE models exploit Lagrange polynomials to build 1D higher-order models; i.e., Lagrange polynomials are used as F_τ cross-sectional functions. In the current research, three types of cross-sectional polynomial sets have been adopted. These are shown in Fig. 3.2 which are namely, four-point polynomials (L4), nine-point polynomials (L9), and sixteen-point polynomials (L16). The isoparametric formulation is exploited to deal with arbitrarily shaped geometries.

Some aspects of the Lagrange polynomials as interpolation functions can be found in [109]. However, for the sake of completeness, an illustrative example of the interpolation function is given below for the case of an L4 beam model.

$$F_\tau = \frac{1}{4}(1 + r\, r_\tau)(1 + s\, s_\tau) \qquad \tau = 1,2,3,4 \tag{3.10}$$

where r and s vary from -1 to $+1$, whereas r_τ and s_τ are the coordinates of the four corner points whose numbering and location in the natural coordinate frame are shown in Fig. 3.2a. In the case of an L9 kinematics, see Fig. 3.2b, the interpolation functions are given by:

$$\begin{aligned} &F_\tau = \tfrac{1}{4}(r^2 + r\, r_\tau)(s^2 + s\, s_\tau) \qquad \tau = 1,3,5,7 \\ &F_\tau = \tfrac{1}{2}s_\tau^2(s^2 - s\, s_\tau)(1 - r^2) + \tfrac{1}{2}r_\tau^2(r^2 - r\, r_\tau)(1 - s^2) \qquad \tau = 2,4,6,8 \\ &F_\tau = (1 - r^2)(1 - s^2) \qquad \tau = 9 \end{aligned} \tag{3.11}$$

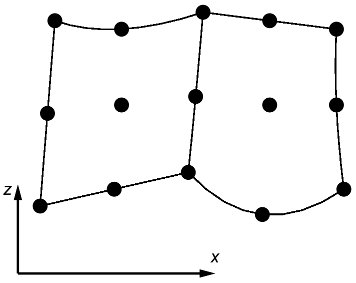

Figure 3.3 Two assembled L9 elements in actual geometry.

Finally, the L16 polynomials with reference to Fig. 3.2c are as follows:

$$F_{\tau IJ} = L_I(r)L_J(s) \qquad I,J = 1,\cdots,4 \tag{3.12}$$

where

$$\begin{aligned} L_1(r) &= \frac{1}{16}(r-1)(1-9r^2) \quad L_2(r) = \frac{9}{16}(3r-1)(r^2-1) \\ L_3(r) &= \frac{9}{16}(3r+1)(1-r^2) \quad L_4(r) = \frac{1}{16}(r+1)(9r^2-1) \end{aligned} \tag{3.13}$$

The complete displacement field of a beam model discretized with one single L9 polynomial is given below for illustrative purposes:

$$\begin{aligned} u_x &= F_1 u_{x_1} + F_2 u_{x_2} + F_3 u_{x_3} + F_4 u_{x_4} + F_5 u_{x_5} + F_6 u_{x_6} + F_7 u_{x_7} + F_8 u_{x_8} + F_9 u_{x_9} \\ u_y &= F_1 u_{y_1} + F_2 u_{y_2} + F_3 u_{y_3} + F_4 u_{y_4} + F_5 u_{y_5} + F_6 u_{y_6} + F_7 u_{y_7} + F_8 u_{y_8} + F_9 u_{y_9} \\ u_z &= F_1 u_{z_1} + F_2 u_{z_2} + F_3 u_{z_3} + F_4 u_{z_4} + F_5 u_{z_5} + F_6 u_{z_6} + F_7 u_{z_7} + F_8 u_{z_8} + F_9 u_{z_9} \end{aligned} \tag{3.14}$$

where $u_{x_1},...,u_{z_9}$ are the displacement variables of the problem, and they represent the translational displacement components in correspondence of the roots of the L9 polynomial. For further refinements, the cross-section can be discretized by using several L-elements as in Fig. 3.3, where two assembled L9 elements are shown in actual geometry. Further details about LE models can be found in the original work of Carrera and Petrolo [110] and in [111].

Chapter 4

Governing differential equations

In this chapter, by taking a recourse to the calculus of variations, the governing differential equations of refined beam models are derived. Attention is particularly focussed on static, free vibration and buckling analyses. Using CUF, the governing differential equations are written in a general, but unified and compact manner. Except for free vibration analysis of axially loaded beams, the same equations can be found in [108], where the same problems are addressed by making use of a slightly different notation.

4.1 Principle of virtual work

Consider a system of particles in equilibrium under applied forces and some prescribed geometrical constraints. The principle of virtual work states that *the sum of all the virtual work, δL, done by the internal and external forces existing in the system in any arbitrary infinitesimal virtual displacements satisfying the prescribed geometrical constraints is zero*:

$$\delta L = 0 \tag{4.1}$$

An alternative form of the principle of virtual work states that, if δL vanishes for any arbitrary infinitesimal virtual displacements satisfying the prescribed geometrical constrains, then the system of particles is in equilibrium. Thus, it is clear that the principle of virtual work is equivalent to the equations of equilibrium of the system. However, as demonstrated in the classical text of Washizu [29], the former has a much wider field of application in the formulation of mechanics problems than the latter. One of the main advantages of the variational calculus (analytical mechanics) as introduced by Euler, Lagrange and Hamilton as opposed to the “vectorial” mechanics of Newton is that in the former, the entire set of governing equations can be developed from one unified principle which considers the system as a whole and provides all these equations. This principle takes the form of minimizing a certain quantity: the potential energy, for example in static problems. It is significant to note that, since a minimum principle is independent of any special reference system, the equations of analytical mechanics hold for any set of coordinates. This allows one to adjust the coordinates employed to the specific nature of each problem [112].

Calculus of variations and analytical[1] mechanics are fascinating topics, but important though they are, details pertaining to the subject are out of the scope of the present work. For further readings, interested readers are referred to [112, 29]. In this thesis, the principle of virtual work is applied mainly to derive the equations of motion of arbitrary higher-order beam models. In general, by considering inertial effects, external loads, and the contribution of an axial pre-stress in the beam structure, Eq. (4.1) can be written as

$$\delta L = \delta L_{\mathrm{int}} + \delta L_{\mathrm{ine}} - \delta L_{\mathrm{ext}} - \delta L_{\sigma^0_{\mathrm{yy}}} = 0 \tag{4.2}$$

where L_{int} stands for the strain energy; L_{ine} is the contribution of the inertial loads; L_{ext} is the work done by the external loadings; $L_{\sigma^0_{\mathrm{yy}}}$ is the work done by the axial pre-stress σ^0_{yy} on the corresponding non-linear strain $\varepsilon^{\mathrm{nl}}_{yy}$; and δ stands for the usual virtual variation operator. In the following sections each of the contributions in the make up of Eq. (4.2) above are considered separately and written in terms of CUF.

4.1.1 Virtual variation of the strain energy

As detailed in [108], the virtual variation of the strain energy is

$$\delta L_{\mathrm{int}} = \int_V \delta \boldsymbol{\varepsilon}^T \boldsymbol{\sigma} \, \mathrm{d}V \tag{4.3}$$

Equation (4.3) is rewritten using Eqs. (3.3), (3.5) and (3.7). After integrations by parts (see [101]), it becomes

$$\delta L_{\mathrm{int}} = \int_L \delta \mathbf{u}_\tau^T \mathbf{K}^{\tau s} \mathbf{u}_s \, \mathrm{d}y + \left[\delta \mathbf{u}_\tau^T \boldsymbol{\Pi}^{\tau s} \mathbf{u}_s \right]_{y=0}^{y=L} \tag{4.4}$$

where $\mathbf{K}^{\tau s}$ is the differential linear stiffness matrix and $\boldsymbol{\Pi}^{\tau s}$ is the matrix of the natural boundary conditions in the form of 3×3 fundamental nuclei. The components of $\mathbf{K}^{\tau s}$ are given below in the case of monoclinic material and they are referred to as $K^{\tau s}_{(rc)}$, where r is the row number ($r = 1,2,3$) and c denotes the column number ($c = 1,2,3$):

---

[1] According to Lanczos [112], the word "analytical" is used here with reference to the mathematical term *analysis*, referring to the application of the principles of infinitesimal calculus to mechanical problems.

$$\begin{aligned}
K^{\tau s}_{(11)} &= E^{22}_{\tau_{,x}s_{,x}} + E^{44}_{\tau_{,z}s_{,z}} + \left(E^{26}_{\tau_{,x}s} - E^{26}_{\tau s_{,x}}\right)\frac{\partial}{\partial y} - E^{66}_{\tau s}\frac{\partial^2}{\partial y^2}\\
K^{\tau s}_{(12)} &= E^{26}_{\tau_{,x}s_{,x}} + E^{45}_{\tau_{,z}s_{,z}} + \left(E^{23}_{\tau_{,x}s} - E^{66}_{\tau s_{,x}}\right)\frac{\partial}{\partial y} - E^{36}_{\tau s}\frac{\partial^2}{\partial y^2}\\
K^{\tau s}_{(13)} &= E^{12}_{\tau_{,x}s_{,z}} + E^{44}_{\tau_{,z}s_{,x}} + \left(E^{45}_{\tau_{,z}s} - E^{16}_{\tau s_{,z}}\right)\frac{\partial}{\partial y}\\
K^{\tau s}_{(21)} &= E^{26}_{\tau_{,x}s_{,x}} + E^{45}_{\tau_{,z}s_{,z}} + \left(E^{66}_{\tau_{,x}s} - E^{23}_{\tau s_{,x}}\right)\frac{\partial}{\partial y} - E^{36}_{\tau s}\frac{\partial^2}{\partial y^2}\\
K^{\tau s}_{(22)} &= E^{66}_{\tau_{,x}s_{,x}} + E^{55}_{\tau_{,z}s_{,z}} + \left(E^{36}_{\tau_{,x}s} - E^{36}_{\tau s_{,x}}\right)\frac{\partial}{\partial y} - E^{33}_{\tau s}\frac{\partial^2}{\partial y^2} \qquad (4.5)\\
K^{\tau s}_{(23)} &= E^{16}_{\tau_{,x}s_{,z}} + E^{45}_{\tau_{,z}s_{,x}} + \left(E^{55}_{\tau_{,z}s} - E^{13}_{\tau s_{,z}}\right)\frac{\partial}{\partial y}\\
K^{\tau s}_{(31)} &= E^{44}_{\tau_{,x}s_{,z}} + E^{12}_{\tau_{,z}s_{,x}} + \left(E^{16}_{\tau_{,z}s} - E^{45}_{\tau s_{,z}}\right)\frac{\partial}{\partial y}\\
K^{\tau s}_{(32)} &= E^{45}_{\tau_{,x}s_{,z}} + E^{16}_{\tau_{,z}s_{,x}} + \left(E^{13}_{\tau_{,z}s} - E^{55}_{\tau s_{,z}}\right)\frac{\partial}{\partial y}\\
K^{\tau s}_{(33)} &= E^{44}_{\tau_{,x}s_{,x}} + E^{11}_{\tau_{,z}s_{,z}} + \left(E^{45}_{\tau_{,x}s} - E^{45}_{\tau s_{,x}}\right)\frac{\partial}{\partial y} - E^{55}_{\tau s}\frac{\partial^2}{\partial y^2}
\end{aligned}$$

The generic term $E^{\alpha\beta}_{\tau_{,\theta}s_{,\zeta}}$ above is a cross-sectional moment parameter given by

$$E^{\alpha\beta}_{\tau_{,\theta}s_{,\zeta}} = \int_{\Omega} \tilde{C}_{\alpha\beta} F_{\tau_{,\theta}} F_{s_{,\zeta}} \,\mathrm{d}\Omega \qquad (4.6)$$

where the cross-sectional functions F_τ have been defined in Chapter 3. The suffix after the comma in Eq. (4.5) denotes the partial derivatives. As far as the boundary conditions are concerned, the components of $\mathbf{\Pi}^{\tau s}$ are

$$\begin{aligned}
&\Pi^{\tau s}_{(11)} = E^{26}_{\tau s,x} + E^{66}_{\tau s}\frac{\partial}{\partial y}, \quad \Pi^{\tau s}_{(12)} = E^{66}_{\tau s,x} + E^{36}_{\tau s}\frac{\partial}{\partial y}, \quad \Pi^{\tau s}_{(13)} = E^{16}_{\tau s,z}\\
&\Pi^{\tau s}_{(21)} = E^{23}_{\tau s,x} + E^{36}_{\tau s}\frac{\partial}{\partial y}, \quad \Pi^{\tau s}_{(22)} = E^{36}_{\tau s,x} + E^{33}_{\tau s}\frac{\partial}{\partial y}, \quad \Pi^{\tau s}_{(23)} = E^{13}_{\tau s,z}\\
&\Pi^{\tau s}_{(31)} = E^{45}_{\tau s,z}, \qquad \Pi^{\tau s}_{(32)} = E^{55}_{\tau s,z}, \qquad \Pi^{\tau s}_{(33)} = E^{45}_{\tau s,x} + E^{55}_{\tau s}\frac{\partial}{\partial y}
\end{aligned} \tag{4.7}$$

It will be shown later that the term $\mathbf{\Pi}^{\tau s}\mathbf{u}_s$ represents the generalized reaction forces at the end of the beam. It is worth to underline that the main property of the fundamental nuclei, $\mathbf{K}^{\tau s}$ and $\mathbf{\Pi}^{\tau s}$ in this section, is that their formal mathematical expression does not depend either on the order of the beam theory or on the geometry of the problem. This aspect will also be discussed more in detail later in the thesis.

4.1.2 Virtual variation of the work done by axial pre-stress

The virtual variation of the work due to the axial pre-stress is given by

$$\delta L_{\sigma^0_{yy}} = \int_L \left(\int_\Omega \sigma^0_{yy} \delta \varepsilon^{\mathrm{nl}}_{yy} \, \mathrm{d}\Omega \right) \mathrm{d}y \tag{4.8}$$

Here, the geometric non-linearities are introduced in the axial strain in the following Green-Lagrange manner:

$$\varepsilon^{\mathrm{nl}}_{yy} = \frac{1}{2}(u^2_{x,y} + u^2_{y,y} + u^2_{z,y}) \tag{4.9}$$

After substituting Eqs. (3.7) and (4.9) into Eq. (4.8) and performing integration by parts, one obtains

$$\delta L_{\sigma^0_{yy}} = -\sigma^0_{yy} \int_L \delta \mathbf{u}^T_\tau \mathbf{K}^{\tau s}_{\sigma^0_{yy}} \mathbf{u}_s \, \mathrm{d}y + \sigma^0_{yy} \left[\delta \mathbf{u}^T_\tau \mathbf{\Pi}^{\tau s}_{\sigma^0_{yy}} \mathbf{u}_s \right]^{y=L}_{y=0} \tag{4.10}$$

where $\mathbf{K}^{\tau s}_{\sigma^0_{yy}}$ as given below is the fundamental nucleus of the differential geometric stiffness matrix.

$$\mathbf{K}^{\tau s}_{\sigma^0_{yy}} = \begin{bmatrix} E_{\tau s}\frac{\partial^2}{\partial y^2} & 0 & 0 \\ 0 & E_{\tau s}\frac{\partial^2}{\partial y^2} & 0 \\ 0 & 0 & E_{\tau s}\frac{\partial^2}{\partial y^2} \end{bmatrix} \tag{4.11}$$

where

$$E_{\tau s} = \int_\Omega F_\tau F_s \, \mathrm{d}\Omega \tag{4.12}$$

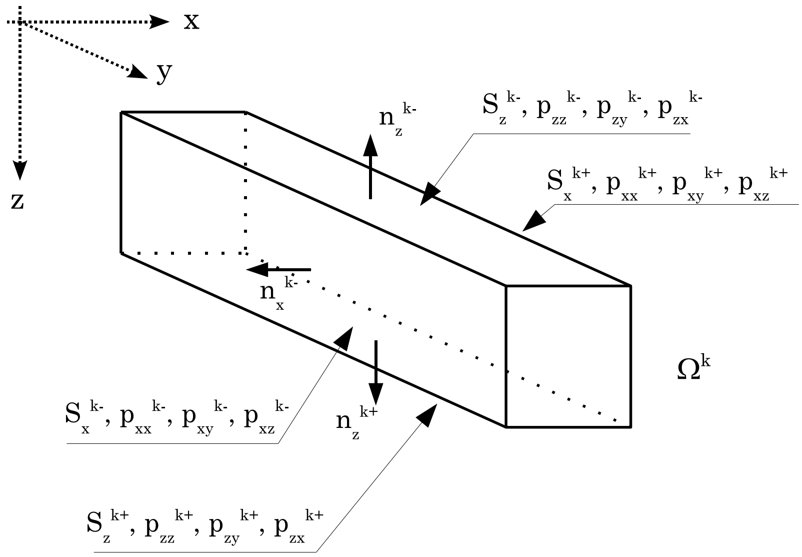
x
y
z
n_z^{k-}
$S_z^{k-}, p_{zz}^{k-}, p_{zy}^{k-}, p_{zx}^{k-}$
$S_x^{k+}, p_{xx}^{k+}, p_{xy}^{k+}, p_{xz}^{k+}$
n_x^{k-}
Ω^k
$S_x^{k-}, p_{xx}^{k-}, p_{xy}^{k-}, p_{xz}^{k-}$
n_z^{k+}
$S_z^{k+}, p_{zz}^{k+}, p_{zy}^{k+}, p_{zx}^{k+}$

Figure 4.1 Components of a surface loading; lateral surfaces and normal vectors of the beam.

The components of $\mathbf{\Pi}^{\tau s}_{\sigma^0_{yy}}$ are

$$\mathbf{\Pi}^{\tau s}_{\sigma^0_{yy}} = \begin{bmatrix} E_{\tau s}\frac{\partial}{\partial y} & 0 & 0 \\ 0 & E_{\tau s}\frac{\partial}{\partial y} & 0 \\ 0 & 0 & E_{\tau s}\frac{\partial}{\partial y} \end{bmatrix} \tag{4.13}$$

4.1.3 Virtual variation of external work

The virtual work done by the external loadings is assumed to be due to a surface loading and a line loading, see Carrera *et al.* [108]. The components of a surface loading acting above a k-th sub-domain of the cross-section are:

$$\mathbf{p}^k = \left\{ \begin{array}{cccccc} p^{k\pm}_{xx} & p^{k\pm}_{xy} & p^{k\pm}_{xz} & p^{k\pm}_{zx} & p^{k\pm}_{zy} & p^{k\pm}_{zz} \end{array} \right\}^T \tag{4.14}$$

The components of the surface load are shown in Fig. 4.1. The lateral surfaces $\left\{S^{k\pm}_{\phi} : \phi = x, z\right\}$ of the beam are defined on the basis of the normal unit vector $\left\{n^{k\pm}_{\phi} : \phi = x, z\right\}$. A normal unit vector with the same orientation as x or z axis identifies a positive lateral surface. The external virtual work due to the pressure loading $\mathbf{p}^k$ is given by

$$\delta L_{\mathrm{ext}} = \left(\delta L^k_{p^{\pm}_{xx}} + \delta L^k_{p^{\pm}_{xy}} + \delta L^k_{p^{\pm}_{xz}} + \delta L^k_{p^{\pm}_{zx}} + \delta L^k_{p^{\pm}_{zy}} + \delta L^k_{p^{\pm}_{zz}}\right)_k \tag{4.15}$$

The explicit forms of the terms in Eq. (4.15) are as follows:

$$
\begin{aligned}
\left(\delta L^k_{p^\pm_{xx}},\ \delta L^k_{p^\pm_{zx}}\right) &= \int_L \delta u_{x\tau} \left(p^{k\pm}_{xx} E^{kz^\pm}_\tau,\ p^{k\pm}_{zx} E^{kx^\pm}_\tau\right)\, dy \\
\left(\delta L^k_{p^\pm_{zz}},\ \delta L^k_{p^\pm_{xz}}\right) &= \int_L \delta u_{z\tau} \left(p^{k\pm}_{zz} E^{kx^\pm}_\tau,\ p^{k\pm}_{xz} E^{kz^\pm}_\tau\right)\, dy \\
\left(\delta L^k_{p^\pm_{zy}},\ \delta L^k_{p^\pm_{xy}}\right) &= \int_L \delta u_{y\tau} \left(p^{k\pm}_{zy} E^{kx^\pm}_\tau,\ p^{k\pm}_{xy} E^{kz^\pm}_\tau\right)\, dy
\end{aligned}
\tag{4.16}
$$

where:

$$
\begin{aligned}
\left(E^{kx^+}_\tau, E^{kx^-}_\tau\right) &= \int_{x^k_1}^{x^k_2} \left(F_\tau\left(z^k_2, x\right), F_\tau\left(z^k_1, x\right)\right)\, dx \\
\left(E^{kz^+}_\tau, E^{kz^-}_\tau\right) &= \int_{z^k_1}^{z^k_2} \left(F_\tau\left(z, x^k_2\right), F_\tau\left(z, x^k_1\right)\right)\, dz
\end{aligned}
\tag{4.17}
$$

$\left[x^k_1, x^k_2\right]$ and $\left[z^k_1, z^k_2\right]$ define the boundaries on the cross-section of the k-th sub-domain where the loading is applied. The components of a line loading $\mathbf{l}^k$ (see Fig. 4.2) are:

$$
\mathbf{l}^k = \left\{\begin{array}{cccccc} l^{k\pm}_{xx} & l^{k\pm}_{xy} & l^{k\pm}_{xz} & l^{k\pm}_{zx} & l^{k\pm}_{zy} & l^{k\pm}_{zz} \end{array}\right\}^T
\tag{4.18}
$$

The external virtual work due to a generic line load is therefore

$$
\delta L_{\text{ext}} = \left(\delta L^k_{l^\pm_{xx}} + \delta L^k_{l^\pm_{zz}} + \delta L^k_{l^\pm_{zy}} + \delta L^k_{l^\pm_{xy}} + \delta L^k_{l^\pm_{zx}} + \delta L^k_{l^\pm_{xz}}\right)_k
\tag{4.19}
$$

whose terms are:

$$
\begin{aligned}
\left(\delta L^k_{l^\pm_{zz}},\ \delta L^k_{l^\pm_{xz}}\right) &= \int_L \delta u_{z\tau} \left(l^{k\pm}_{zz} F_\tau\left(z^k_{l^\pm_{zz}}, x^k_{l^\pm_{zz}}\right),\ l^{k\pm}_{xz} F_\tau\left(z^k_{l^\pm_{xz}}, x^k_{l^\pm_{xz}}\right)\right)\, dy \\
\left(\delta L^k_{l^\pm_{xx}},\ \delta L^k_{l^\pm_{zx}}\right) &= \int_L \delta u_{x\tau} \left(l^{k\pm}_{xx} F_\tau\left(z^k_{l^\pm_{xx}}, x^k_{l^\pm_{xx}}\right),\ l^{k\pm}_{zx} F_\tau\left(z^k_{l^\pm_{zx}}, x^k_{l^\pm_{zx}}\right)\right)\, dy \\
\left(\delta L^k_{l^\pm_{zy}},\ \delta L^k_{l^\pm_{xy}}\right) &= \int_L \delta u_{y\tau} \left(l^{k\pm}_{zy} F_\tau\left(z^k_{l^\pm_{zy}}, x^k_{l^\pm_{zy}}\right),\ l^{k\pm}_{xy} F_\tau\left(z^k_{l^\pm_{xy}}, x^k_{l^\pm_{xy}}\right)\right)\, dy
\end{aligned}
\tag{4.20}
$$

In Eq. (4.20), $z^k_{l^{\pm}_{ij}}$ and $x^k_{l^{\pm}_{ij}}$ are the coordinates of the line loading application point above a k-th sub-domain of the cross-section.

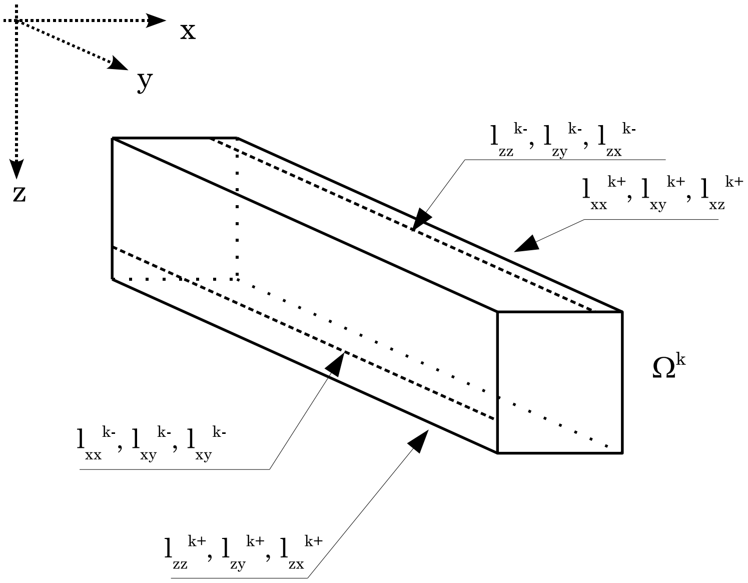
x
y
z
$l_{zz}^{k-}, l_{zy}^{k-}, l_{zx}^{k-}$
$l_{xx}^{k+}, l_{xy}^{k+}, l_{xz}^{k+}$
Ω^k
$l_{xx}^{k-}, l_{xy}^{k-}, l_{xy}^{k-}$
$l_{zz}^{k+}, l_{zy}^{k+}, l_{zx}^{k+}$

Figure 4.2 Components of a line loading.

4.1.4 Virtual variation of inertial work

The virtual variation of the inertial work is given by

$$\delta L_{\text{ine}} = \int_L \delta \mathbf{u}_\tau \int_\Omega \rho F_\tau F_s \, \mathrm{d}\Omega \, \ddot{\mathbf{u}}_s \, \mathrm{d}y = \int_L \delta \mathbf{u}_\tau \mathbf{M}^{\tau s} \ddot{\mathbf{u}}_s \, \mathrm{d}y \tag{4.21}$$

where $\mathbf{M}^{\tau s}$ is the fundamental nucleus of the mass matrix and double over dots stand as second derivative with respect to time (t). The components of matrix $\mathbf{M}^{\tau s}$ are

$$\mathbf{M}^{\tau s} = \begin{bmatrix} E^{\rho}_{\tau s} & 0 & 0 \\ 0 & E^{\rho}_{\tau s} & 0 \\ 0 & 0 & E^{\rho}_{\tau s} \end{bmatrix} \tag{4.22}$$

where ρ is the material density and

$$E^{\rho}_{\tau s} = \int_\Omega \rho F_\tau F_s \, \mathrm{d}\Omega \tag{4.23}$$

4.2 Strong-form equations of unified beam theory

The governing differential equations are obtained by substituting the explicit expressions of the virtual variations of the internal, external and inertial works as well as the work of the pre-stresses into the principle of virtual displacements. Different problems are considered and they are obtained as particular cases of Eq. (4.2).

4.2.1 Static analysis

In the case of static analysis, the principle of virtual work holds

$$\delta L_{\text{int}} = \delta L_{\text{ext}} \tag{4.24}$$

The governing equations can be therefore written in the following compact form by using Eqs. (4.4), (4.15), and (4.19):

$$\delta \mathbf{u}_\tau : \quad \mathbf{K}^{\tau s}\mathbf{u}_s = \mathbf{p}_k^\tau \tag{4.25}$$

where $\mathbf{u}_s(y) = \left\{u_{xs}\; u_{ys}\; u_{zs}\right\}^T$ is the vector of the unknown generalised displacements and $\mathbf{p}_k^\tau$ is the fundamental nucleus of the loading vector containing both surface pressures and line loading terms. The explicit expression for $\mathbf{p}_k^\tau$ is not given here, but it can be easily obtained from Section (4.1.3).

Letting $\mathbf{P}_\tau(y) = \left\{ \begin{array}{ccc} P_{x\tau} & P_{y\tau} & P_{z\tau} \end{array} \right\}^T$ be the vector of the generalized forces applied at the end of the beam (see Fig. 4.3) , the natural boundary conditions can be written as

$$\left[\mathbf{P}_s\right]_{y=0}^{y=L} = 0 \tag{4.26}$$

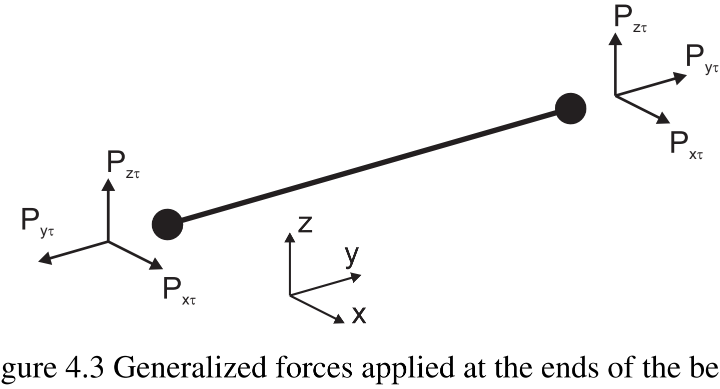

Figure 4.3 Generalized forces applied at the ends of the beam.

According to Eq. (4.4), Eq. (4.26) yields

$$\delta \mathbf{u}_\tau : \quad \left[\mathbf{\Pi}^{\tau s}\mathbf{u}_s\right]_{y=0}^{y=L} = 0 \tag{4.27}$$

The equations above can be written in explicit differential form by using Eqs. (4.5), (4.16), (4.20), and (4.7). The governing equations are:

$$\begin{aligned}
\delta u_{x\tau} : \quad & -E^{66}_{\tau s} u_{xs_{,yy}} + \left(E^{26}_{\tau_{,x}s} - E^{26}_{\tau s_{,x}}\right) u_{xs_{,y}} + \left(E^{22}_{\tau_{,x}s_{,x}} + E^{44}_{\tau_{,z}s_{,z}}\right) u_{xs} \\
& -E^{36}_{\tau s} u_{ys_{,yy}} + \left(E^{23}_{\tau_{,x}s} - E^{66}_{\tau s_{,x}}\right) u_{ys_{,y}} + \left(E^{26}_{\tau_{,x}s_{,x}} + E^{45}_{\tau_{,z}s_{,z}}\right) u_{ys} \\
& +\left(E^{45}_{\tau_{,z}s} - E^{16}_{\tau s_{,z}}\right) u_{zs_{,y}} + \left(E^{44}_{\tau_{,z}s_{,x}} + E^{12}_{\tau_{,x}s_{,z}}\right) u_{zs} = \Big[p^{k\pm}_{xx} E^{kz^{\pm}}_{\tau} \\
& +p^{k\pm}_{zx} E^{kx^{\pm}}_{\tau} + l^{k\pm}_{xx} F_\tau\left(z^k_{l^{\pm}_{xx}}, x^k_{l^{\pm}_{xx}}\right) + l^{k\pm}_{zx} F_\tau\left(z^k_{l^{\pm}_{zx}}, x^k_{l^{\pm}_{zx}}\right)\Big]_k \\
\delta u_{y\tau} : \quad & -E^{36}_{\tau s} u_{xs_{,yy}} + \left(E^{66}_{\tau_{,x}s} - E^{23}_{\tau s_{,x}}\right) u_{xs_{,y}} + \left(E^{26}_{\tau_{,x}s_{,x}} + E^{45}_{\tau_{,z}s_{,z}}\right) u_{xs} \\
& -E^{33}_{\tau s} u_{ys_{,yy}} + \left(E^{36}_{\tau_{,x}s} - E^{36}_{\tau s_{,x}}\right) u_{ys_{,y}} + \left(E^{66}_{\tau_{,x}s_{,x}} + E^{55}_{\tau_{,z}s_{,z}}\right) u_{ys} \\
& +\left(E^{55}_{\tau_{,z}s} - E^{13}_{\tau s_{,z}}\right) u_{zs,y} + \left(E^{16}_{\tau_{,x}s_{,z}} + E^{45}_{\tau_{,z}s_{,x}}\right) u_{zs} = \Big[p^{k\pm}_{zy} E^{kx^{\pm}}_{\tau} \\
& +p^{k\pm}_{xy} E^{kz^{\pm}}_{\tau} + l^{k\pm}_{zy} F_\tau\left(z^k_{l^{\pm}_{zy}}, x^k_{l^{\pm}_{zy}}\right) + l^{k\pm}_{xy} F_\tau\left(z^k_{l^{\pm}_{xy}}, x^k_{l^{\pm}_{xy}}\right)\Big]_k \\
\delta u_{z\tau} : \quad & \left(E^{16}_{\tau_{,z}s} - E^{45}_{\tau s_{,z}}\right) u_{xs_{,y}} + \left(E^{44}_{\tau_{,x}s_{,z}} + E^{12}_{\tau_{,z}s_{,x}}\right) u_{xs} \\
& +\left(E^{13}_{\tau_{,z}s} - E^{55}_{\tau s_{,z}}\right) u_{ys_{,y}} + \left(E^{45}_{\tau_{,x}s_{,z}} + E^{16}_{\tau_{,z}s_{,x}}\right) u_{ys} - E^{55}_{\tau s} u_{zs_{,yy}} \\
& +\left(E^{45}_{\tau_{,x}s} - E^{45}_{\tau s_{,x}}\right) u_{zs_{,y}} + \left(E^{44}_{\tau_{,x}s_{,x}} + E^{11}_{\tau_{,z}s_{,z}}\right) u_{zs} = \Big[p^{k\pm}_{zz} E^{kx^{\pm}}_{\tau} \\
& +p^{k\pm}_{xz} E^{kz^{\pm}}_{\tau} + l^{k\pm}_{zz} F_\tau\left(z^k_{l^{\pm}_{zz}}, x^k_{l^{\pm}_{zz}}\right) + l^{k\pm}_{xz} F_\tau\left(z^k_{l^{\pm}_{xz}}, x^k_{l^{\pm}_{xz}}\right)\Big]_k
\end{aligned} \tag{4.28}$$

Similarly, the natural boundary conditions are:

$$
\begin{aligned}
\delta u_{x\tau}: &\quad \left[E^{66}_{\tau s}u_{xs,y} + E^{26}_{\tau s,x}u_{xs} + E^{36}_{\tau s}u_{ys,y} + E^{66}_{\tau s,x}u_{ys} + E^{16}_{\tau s,z}u_{zs}\right]^{y=L}_{y=0} = 0 \\
\delta u_{y\tau}: &\quad \left[E^{36}_{\tau s}u_{xs,y} + E^{23}_{\tau s,x}u_{xs} + E^{33}_{\tau s}u_{ys,y} + E^{36}_{\tau s,x}u_{ys} + E^{13}_{\tau s,z}u_{zs}\right]^{y=L}_{y=0} = 0 \\
\delta u_{z\tau}: &\quad \left[E^{45}_{\tau s,z}u_{xs} + E^{55}_{\tau s,z}u_{ys} + E^{55}_{\tau s}u_{zs,y} + E^{45}_{\tau s,x}u_{zs}\right]^{y=L}_{y=0} = 0
\end{aligned}
\tag{4.29}
$$

Equations (4.28) and (4.29) represent the governing differential equations and boundary conditions of the generic beam model subjected to static surface pressure and line loads. (Any other loading condition can be treated similarly.) These equations are written in terms of fundamental nuclei. This means that although Eqs. (4.28) and (4.29) are two systems of three coupled Ordinary Differential Equations (ODEs) with constant coefficients in the three unknowns u_{xs}, u_{ys} and u_{zs}, they can be automatically expanded for any order beam model. In other words, for a fixed approximation order (i.e., given the functions F_τ and the number of terms of the expansion M), the nuclei have to be expanded using the indexes τ and s in order to obtain the governing equations and the boundary conditions that concern the desired model. For example, the governing equations of the generic beam model having 6 terms in the displacement field ($M = 6$) can be automatically derived from the equation above resulting in the following relationship:

$$
\begin{bmatrix}
\mathbf{K}^{11} & \mathbf{K}^{12} & \dots & \mathbf{K}^{16} \\
\mathbf{K}^{21} & \mathbf{K}^{22} & \dots & \mathbf{K}^{26} \\
\vdots & \vdots & \ddots & \vdots \\
\mathbf{K}^{61} & \mathbf{K}^{62} & \dots & \mathbf{K}^{66}
\end{bmatrix}
\begin{Bmatrix}
\mathbf{u}_1 \\ \mathbf{u}_2 \\ \vdots \\ \mathbf{u}_6
\end{Bmatrix}
=
\begin{Bmatrix}
\mathbf{p}^1_k \\ \mathbf{p}^2_k \\ \vdots \\ \mathbf{p}^6_k
\end{Bmatrix}
\tag{4.30}
$$

where $\mathbf{K}^{\tau s}$ has already been defined in Eqs. (4.5) and (4.25). Equation (4.30) is a system of 18 ODEs in the 18 unknowns u_{x1}, u_{y1},u_{z1}, ..., u_{x6}, u_{y6},u_{z6}. If F_τ polynomials as in Table 3.1 are used, Eq. (4.30) will represent the governing equations of the second-order ($N = 2$) TE beam model under the action of static loadings.

4.2.2 Free vibration analysis

In the case of modal analysis, the principle of virtual displacement holds

$$\delta L_{\text{int}} = -\delta L_{\text{ine}} \tag{4.31}$$

The governing differential equations of the undamped free vibration problem can therefore be written in the following compact form by using Eqs. (4.4) and (4.21):

$$\delta \mathbf{u}_\tau : \quad \mathbf{K}^{\tau s}\mathbf{u}_s = -\mathbf{M}^{\tau s}\ddot{\mathbf{u}}_s \tag{4.32}$$

The natural boundary conditions are the same as in Eqs. (4.27) and (4.29).

The explicit form of the governing equations is obtained by substituting Eqs. (4.5) and (4.22) into Eq. (4.32) to give

$$\begin{aligned}
\delta u_{x\tau} : \quad & -E^{66}_{\tau s} u_{xs_{,yy}} + \left(E^{26}_{\tau_{,x}s} - E^{26}_{\tau s_{,x}}\right) u_{xs_{,y}} + \left(E^{22}_{\tau_{,x}s_{,x}} + E^{44}_{\tau_{,z}s_{,z}}\right) u_{xs} \\
& -E^{36}_{\tau s} u_{ys_{,yy}} + \left(E^{23}_{\tau_{,x}s} - E^{66}_{\tau s_{,x}}\right) u_{ys_{,y}} + \left(E^{26}_{\tau_{,x}s_{,x}} + E^{45}_{\tau_{,z}s_{,z}}\right) u_{ys} \\
& +\left(E^{45}_{\tau_{,z}s} - E^{16}_{\tau s_{,z}}\right) u_{zs_{,y}} + \left(E^{44}_{\tau_{,z}s_{,x}} + E^{12}_{\tau_{,x}s_{,z}}\right) u_{zs} = -E^{\rho}_{\tau s}\ddot{u}_{xs} \\
\delta u_{y\tau} : \quad & -E^{36}_{\tau s} u_{xs_{,yy}} + \left(E^{66}_{\tau_{,x}s} - E^{23}_{\tau s_{,x}}\right) u_{xs_{,y}} + \left(E^{26}_{\tau_{,x}s_{,x}} + E^{45}_{\tau_{,z}s_{,z}}\right) u_{xs} \\
& -E^{33}_{\tau s} u_{ys_{,yy}} + \left(E^{36}_{\tau_{,x}s} - E^{36}_{\tau s_{,x}}\right) u_{ys_{,y}} + \left(E^{66}_{\tau_{,x}s_{,x}} + E^{55}_{\tau_{,z}s_{,z}}\right) u_{ys} \\
& +\left(E^{55}_{\tau_{,z}s} - E^{13}_{\tau s_{,z}}\right) u_{zs,y} + \left(E^{16}_{\tau_{,x}s_{,z}} + E^{45}_{\tau_{,z}s_{,x}}\right) u_{zs} = -E^{\rho}_{\tau s}\ddot{u}_{ys} \\
\delta u_{z\tau} : \quad & \left(E^{16}_{\tau_{,z}s} - E^{45}_{\tau s_{,z}}\right) u_{xs_{,y}} + \left(E^{44}_{\tau_{,x}s_{,z}} + E^{12}_{\tau_{,z}s_{,x}}\right) u_{xs} \\
& +\left(E^{13}_{\tau_{,z}s} - E^{55}_{\tau s_{,z}}\right) u_{ys_{,y}} + \left(E^{45}_{\tau_{,x}s_{,z}} + E^{16}_{\tau_{,z}s_{,x}}\right) u_{ys} - E^{55}_{\tau s} u_{zs_{,yy}} \\
& +\left(E^{45}_{\tau_{,x}s} - E^{45}_{\tau s_{,x}}\right) u_{zs_{,y}} + \left(E^{44}_{\tau_{,x}s_{,x}} + E^{11}_{\tau_{,z}s_{,z}}\right) u_{zs} = -E^{\rho}_{\tau s}\ddot{u}_{zs}
\end{aligned} \tag{4.33}$$

Analogous to the static analysis case, for a fixed theory order N, Eqs. (4.33) and (4.29) have to be expanded using the indices τ and s in order to obtain the equations of motion and the natural boundary conditions of the desired model.

4.2.3 Buckling analysis

Buckling analysis of beam-columns has been widely investigated in the past and also in recent years because the subject matter plays an important role in the design of structures. Several methodologies have therefore been developed and there are excellent texts on the subject, see for example Timoshenko [113]. In most of the classical works on beam-column buckling, it has been assumed that when the equilibrium of the column is disturbed, it becomes unstable due to bending in the plane of smaller second moment of area. However, there are cases of practical interest where the column may buckle due to twisting, a combination of both twisting and bending, or due to higher-order kinematic effects.

Here we derive the governing equations of the buckled beam-column in terms of CUF and arbitrary kinematics. These equations are derived by retaining the terms related to the internal strain energy and pre-stress, so that the principle of virtual work gives

$$\delta L_{\mathrm{int}} - \delta L_{\sigma^0_{\mathrm{yy}}} = 0 \tag{4.34}$$

The governing equations can be written in the following compact form by using Eqs. (4.4) and (4.10):

$$\delta \mathbf{u}_\tau : \quad \left(\mathbf{K}^{\tau s} + \sigma^0_{yy} \mathbf{K}^{\tau s}_{\sigma^0_{yy}} \right) \mathbf{u}_s = 0 \tag{4.35}$$

Note that because of the choice of the sign convention, σ^0_{yy} is a compressive axial pre-stress, considered positive in Eq. (4.35).

According to Eqs. (4.26) and (4.10), the natural boundary conditions can be written as:

$$\delta \mathbf{u}_\tau : \quad \left[\mathbf{\Pi}^{\tau s} - \sigma^0_{yy} \mathbf{\Pi}^{\tau s}_{\sigma^0_{yy}} \mathbf{u}_s \right]^{y=L}_{y=0} = 0 \tag{4.36}$$

Thus, the explicit form of the linearized governing equations for buckling problem is written in terms of fundamental nucleus as follows:

$$
\begin{aligned}
\delta u_{x\tau}: \quad & (\sigma^0_{yy}E_{\tau s} - E^{66}_{\tau s})u_{xs_{,yy}} + \left(E^{26}_{\tau_{,x}s} - E^{26}_{\tau s_{,x}}\right)u_{xs_{,y}} + \left(E^{22}_{\tau_{,x}s_{,x}} + E^{44}_{\tau_{,z}s_{,z}}\right)u_{xs} \\
& -E^{36}_{\tau s}u_{ys_{,yy}} + \left(E^{23}_{\tau_{,x}s} - E^{66}_{\tau s_{,x}}\right)u_{ys_{,y}} + \left(E^{26}_{\tau_{,x}s_{,x}} + E^{45}_{\tau_{,z}s_{,z}}\right)u_{ys} \\
& +\left(E^{45}_{\tau_{,z}s} - E^{16}_{\tau s_{,z}}\right)u_{zs_{,y}} + \left(E^{44}_{\tau_{,z}s_{,x}} + E^{12}_{\tau_{,x}s_{,z}}\right)u_{zs} = 0 \\
\delta u_{y\tau}: \quad & -E^{36}_{\tau s}u_{xs_{,yy}} + \left(E^{66}_{\tau_{,x}s} - E^{23}_{\tau s_{,x}}\right)u_{xs_{,y}} + \left(E^{26}_{\tau_{,x}s_{,x}} + E^{45}_{\tau_{,z}s_{,z}}\right)u_{xs} \\
& +(\sigma^0_{yy}E_{\tau s} - E^{33}_{\tau s})u_{ys_{,yy}} + \left(E^{36}_{\tau_{,x}s} - E^{36}_{\tau s_{,x}}\right)u_{ys_{,y}} + \left(E^{66}_{\tau_{,x}s_{,x}} + E^{55}_{\tau_{,z}s_{,z}}\right)u_{ys} \qquad (4.37) \\
& +\left(E^{55}_{\tau_{,z}s} - E^{13}_{\tau s_{,z}}\right)u_{zs,y} + \left(E^{16}_{\tau_{,x}s_{,z}} + E^{45}_{\tau_{,z}s_{,x}}\right)u_{zs} = 0 \\
\delta u_{z\tau}: \quad & \left(E^{16}_{\tau_{,z}s} - E^{45}_{\tau s_{,z}}\right)u_{xs_{,y}} + \left(E^{44}_{\tau_{,x}s_{,z}} + E^{12}_{\tau_{,z}s_{,x}}\right)u_{xs} \\
& +\left(E^{13}_{\tau_{,z}s} - E^{55}_{\tau s_{,z}}\right)u_{ys_{,y}} + \left(E^{45}_{\tau_{,x}s_{,z}} + E^{16}_{\tau_{,z}s_{,x}}\right)u_{ys} \\
& +(\sigma^0_{yy}E_{\tau s} - E^{55}_{\tau s})u_{zs_{,yy}} + \left(E^{45}_{\tau_{,x}s} - E^{45}_{\tau s_{,x}}\right)u_{zs_{,y}} + \left(E^{44}_{\tau_{,x}s_{,x}} + E^{11}_{\tau_{,z}s_{,z}}\right)u_{zs} = 0
\end{aligned}
$$

The related natural boundary conditions are

$$
\begin{aligned}
\delta u_{x\tau}: \quad & \left[(E^{66}_{\tau s} - \sigma^0_{yy}E_{\tau s})u_{xs_{,y}} + E^{26}_{\tau s_{,x}}u_{xs} + E^{36}_{\tau s}u_{ys_{,y}} + E^{66}_{\tau s_{,x}}u_{ys} + E^{16}_{\tau s_{,z}}u_{zs}\right]_{y=0}^{y=L} = 0 \\
\delta u_{y\tau}: \quad & \left[E^{36}_{\tau s}u_{xs_{,y}} + E^{23}_{\tau s_{,x}}u_{xs} + (E^{33}_{\tau s} - \sigma^0_{yy}E_{\tau s})u_{ys_{,y}} + E^{36}_{\tau s_{,x}}u_{ys} + E^{13}_{\tau s_{,z}}u_{zs}\right]_{y=0}^{y=L} = 0 \qquad (4.38) \\
\delta u_{z\tau}: \quad & \left[E^{45}_{\tau s_{,z}}u_{xs} + E^{55}_{\tau s_{,z}}u_{ys} + (E^{55}_{\tau s} - \sigma^0_{yy}E_{\tau s})u_{zs_{,y}} + E^{45}_{\tau s_{,x}}u_{zs}\right]_{y=0}^{y=L} = 0
\end{aligned}
$$

4.2.4 Free vibration of axially loaded beams

Another problem of interest in this thesis concerns the determination of natural frequencies of beam-columns. In this case, the inertial term and the work of the axial pre-stress are used in conjunction with the strain energy in the principle of virtual displacements:

$$\delta L_{\mathrm{int}} - \delta L_{\sigma^0_{\mathrm{yy}}} = -\delta L_{\mathrm{ine}} \tag{4.39}$$

The compact form of the governing equations can be easily obtained by using Eqs. (4.4), (4.21) and (4.10), to arrive at

$$\delta \mathbf{u}_\tau : \quad \left(\mathbf{K}^{\tau s} + \sigma^0_{yy}\mathbf{K}^{\tau s}_{\sigma^0_{yy}}\right)\mathbf{u}_s = -\mathbf{M}^{\tau s}\ddot{\mathbf{u}}_s \tag{4.40}$$

For this type of analysis, the natural boundary conditions are the same as in the case of buckling analysis (see Eqs. (4.36) and (4.38)).

The explicit form of the governing equations are given below for the sake of completeness, and they are obtained by substituting Eqs. (4.5), (4.11) and (4.22) into Eq. (4.40):

$$\begin{aligned}
\delta u_{x\tau} : \quad & (\sigma^0_{yy}E_{\tau s} - E^{66}_{\tau s})u_{xs_{,yy}} + \left(E^{26}_{\tau_{,x}s} - E^{26}_{\tau s_{,x}}\right)u_{xs_{,y}} + \left(E^{22}_{\tau_{,x}s_{,x}} + E^{44}_{\tau_{,z}s_{,z}}\right)u_{xs} \\
& -E^{36}_{\tau s}u_{ys_{,yy}} + \left(E^{23}_{\tau_{,x}s} - E^{66}_{\tau s_{,x}}\right)u_{ys_{,y}} + \left(E^{26}_{\tau_{,x}s_{,x}} + E^{45}_{\tau_{,z}s_{,z}}\right)u_{ys} \\
& +\left(E^{45}_{\tau_{,z}s} - E^{16}_{\tau s_{,z}}\right)u_{zs_{,y}} + \left(E^{44}_{\tau_{,z}s_{,x}} + E^{12}_{\tau_{,x}s_{,z}}\right)u_{zs} = -E^{\rho}_{\tau s}\ddot{u}_{xs} \\
\delta u_{y\tau} : \quad & -E^{36}_{\tau s}u_{xs_{,yy}} + \left(E^{66}_{\tau_{,x}s} - E^{23}_{\tau s_{,x}}\right)u_{xs_{,y}} + \left(E^{26}_{\tau_{,x}s_{,x}} + E^{45}_{\tau_{,z}s_{,z}}\right)u_{xs} \\
& +(\sigma^0_{yy}E_{\tau s} - E^{33}_{\tau s})u_{ys_{,yy}} + \left(E^{36}_{\tau_{,x}s} - E^{36}_{\tau s_{,x}}\right)u_{ys_{,y}} + \left(E^{66}_{\tau_{,x}s_{,x}} + E^{55}_{\tau_{,z}s_{,z}}\right)u_{ys} \\
& +\left(E^{55}_{\tau_{,z}s} - E^{13}_{\tau s_{,z}}\right)u_{zs,y} + \left(E^{16}_{\tau_{,x}s_{,z}} + E^{45}_{\tau_{,z}s_{,x}}\right)u_{zs} = -E^{\rho}_{\tau s}\ddot{u}_{ys} \\
\delta u_{z\tau} : \quad & \left(E^{16}_{\tau_{,z}s} - E^{45}_{\tau s_{,z}}\right)u_{xs_{,y}} + \left(E^{44}_{\tau_{,x}s_{,z}} + E^{12}_{\tau_{,z}s_{,x}}\right)u_{xs} + \left(E^{13}_{\tau_{,z}s} - E^{55}_{\tau s_{,z}}\right)u_{ys_{,y}} \\
& +\left(E^{45}_{\tau_{,x}s_{,z}} + E^{16}_{\tau_{,z}s_{,x}}\right)u_{ys} + (\sigma^0_{yy}E_{\tau s} - E^{55}_{\tau s})u_{zs_{,yy}} + \left(E^{45}_{\tau_{,x}s} - E^{45}_{\tau s_{,x}}\right)u_{zs_{,y}} \\
& +\left(E^{44}_{\tau_{,x}s_{,x}} + E^{11}_{\tau_{,z}s_{,z}}\right)u_{zs} = -E^{\rho}_{\tau s}\ddot{u}_{zs}
\end{aligned} \tag{4.41}$$

In the next chapters, analytical and numerical procedures for the solutions of the aforementioned differential equations are addressed. The methodologies to be used will be in CUF notation, in order to preserve generality. In this way, approximate and numerical solutions for strong form governing equations of arbitrary higher-order beam theories will be obtained.

Chapter 5

Closed-form analytical solution

It is well recognized that the governing differential equations of 3D elasticity problems can be solved only for a narrow range of problems. If 1D approximation is adopted, closed-form solutions are available for a wider (but still limited) class of structures. In this chapter, Navier-type solutions that allow transformation of the differential equations discussed in the previous chapter into algebraic equations are analytically developed. An approach to closed-form solutions is particularly adopted for the first time in this thesis to solve static and free vibration problems using LE-based CUF theories. For Navier-type solutions of TE models, interested readers are referred to [108].

5.1 Displacement field and loading

The solution of the differential governing equations presented in Chapter 4 is sought in the form:

$$\begin{aligned} u_{x\tau}(y) &= U_{x\tau}\sin(\alpha y) \\ u_{y\tau}(y) &= U_{y\tau}\cos(\alpha y) \\ u_{z\tau}(y) &= U_{z\tau}\sin(\alpha y) \end{aligned} \tag{5.1}$$

Also, assume the external loadings to vary along the beam axis y in the following manner:

$$\mathbf{p}^k = \begin{Bmatrix} p_{xx}^{k\pm}\sin(\alpha y) \\ p_{xy}^{k\pm}\cos(\alpha y) \\ p_{xz}^{k\pm}\sin(\alpha y) \\ p_{zx}^{k\pm}\sin(\alpha y) \\ p_{zy}^{k\pm}\cos(\alpha y) \\ p_{zz}^{k\pm}\sin(\alpha y) \end{Bmatrix}, \quad \mathbf{l}^k = \begin{Bmatrix} l_{xx}^{k\pm}\sin(\alpha y) \\ l_{xy}^{k\pm}\cos(\alpha y) \\ l_{xz}^{k\pm}\sin(\alpha y) \\ l_{zx}^{k\pm}\sin(\alpha y) \\ l_{zy}^{k\pm}\cos(\alpha y) \\ l_{zz}^{k\pm}\sin(\alpha y) \end{Bmatrix} \tag{5.2}$$

where $\mathbf{p}^k$ and $\mathbf{l}^k$ represent pressure and line loadings, respectively. The assumption on external loading does not represent a loss of generality, since a generic loading can be approximated via Fourier series expansion (see [114, 115]). The term α in Eqs. (5.1) and (5.2) is given by

$$\alpha = \frac{m\pi}{L} \tag{5.3}$$

where m represents the half-wave number along the beam axis. $U_{x\tau}$, $U_{y\tau}$, $U_{z\tau}$ are the maximum displacement amplitudes function of the motion and $p_{xx}^{k\pm}$, $p_{xy}^{k\pm}$, ..., $p_{zz}^{k\pm}$, $l_{xx}^{k\pm}$, $l_{xy}^{k\pm}$, ..., $l_{zz}^{k\pm}$ are the maximum amplitudes of the surface and line loadings.

Equation (5.1) represents the displacement field of a simply supported beam and it satisfies the boundary conditions in Eq. (4.29). Thus, according to Eq. (5.1), one has

$$\begin{aligned} &u_{x\tau}(0) = u_{x\tau}(L) = 0 \\ &u_{y\tau,_y}(0) = u_{y\tau,_y}(L) = 0 \\ &u_{z\tau}(0) = u_{z\tau}(L) = 0 \end{aligned} \tag{5.4}$$

5.2 Governing differential equations in explicit algebraic form

5.2.1 Static analysis

By using the hypotheses introduced in the previous section, the ODEs describing the mechanical behaviour of the generic beam theory can be transformed into coupled algebraic equations. Equations (5.1) and (5.2) are substituted into Eq. (4.28) to give

$$
\begin{aligned}
\delta U_{x\tau}: \quad & \alpha^2 E^{66}_{\tau s} U_{xs} \sin(\alpha y) + \alpha \left(E^{26}_{\tau_{,x} s} - E^{26}_{\tau s_{,x}} \right) U_{xs} \cos(\alpha y) + \left(E^{22}_{\tau_{,x} s_{,x}} + E^{44}_{\tau_{,z} s_{,z}} \right) U_{xs} \sin(\alpha y) \\
& + \alpha^2 E^{36}_{\tau s} U_{ys} \cos(\alpha y) - \alpha \left(E^{23}_{\tau_{,x} s} - E^{66}_{\tau s_{,x}} \right) U_{ys} \sin(\alpha y) + \left(E^{26}_{\tau_{,x} s_{,x}} + E^{45}_{\tau_{,z} s_{,z}} \right) U_{ys} \cos(\alpha y) \\
& + \alpha \left(E^{45}_{\tau_{,z} s} - E^{16}_{\tau s_{,z}} \right) U_{zs} \cos(\alpha y) + \left(E^{44}_{\tau_{,z} s_{,x}} + E^{12}_{\tau_{,x} s_{,z}} \right) U_{zs} \sin(\alpha y) = \Big[p^{k\pm}_{xx} E^{kz^{\pm}}_{\tau} \\
& + p^{k\pm}_{zx} E^{kx^{\pm}}_{\tau} + l^{k\pm}_{xx} F_{\tau} \left(z^{k}_{l^{\pm}_{xx}}, x^{k}_{l^{\pm}_{xx}} \right) + l^{k\pm}_{zx} F_{\tau} \left(z^{k}_{l^{\pm}_{zx}}, x^{k}_{l^{\pm}_{zx}} \right) \Big]_k \sin(\alpha y) \\
\delta U_{y\tau}: \quad & \alpha^2 E^{36}_{\tau s} U_{xs} \sin(\alpha y) + \alpha \left(E^{66}_{\tau_{,x} s} - E^{23}_{\tau s_{,x}} \right) U_{xs} \cos(\alpha y) + \left(E^{26}_{\tau_{,x} s_{,x}} + E^{45}_{\tau_{,z} s_{,z}} \right) U_{xs} \sin(\alpha y) \\
& + \alpha^2 E^{33}_{\tau s} U_{ys} \cos(\alpha y) - \alpha \left(E^{36}_{\tau_{,x} s} - E^{36}_{\tau s_{,x}} \right) U_{ys} \sin(\alpha y) + \left(E^{66}_{\tau_{,x} s_{,x}} + E^{55}_{\tau_{,z} s_{,z}} \right) U_{ys} \cos(\alpha y) \\
& + \alpha \left(E^{55}_{\tau_{,z} s} - E^{13}_{\tau s_{,z}} \right) U_{zs} \cos(\alpha y) + \left(E^{16}_{\tau_{,x} s_{,z}} + E^{45}_{\tau_{,z} s_{,x}} \right) U_{zs} \sin(\alpha y) = \Big[p^{k\pm}_{zy} E^{kx^{\pm}}_{\tau} \\
& + p^{k\pm}_{xy} E^{kz^{\pm}}_{\tau} + l^{k\pm}_{zy} F_{\tau} \left(z^{k}_{l^{\pm}_{zy}}, x^{k}_{l^{\pm}_{zy}} \right) + l^{k\pm}_{xy} F_{\tau} \left(z^{k}_{l^{\pm}_{xy}}, x^{k}_{l^{\pm}_{xy}} \right) \Big]_k \cos(\alpha y) \\
\delta U_{z\tau}: \quad & \alpha \left(E^{16}_{\tau_{,z} s} - E^{45}_{\tau s_{,z}} \right) U_{xs} \cos(\alpha y) + \left(E^{44}_{\tau_{,x} s_{,z}} + E^{12}_{\tau_{,z} s_{,x}} \right) U_{xs} \sin(\alpha y) \\
& - \alpha \left(E^{13}_{\tau_{,z} s} - E^{55}_{\tau s_{,z}} \right) U_{ys} \sin(\alpha y) + \left(E^{45}_{\tau_{,x} s_{,z}} + E^{16}_{\tau_{,z} s_{,x}} \right) U_{ys} \cos(\alpha y) + \alpha^2 E^{55}_{\tau s} U_{zs} \sin(\alpha y) \\
& + \alpha \left(E^{45}_{\tau_{,x} s} - E^{45}_{\tau s_{,x}} \right) U_{zs} \cos(\alpha y) + \left(E^{44}_{\tau_{,x} s_{,x}} + E^{11}_{\tau_{,z} s_{,z}} \right) U_{zs} \sin(\alpha y) = \Big[p^{k\pm}_{zz} E^{kx^{\pm}}_{\tau} \\
& + p^{k\pm}_{xz} E^{kz^{\pm}}_{\tau} + l^{k\pm}_{zz} F_{\tau} \left(z^{k}_{l^{\pm}_{zz}}, x^{k}_{l^{\pm}_{zz}} \right) + l^{k\pm}_{xz} F_{\tau} \left(z^{k}_{l^{\pm}_{xz}}, x^{k}_{l^{\pm}_{xz}} \right) \Big]_k \sin(\alpha y)
\end{aligned}
\tag{5.5}
$$

If *isotropic* or *symmetric and balanced cross-ply* laminated beams are considered, the axial motions will be decoupled from the transversal ones. For these cases, the material coefficients $\widetilde{C}_{16}$, $\widetilde{C}_{26}$, $\widetilde{C}_{36}$ and $\widetilde{C}_{45}$ are null, so that the governing equations can be decoupled and simplified in the following algebraic form:

$$\begin{aligned}
\delta U_{x\tau}: \quad & \left(\alpha^2 E^{66}_{\tau s} + E^{22}_{\tau_{,x} s_{,x}} + E^{44}_{\tau_{,z} s_{,z}}\right) U_{xs} - \alpha\left(E^{23}_{\tau_{,x} s} - E^{66}_{\tau s_{,x}}\right) U_{ys} \\
& + \left(E^{44}_{\tau_{,z} s_{,x}} + E^{12}_{\tau_{,x} s_{,z}}\right) U_{zs} = \Big[p^{k\pm}_{xx} E^{kz^{\pm}}_{\tau} + p^{k\pm}_{zx} E^{kx^{\pm}}_{\tau} \\
& + l^{k\pm}_{xx} F_\tau\left(z^k_{l^{\pm}_{xx}}, x^k_{l^{\pm}_{xx}}\right) + l^{k\pm}_{zx} F_\tau\left(z^k_{l^{\pm}_{zx}}, x^k_{l^{\pm}_{zx}}\right) \Big]_k \\
\delta U_{y\tau}: \quad & \alpha\left(E^{66}_{\tau_{,x} s} - E^{23}_{\tau s_{,x}}\right) U_{xs} + \left(\alpha^2 E^{33}_{\tau s} + E^{66}_{\tau_{,x} s_{,x}} + E^{55}_{\tau_{,z} s_{,z}}\right) U_{ys} \\
& + \alpha\left(E^{55}_{\tau_{,z} s} - E^{13}_{\tau s_{,z}}\right) U_{zs} = \Big[p^{k\pm}_{zy} E^{kx^{\pm}}_{\tau} + p^{k\pm}_{xy} E^{kz^{\pm}}_{\tau} \\
& + l^{k\pm}_{zy} F_\tau\left(z^k_{l^{\pm}_{zy}}, x^k_{l^{\pm}_{zy}}\right) + l^{k\pm}_{xy} F_\tau\left(z^k_{l^{\pm}_{xy}}, x^k_{l^{\pm}_{xy}}\right) \Big]_k \\
\delta U_{z\tau}: \quad & \left(E^{44}_{\tau_{,x} s_{,z}} + E^{12}_{\tau_{,z} s_{,x}}\right) U_{xs} - \alpha\left(E^{13}_{\tau_{,z} s} - E^{55}_{\tau s_{,z}}\right) U_{ys} + \left(\alpha^2 E^{55}_{\tau s}\right. \\
& \left. + E^{44}_{\tau_{,x} s_{,x}} + E^{11}_{\tau_{,z} s_{,z}}\right) U_{zs} = \Big[p^{k\pm}_{zz} E^{kx^{\pm}}_{\tau} + p^{k\pm}_{xz} E^{kz^{\pm}}_{\tau} \\
& + l^{k\pm}_{zz} F_\tau\left(z^k_{l^{\pm}_{zz}}, x^k_{l^{\pm}_{zz}}\right) + l^{k\pm}_{xz} F_\tau\left(z^k_{l^{\pm}_{xz}}, x^k_{l^{\pm}_{xz}}\right) \Big]_k
\end{aligned} \tag{5.6}$$

Equation (5.6) is the algebraic system of equations of the generic simply supported beam subjected to pressure and line loads. The above equations are written in terms of a fundamental nucleus, which can be automatically expanded according to the summation indexes τ, s and the cross-sectional functions F_τ.

5.2.2 Free vibration analysis

In the case of free vibration problems, the amplitudes of the time-dependant displacements are supposed to vary harmonically.

$$\begin{aligned}
u_{x\tau}(y;t) &= U_{x\tau}\, e^{\mathrm{i}\omega t} \sin(\alpha y) \\
u_{y\tau}(y;t) &= U_{y\tau}\, e^{\mathrm{i}\omega t} \cos(\alpha y) \\
u_{z\tau}(y;t) &= U_{z\tau}\, e^{\mathrm{i}\omega t} \sin(\alpha y)
\end{aligned} \tag{5.7}$$

where ω is an arbitrary circular or angular frequency, and i is the usual imaginary unit $\sqrt{-1}$. By substituting Eq. (5.7) into the equations of motion Eq. (4.33) and considering symmetric and balanced cross-ply laminated (or isotropic) beams, one has

$$
\begin{aligned}
\delta U_{x\tau}: \quad & \big(\alpha^2 E^{66}_{\tau s} + E^{22}_{\tau_{,x}s_{,x}} + E^{44}_{\tau_{,z}s_{,z}} - \omega^2 E^{\rho}_{\tau s}\big) U_{xs} \\
& -\alpha\big(E^{23}_{\tau_{,x}s} - E^{66}_{\tau s_{,x}}\big) U_{ys} + \big(E^{44}_{\tau_{,z}s_{,x}} + E^{12}_{\tau_{,x}s_{,z}}\big) U_{zs} = 0 \\
\delta U_{y\tau}: \quad & \alpha\big(E^{66}_{\tau_{,x}s} - E^{23}_{\tau s_{,x}}\big) U_{xs} + \big(\alpha^2 E^{33}_{\tau s} + E^{66}_{\tau_{,x}s_{,x}} + E^{55}_{\tau_{,z}s_{,z}} \\
& - \omega^2 E^{\rho}_{\tau s}\big) U_{ys} + \alpha\big(E^{55}_{\tau_{,z}s} - E^{13}_{\tau s_{,z}}\big) U_{zs} = 0 \\
\delta U_{z\tau}: \quad & \big(E^{44}_{\tau_{,x}s_{,z}} + E^{12}_{\tau_{,z}s_{,x}}\big) U_{xs} - \alpha\big(E^{13}_{\tau_{,z}s} - E^{55}_{\tau s_{,z}}\big) U_{ys} + \big(\alpha^2 E^{55}_{\tau s} \\
& + E^{44}_{\tau_{,x}s_{,x}} + E^{11}_{\tau_{,z}s_{,z}} - \omega^2 E^{\rho}_{\tau s}\big) U_{zs} = 0
\end{aligned}
\tag{5.8}
$$

Equation (5.8) represents a classical linear eigenvalue problem. Given the order of the beam theory and its class, Eq. (5.8) can be automatically expanded as was the case in Eq. (4.30) to finally arrive at a linear eigenvalue problem that can be solved by classical methods.

Any other problems discussed in Chapter 4, such as buckling and vibration of beam-columns, can also be solved analogously by following the same procedure outlined above.

5.3 Limitations of the method

One of the main limitation of the theory presented in this chapter is that it can be applied only to simply supported beams. Moreover, the transcendental governing equations (see Eq. (5.5)) can be simplified into an algebraic system of equations (Eqs. (5.6) and (5.8)) only if the axial motions are decoupled from the transversal ones. This is only possible if the material coupling is absent, i.e. if the structure is homogeneous or the laminae of the composite beam are isotropic or the resulting laminate is symmetric and balanced cross-ply. Another limitation is that only prismatic beams whose material characteristics are homogeneous along the axis can be addressed by using a Navier-type solution. In the following chapters, numerical methods that will overcome all of the above limitations are addressed to deal with general cases with no restriction on boundary conditions and/or cross-sections.

Chapter 6

Radial Basis Functions

Analytical solutions of higher-order CUF beam theories are available only for a limited class of problems. In this chapter, approximate solutions of the strong form governing equations by using Radial Basis Functions (RBFs) are developed. With this method, boundary conditions and stacking sequences for composites can be chosen with no limitations by accepting numerical uncertainties. Here attention is focused on free vibration problems although RBFs have several other applications and the method can be applied to other problems in an analogous manner.

6.1 Collocation of the unknowns

The governing differential equations for free vibration analysis (Eqs. (4.32) and (4.27)) are recalled here for the sake of clarity and completeness.

$$\delta \mathbf{u}_\tau : \quad \mathbf{K}^{\tau s} \mathbf{u}_s = -\mathbf{M}^{\tau s} \ddot{\mathbf{u}}_s \tag{6.1}$$

$$\delta \mathbf{u}_\tau : \quad \left[\mathbf{\Pi}^{\tau s} \mathbf{u}_s \right]_{y=0}^{y=L} = 0 \tag{6.2}$$

In the case of harmonic motion, the solution of Eqs. (6.1) is sought in the form

$$\mathbf{u}_\tau(y;t) = \mathbf{U}_\tau(y)\, \mathrm{e}^{\mathrm{i}\omega t} \tag{6.3}$$

Note that $\mathbf{U}_\tau(y)$ in Eq. (6.3) should not be confused with $\mathbf{U}_\tau$ in Eqs. (5.1) and (5.7). The former is a function of the beam axis y whereas the latter is a vector of scalar parameters. By substituting Eq. (6.3) into Eqs. (6.1) and (6.2), one obtains

$$\delta \mathbf{U}_\tau : \quad (\mathbf{K}^{\tau s} - \omega^2 \mathbf{M}^{\tau s}) \mathbf{U}_s = 0 \tag{6.4}$$

$$\delta \mathbf{U}_\tau : \quad \left[\mathbf{\Pi}^{\tau s} \mathbf{U}_s \right]_{y=0}^{y=L} = 0 \tag{6.5}$$

Equation (6.4) represents a system of second-order differential equations with constant coefficients and Eq. (6.5) gives the associated boundary conditions.

RBFs approximations are essentially collocation schemes that can exploit accurate representations of the boundary. They are easy to implement and can be spectrally accurate. In solid mechanics, they are generally used to approximate the unknown derivatives and this is the basic step of the methodology described hereafter. Within the framework of the RBFs method, the amplitude of the harmonically varying generalized displacement vector, $\mathbf{U}_s(y)$, is approximated with a linear combination of the radial basis functions ϕ_i.

$$\mathbf{U}_s(y) = \mathbf{q}_{s\,i} \phi_i \left(\|y - y_i\|_2 \right) \tag{6.6}$$

where $\mathbf{q}_{s\,i}$ is the vector of the unknown parameters at the coordinate y_i of the finite set of n distinct points (centres) and $\|y - y_i\|_2$ is the Euclidian distance r_i, which in the case of 1D problems corresponds to $|y - y_i|$. In Eq. (6.6), index i indicates summation over $i = 1, ..., \mathsf{n}$. Derivatives of $\mathbf{U}_s(y)$ over y can be treated similarly.

$$\begin{aligned} \mathbf{U}_{s,_y}(y) &= \mathbf{q}_{s\,i} \phi_{i,_y} \left(|y - y_i| \right) \\ \mathbf{U}_{s,_{yy}}(y) &= \mathbf{q}_{s\,i} \phi_{i,_{yy}} \left(|y - y_i| \right) \end{aligned} \tag{6.7}$$

In this work, uniform and Chebyshev grid distributions of points y_i are respectively used. The latter distribution, in particular, is known to be the best choice in terms of stability (see for example [116–118]). A Chebyshev grid is defined by

$$y_i = \frac{L}{2} \left[1 - cos \left(\frac{i-1}{\mathsf{n}-1} \pi \right) \right], \qquad i = 1, ..., \mathsf{n} \tag{6.8}$$

Several RBFs have been formulated over the years and they are given coverage in a large volume of literature. In the present work, locally supported Wendland's C^6 functions [119] are chosen as ϕ_i, so that

$$\phi_i(r_i, c) = max\big((1 - c\, r_i)^8, 0\big) + \big(32\, c^3 r_i^3 + 25\, c^2 r_i^2 + 8\, c\, r_i + 1\big) \tag{6.9}$$

where c is a positive shape parameter.

The shape parameter c is known to play a very important role in collocation with RBFs for approximating functions and solving partial differential equations, see for example [120, 121]. The accuracy of the solution can vary significantly depending on the choice of the shape parameter. In the literature, several solutions for the evaluation of an optimal value of c have been proposed depending upon the number of nodes, the distance between the nodes and the type of the RBFs. For instance, in [122] a shape parameter inversely proportional to the square root of the number of grid points was proposed in the case of multiquadrics RBFs. However, finding a good value of the parameter c is not always an easy task. As specified in [123], smaller values of c generally lead to higher accuracy. On the other hand, unstable numerical solutions may occur as the value of c is decreased (see [124]).

In this thesis, a constant value of c is used for the sake of simplicity and no optimization procedures are employed. An optimization technique, such as the one recently introduced by Fantuzzi *et al.* [125], will be the subject of future work.

6.2 Formulation of the eigenvalue problem with radial basis functions

Let the domain of the problem be denoted by Γ and let $\partial\Gamma$ be its boundary. Then, consider n_I nodes in Γ and n_B nodes on $\partial\Gamma$, with $\mathsf{n} = \mathsf{n}_I + \mathsf{n}_B$. In the particular case of 1D beam theories as in this work, $\mathsf{n}_B = 2$ (i.e. the two ends of the beam). By substituting Eqs. (6.6) and (6.7) into Eq. (6.4), the differential equations of motion are reduced to a classical eigenvalue problem. For a node $y_j \in \Gamma$, it reads:

$$(\mathbf{K}^{\tau s i j} - \omega^2 \mathbf{M}^{\tau s i j})\mathbf{q}_{si} = 0 \tag{6.10}$$

where $\mathbf{K}^{\tau s i j}$ and $\mathbf{M}^{\tau s i j}$ are the 3×3 fundamental nuclei which contains the coefficients of the algebraic equations of motion. In the case of composite material, the components of matrix $\mathbf{K}^{\tau s i j}$ are

$$\begin{aligned}
K_{(11)}^{\tau sij} &= \left(E^{22}_{\tau_{,x}s_{,x}} + E^{44}_{\tau_{,z}s_{,z}}\right)\phi_{ij} + \left(E^{26}_{\tau_{,x}s} - E^{26}_{\tau s_{,x}}\right)\phi_{ij_{,y}} - E^{66}_{\tau s}\phi_{ij_{,yy}} \\
K_{(12)}^{\tau sij} &= \left(E^{26}_{\tau_{,x}s_{,x}} + E^{45}_{\tau_{,z}s_{,z}}\right)\phi_{ij} + \left(E^{23}_{\tau_{,x}s} - E^{66}_{\tau s_{,x}}\right)\phi_{ij_{,y}} - E^{36}_{\tau s}\phi_{ij_{,yy}} \\
K_{(13)}^{\tau sij} &= \left(E^{12}_{\tau_{,x}s_{,z}} + E^{44}_{\tau_{,z}s_{,x}}\right)\phi_{ij} + \left(E^{45}_{\tau_{,z}s} - E^{16}_{\tau s_{,z}}\right)\phi_{ij_{,y}} \\
K_{(21)}^{\tau sij} &= \left(E^{26}_{\tau_{,x}s_{,x}} + E^{45}_{\tau_{,z}s_{,z}}\right)\phi_{ij} + \left(E^{66}_{\tau_{,x}s} - E^{23}_{\tau s_{,x}}\right)\phi_{ij_{,y}} - E^{36}_{\tau s}\phi_{ij_{,yy}} \\
K_{(22)}^{\tau sij} &= \left(E^{66}_{\tau_{,x}s_{,x}} + E^{55}_{\tau_{,z}s_{,z}}\right)\phi_{ij} + \left(E^{36}_{\tau_{,x}s} - E^{36}_{\tau s_{,x}}\right)\phi_{ij_{,y}} - E^{33}_{\tau s}\phi_{ij_{,yy}} \\
K_{(23)}^{\tau sij} &= \left(E^{16}_{\tau_{,x}s_{,z}} + E^{45}_{\tau_{,z}s_{,x}}\right)\phi_{ij} + \left(E^{55}_{\tau_{,z}s} - E^{13}_{\tau s_{,z}}\right)\phi_{ij_{,y}} \\
K_{(31)}^{\tau sij} &= \left(E^{44}_{\tau_{,x}s_{,z}} + E^{12}_{\tau_{,z}s_{,x}}\right)\phi_{ij} + \left(E^{16}_{\tau_{,z}s} - E^{45}_{\tau s_{,z}}\right)\phi_{ij_{,y}} \\
K_{(32)}^{\tau sij} &= \left(E^{45}_{\tau_{,x}s_{,z}} + E^{16}_{\tau_{,z}s_{,x}}\right)\phi_{ij} + \left(E^{13}_{\tau_{,z}s} - E^{55}_{\tau s_{,z}}\right)\phi_{ij_{,y}} \\
K_{(33)}^{\tau sij} &= \left(E^{44}_{\tau_{,x}s_{,x}} + E^{11}_{\tau_{,z}s_{,z}}\right)\phi_{ij} + \left(E^{45}_{\tau_{,x}s} - E^{45}_{\tau s_{,x}}\right)\phi_{ij_{,y}} - E^{55}_{\tau s}\phi_{ij_{,yy}}
\end{aligned} \tag{6.11}$$

The components of matrix $\mathbf{M}^{\tau sij}$ are

$$\begin{aligned}
&M_{(11)}^{\tau sij} = M_{(22)}^{\tau sij} = M_{(33)}^{\tau sij} = E^{\rho}_{\tau s}\phi_{ij} \\
&M_{(12)}^{\tau sij} = M_{(13)}^{\tau sij} = M_{(21)}^{\tau sij} = M_{(23)}^{\tau sij} = M_{(31)}^{\tau sij} = M_{(32)}^{\tau sij} = 0
\end{aligned} \tag{6.12}$$

In Eqs. (6.11) and (6.12), ϕ_{ij} stands for $\phi_i(|y_j - y_i|)$. For a given beam theory - i.e., given the expansion functions F_τ and the number of terms in the theory kinematics M -, the eigenvalue problem describing the motion of the beam in free vibration is obtained by expanding $\mathbf{K}^{\tau sij}$ and $\mathbf{M}^{\tau sij}$ for $\tau = 1, 2, ..., M$, $s = 1, 2, ..., M$, $i = 1, ..., \mathsf{n}$, and $j = 1, ..., \mathsf{n}_I$. Finally the problem essentially becomes

$$(\mathbf{K}^I - \omega^2 \mathbf{M}^I)\mathbf{q} = 0 \tag{6.13}$$

where the superscript I denotes the fact that Eq. (6.13) applies in Γ. In a similar way, the natural boundary conditions can be written in algebraic form by substituting Eqs. (6.6) and (6.7) into Eq. (6.5). For a node $y_j \in \partial\Gamma$, it is represented by

$$\left[\mathbf{\Pi}^{\tau sij}\,\mathbf{q}_{si}\right]_{y=0}^{y=L} = 0 \tag{6.14}$$

where the components of the algebraic fundamental nucleus $\mathbf{\Pi}^{\tau sij}$ are as follows:

$$\begin{aligned}
&\Pi^{\tau sij}_{(11)} = E^{26}_{\tau s_{,x}}\phi_{ij} + E^{66}_{\tau s}\phi_{ij_{,y}}, \quad \Pi^{\tau sij}_{(12)} = E^{66}_{\tau s_{,x}}\phi_{ij} + E^{66}_{\tau s_{,x}}\phi_{ij_{,y}}, \quad \Pi^{\tau sij}_{(13)} = E^{16}_{\tau s_{,z}}\phi_{ij}\\
&\Pi^{\tau sij}_{(21)} = E^{23}_{\tau s_{,x}}\phi_{ij} + E^{36}_{\tau s}\phi_{ij_{,y}}, \quad \Pi^{\tau sij}_{(22)} = E^{36}_{\tau s_{,x}}\phi_{ij} + E^{33}_{\tau s}\phi_{ij_{,y}}, \quad \Pi^{\tau sij}_{(23)} = E^{13}_{\tau s_{,z}}\phi_{ij}\\
&\Pi^{\tau sij}_{(31)} = E^{45}_{\tau s_{,z}}\phi_{ij}, \qquad \Pi^{\tau sij}_{(32)} = E^{55}_{\tau s_{,z}}\phi_{ij}, \qquad \Pi^{\tau sij}_{(33)} = E^{45}_{\tau s_{,x}}\phi_{ij} + E^{55}_{\tau s}\phi_{ij_{,y}}
\end{aligned} \tag{6.15}$$

Similarly as above, the fundamental nucleus $\mathbf{\Pi}^{\tau sij}$ can be automatically expanded for $\tau = 1,2,...,M$, $s = 1,2,...,M$, $i = 1,...,\mathsf{n}$, and $j = \mathsf{n}_I + 1,...,\mathsf{n}$. In the case of homogeneous natural boundary condition one has

$$\mathbf{\Pi}^B\,\mathbf{q} = 0 \tag{6.16}$$

where superscript B denotes the fact that Eq. (6.16) applies to $\partial\Gamma$. The matrix $\mathbf{\Pi}^B$ is not derived in this thesis in the case of essential boundary conditions for the sake of brevity, but it is fairly straightforward. Now, essential boundary conditions can be applied by imposing a certain value to the amplitude of the harmonically varying generalized displacement $\mathbf{U}_s(y) = \overline{\mathbf{U}}_s(y)$.

Once matrices $\mathbf{K}^I$, $\mathbf{M}^I$, and $\mathbf{\Pi}^B$ are obtained, the final eigenvalue problem can be formulated and solved as

$$\left(\begin{bmatrix} \mathbf{K}^I \\ \mathbf{\Pi}^B \end{bmatrix} - \omega_k^2 \begin{bmatrix} \mathbf{M}^I \\ \mathbf{0} \end{bmatrix}\right)\mathbf{q}_k = 0 \tag{6.17}$$

where $\mathbf{q}_k$ is the k-th eigenvector. It is well known that some RBFs produce ill-conditioned matrices and this problem is further exacerbated as the number of grid points increases. Some authors reduce the conditioning number by using preconditioners, see [126]. Results discussed later show that by increasing the order of the beam theory (e.g., N in the case of TE models), the problem can become severely ill-conditioned. However, scaling the matrices $\mathbf{K}^I$ and $\mathbf{M}^I$ as well as the matrix of natural (not essential) boundary conditions $\mathbf{\Pi}^B$ by the maximum coefficient of the stiffness matrix itself, was sufficient to obtain a well-conditioned problem for each case considered in this thesis. In order to improve the accuracy of the solution further, the generalized displacements on the boundary centres could be condensed with respect to those related to the internal nodes, as explained in [127].

Chapter 7

Dynamic Stiffness Method

In the previous chapters, the solutions of the strong form equations of higher-order beam models have been sought both in exact as well as numerical forms. In the case of former, the differential equations have been transformed into algebraic problems specially by imposing simply supported boundary conditions. The numerical solutions which are approximated, on the other hand, are based on the use of RBFs with no limitations regarding boundary conditions and effects of material couplings. Nonetheless, RBFs method may present some numerical difficulty as it will be shown later in the computed results.

Owing to the rapid developments in computer technology in recent years, tremendous progress has been made in computational methods as applied in engineering. RBFs and, in general, collocation schemes are not necessarily the most effective tools to tackle the problems discussed in this thesis. Among the methods based on weak form solutions (which are, however, out of the scope of this work), the Finite Element Method (FEM) has been probably the most popular. Although FEM is versatile and applicable to arbitrary geometries, boundary conditions and material variations, it can be sometimes very expensive from a computational standpoint. There are other limitations of FEM as well. For example, the conventional FEM (and the majority of numerical methods, including RBFs) may not capture all necessary high frequency wave modes of interest, which can play an important role in the correct characterization of the entire vibration pattern of a structure. One of the reasons for this is that FEM uses assumed (frequency-independent) shape functions.

An alternative approach to improve the solution accuracy is to use frequency dependent shape functions, i.e. dynamic shape functions [128]. As the dynamic shape functions can capture all necessary high frequency wave modes, much accurate solutions can eventually be achieved. This elegant approach has led to the development of the Dynamic Stiffness Method (DSM), whose application to strong-form governing differential equations in conjunction with CUF is the main subject of this chapter and, in part, represents the important novelty of this entire work.

DSM makes use of dynamic shape functions that are derived from the exact wave solutions of the governing differential equations to formulate the Dynamic Stiffness (DS) matrix. To obtain the exact wave solutions in the frequency domain, the governing equations are transformed into the frequency domain by assuming harmonic solutions of a single frequency. Thus, the dynamic stiffness matrix is frequency dependent, consisting of a mixture of inertia and stiffness properties of the structure. As the dynamic stiffness matrix is constructed by using the exact solutions of the governing equations, it is clear that it deals with continuous mass and stiffness distributions in a structure exactly. As a consequence, DSM guarantees exact solutions of the governing equations in the frequency domain and this is the reason why it is referred as an *exact* method in the literature. In fact, only one single element is sufficient for a regular part of a structure to acquire exact solutions of the given governing equations with no limitations of geometry, boundary conditions or material couplings. It should be recognized that DSM results in a non-linear eigenvalue problem, which requires the adoption of an iterative algorithm for which the known best method is the application of the Wittrick-Williams algorithm [49]. The algorithm has certainly enhanced the applicability of DSM. It allows one to automatically calculate undamped natural frequencies (or critical loads in the case of buckling problems) within any desired accuracy.

In the following sections, the elegance of the DSM when applied to CUF beam theories is discussed. Attention is primarily focused on free vibration and buckling analyses.

7.1 L-matrix form of the governing differential equations

The procedure to obtain the Dynamic Stiffness (DS) matrix for a structural problem can be summarised as follows: (i) Seek a closed form analytical solution of the governing differential equations of the structural element; (ii) Apply a number of general boundary conditions equal to twice the number of integration constants in algebraic form, which are usually the nodal displacements and forces; (iii) Eliminate the integration constants by relating the amplitudes of the generalized nodal forces to the corresponding generalized displacements generating the DS matrix.

The above steps are briefly described below when developing the DS matrix for typical problems. First, the governing equations for free vibration of beams and beam-columns as well as for linearized buckling problems are transformed into a suitable form to obtain the exact wave solutions in the frequency domain before formulating the DS matrix. The

Wittrick-Williams algorithm [49] is finally introduced as the most effective solution technique to solve the transcendental eigenvalue problems.

7.1.1 Free vibration analysis

In the case of harmonic motion (Eq. (6.3)), the ordinary differential equations of the beam in free vibration (i.e., Eq. (6.4)) are written in the following compact form:

$$\delta \mathbf{U}_\tau : \quad \mathbf{L}^{\tau s} \tilde{\mathbf{U}}_s = 0 \tag{7.1}$$

where

$$\tilde{\mathbf{U}}_s = \left\{ \begin{array}{ccccccccc} U_{xs} & U_{xs,y} & U_{xs,yy} & U_{ys} & U_{ys,y} & U_{ys,yy} & U_{zs} & U_{zs,y} & U_{zs,yy} \end{array} \right\}^T \tag{7.2}$$

and $\mathbf{L}^{\tau s}$ is the 3×9 fundamental nucleus of the matrix containing the coefficients of the ordinary differential equations. The components of matrix $\mathbf{L}^{\tau s}$ are provided below in the case of monoclinic materials (e.g., fibre reinforced beam) and they are referred to as $L^{\tau s}_{(rc)}$, where r is the row number ($r = 1,2,3$) and c is the column number ($j = 1,2,...,9$). For the notation employed, the reader is referred to Chapter 4.

$$\begin{aligned}
&L^{\tau s}_{(11)} = -\omega^2 E^{\rho}_{\tau s} + E^{22}_{\tau_{,x} s_{,x}} + E^{44}_{\tau_{,z} s_{,z}}, && L^{\tau s}_{(12)} = E^{26}_{\tau_{,x} s} - E^{26}_{\tau s_{,x}}, && L^{\tau s}_{(13)} = -E^{66}_{\tau s} \\
&L^{\tau s}_{(14)} = E^{26}_{\tau_{,x} s_{,x}} + E^{45}_{\tau_{,z} s_{,z}}, && L^{\tau s}_{(15)} = E^{23}_{\tau s_{,x}} - E^{66}_{\tau s_{,x}}, && L^{\tau s}_{(16)} = -E^{36}_{\tau s} \\
&L^{\tau s}_{(17)} = E^{12}_{\tau_{,x} s_{,z}} + E^{44}_{\tau_{,z} s_{,x}}, && L^{\tau s}_{(18)} = E^{45}_{\tau_{,z} s} - E^{16}_{\tau s_{,z}}, && L^{\tau s}_{(19)} = 0 \\
&L^{\tau s}_{(21)} = E^{26}_{\tau_{,x} s_{,x}} + E^{45}_{\tau_{,z} s_{,z}}, && L^{\tau s}_{(22)} = E^{66}_{\tau_{,x} s} - E^{23}_{\tau s_{,x}}, && L^{\tau s}_{(23)} = -E^{36}_{\tau s} \\
&L^{\tau s}_{(24)} = -\omega^2 E^{\rho}_{\tau s} + E^{66}_{\tau_{,x} s_{,x}} + E^{55}_{\tau_{,z} s_{,z}}, && L^{\tau s}_{(25)} = E^{36}_{\tau_{,x} s} - E^{36}_{\tau s_{,x}}, && L^{\tau s}_{(26)} = -E^{33}_{\tau s} \\
&L^{\tau s}_{(27)} = E^{16}_{\tau_{,x} s_{,z}} + E^{45}_{\tau_{,z} s_{,x}}, && L^{\tau s}_{(28)} = E^{55}_{\tau_{,z} s} - E^{13}_{\tau s_{,z}}, && L^{\tau s}_{(29)} = 0 \\
&L^{\tau s}_{(31)} = E^{44}_{\tau_{,x} s_{,z}} + E^{12}_{\tau_{,z} s_{,x}}, && L^{\tau s}_{(32)} = E^{16}_{\tau_{,z} s_{,x}} - E^{45}_{\tau s_{,z}}, && L^{\tau s}_{(33)} = 0 \\
&L^{\tau s}_{(34)} = E^{45}_{\tau_{,x} s_{,z}} + E^{16}_{\tau_{,z} s_{,x}}, && L^{\tau s}_{(35)} = E^{13}_{\tau_{,z} s} - E^{55}_{\tau s_{,z}}, && L^{\tau s}_{(36)} = 0 \\
&L^{\tau s}_{(37)} = -\omega^2 E^{\rho}_{\tau s} + E^{44}_{\tau_{,x} s_{,x}} + E^{11}_{\tau_{,z} s_{,z}}, && L^{\tau s}_{(38)} = E^{45}_{\tau_{,x} s} - E^{45}_{\tau s_{,x}}, && L^{\tau s}_{(39)} = -E^{55}_{\tau s}
\end{aligned} \tag{7.3}$$

For a given expansion order beam theory, the equations of motion in the frequency domain can be obtained in the form of Eq. (7.4), as given below, by expanding out $\mathbf{L}^{\tau s}$ for indexes τ and s to give $\mathbf{L}$ and $\tilde{\mathbf{U}}$ to include all the terms in the expansion. Thus

$$\mathbf{L}\tilde{\mathbf{U}} = 0 \tag{7.4}$$

In the case of TE models, for example, the expansion of the fundamental nuclei $\mathbf{L}^{\tau s}$ is conducted for for $\tau = 1,2,...,(N+1)(N+2)/2$ and $s = 1,2,...,(N+1)(N+2)/2$. Figure 7.1 illustrates the expansion of $\mathbf{L}^{\tau s}$ in the case of linear and quadratic TE models.

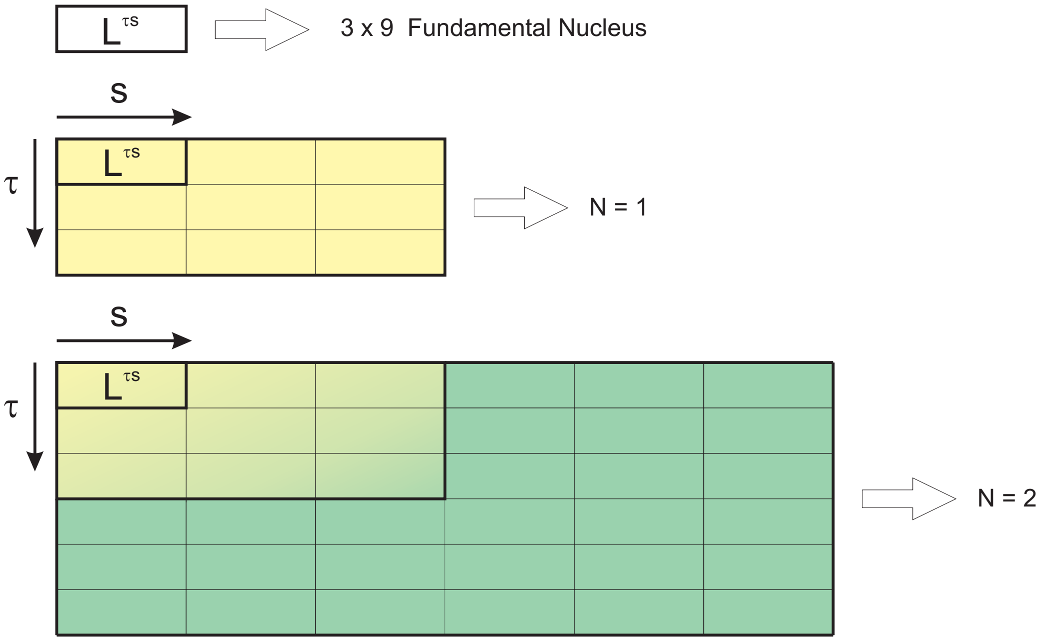

Figure 7.1 Expansion of the matrix $\mathbf{L}^{\tau s}$ for a given expansion order and TE.

Similarly, the boundary conditions in Eq. (6.5) can be written in a matrix form as

$$\delta\mathbf{U}_\tau: \quad \mathbf{P}_s = \mathbf{B}^{\tau s}\hat{\mathbf{U}}_s \tag{7.5}$$

where $\mathbf{P}_s$ is the amplitude of the harmonically varying load and

$$\hat{\mathbf{U}}_s = \left\{ \begin{array}{cccccc} U_{xs} & U_{xs,_y} & U_{ys} & U_{ys,_y} & U_{zs} & U_{zs,_y} \end{array} \right\}^T \tag{7.6}$$

$\mathbf{B}^{\tau s}$ is the 3×6 fundamental nucleus which contains the coefficients of the natural boundary conditions

$$\mathbf{B}^{\tau s} = \begin{bmatrix} E^{26}_{\tau s_{,x}} & E^{66}_{\tau s} & E^{66}_{\tau s_{,x}} & E^{36}_{\tau s} & E^{16}_{\tau s_{,z}} & 0 \\ E^{23}_{\tau s_{,x}} & E^{36}_{\tau s} & E^{36}_{\tau s_{,x}} & E^{33}_{\tau s} & E^{13}_{\tau s_{,z}} & 0 \\ E^{45}_{\tau s_{,z}} & 0 & E^{55}_{\tau s_{,z}} & 0 & E^{45}_{\tau s_{,x}} & E^{55}_{\tau s} \end{bmatrix} \tag{7.7}$$

Given the number of the terms in the beam kinematics, M, and the cross-sectional functions, F_τ, the natural boundary conditions can be obtained in the form of Eq. (7.8) by expanding $\mathbf{B}^{\tau s}$ in the same way as $\mathbf{L}^{\tau s}$ to finally give

$$\mathbf{P} = \mathbf{B}\hat{\mathbf{U}} \tag{7.8}$$

7.1.2 Free vibration analysis of axially loaded beams

In the case of beam-columns with the assumption of harmonic motion (Eq. (6.3)), the governing equations (Eqs. (4.39) to (4.41)) can be written in a compact form similar to those of Eq. (7.1). In this case, the components of matrix $L^{\tau s}$ are

$$\begin{aligned}
&L^{\tau s}_{(11)} = -\omega^2 E^{\rho}_{\tau s} + E^{22}_{\tau_{,x}s_{,x}} + E^{44}_{\tau_{,z}s_{,z}}, && L^{\tau s}_{(12)} = E^{26}_{\tau_{,x}s} - E^{26}_{\tau s_{,x}}, && L^{\tau s}_{(13)} = \sigma^0_{yy} E_{\tau s} - E^{66}_{\tau s} \\
&L^{\tau s}_{(14)} = E^{26}_{\tau_{,x}s_{,x}} + E^{45}_{\tau_{,z}s_{,z}}, && L^{\tau s}_{(15)} = E^{23}_{\tau s_{,x}} - E^{66}_{\tau s_{,x}}, && L^{\tau s}_{(16)} = -E^{36}_{\tau s} \\
&L^{\tau s}_{(17)} = E^{12}_{\tau_{,x}s_{,z}} + E^{44}_{\tau_{,z}s_{,x}}, && L^{\tau s}_{(18)} = E^{45}_{\tau_{,z}s} - E^{16}_{\tau s_{,z}}, && L^{\tau s}_{(19)} = 0 \\
&L^{\tau s}_{(21)} = E^{26}_{\tau_{,x}s_{,x}} + E^{45}_{\tau_{,z}s_{,z}}, && L^{\tau s}_{(22)} = E^{66}_{\tau_{,x}s} - E^{23}_{\tau s_{,x}}, && L^{\tau s}_{(23)} = -E^{36}_{\tau s} \\
&L^{\tau s}_{(24)} = -\omega^2 E^{\rho}_{\tau s} + E^{66}_{\tau_{,x}s_{,x}} + E^{55}_{\tau_{,z}s_{,z}}, && L^{\tau s}_{(25)} = E^{36}_{\tau_{,x}s} - E^{36}_{\tau s_{,x}}, && L^{\tau s}_{(26)} = \sigma^0_{yy} E_{\tau s} - E^{33}_{\tau s} \\
&L^{\tau s}_{(27)} = E^{16}_{\tau_{,x}s_{,z}} + E^{45}_{\tau_{,z}s_{,x}}, && L^{\tau s}_{(28)} = E^{55}_{\tau_{,z}s} - E^{13}_{\tau s_{,z}}, && L^{\tau s}_{(29)} = 0 \\
&L^{\tau s}_{(31)} = E^{44}_{\tau_{,x}s_{,z}} + E^{12}_{\tau_{,z}s_{,x}}, && L^{\tau s}_{(32)} = E^{16}_{\tau_{,z}s_{,x}} - E^{45}_{\tau s_{,z}}, && L^{\tau s}_{(33)} = 0 \\
&L^{\tau s}_{(34)} = E^{45}_{\tau_{,x}s_{,z}} + E^{16}_{\tau_{,z}s_{,x}}, && L^{\tau s}_{(35)} = E^{13}_{\tau_{,z}s} - E^{55}_{\tau s_{,z}}, && L^{\tau s}_{(36)} = 0 \\
&L^{\tau s}_{(37)} = -\omega^2 E^{\rho}_{\tau s} + E^{44}_{\tau_{,x}s_{,x}} + E^{11}_{\tau_{,z}s_{,z}}, && L^{\tau s}_{(38)} = E^{45}_{\tau_{,x}s} - E^{45}_{\tau s_{,x}}, && L^{\tau s}_{(39)} = \sigma^0_{yy} E_{\tau s} - E^{55}_{\tau s}
\end{aligned} \tag{7.9}$$

For a given expansion order, the equations of motion in the frequency domain can be obtained in the form of Eq. (7.4), as given below, by expanding $\mathbf{L}^{\tau s}$ for indexes τ and s to give

$$\mathbf{L}\tilde{\mathbf{U}} = 0 \tag{7.10}$$

In a similar manner, the boundary conditions of Eq. (4.38) can be written in a matrix form as

$$\delta\mathbf{U}_\tau : \quad \mathbf{P}_s = \mathbf{B}^{\tau s}\hat{\mathbf{U}}_s \tag{7.11}$$

where

$$\mathbf{B}^{\tau s} = \begin{bmatrix} E^{26}_{\tau s_{,x}} & (E^{66}_{\tau s} - \sigma^0_{yy}E_{\tau s}) & E^{66}_{\tau s_{,x}} & E^{36}_{\tau s} & E^{16}_{\tau s_{,z}} & 0 \\ E^{23}_{\tau s_{,x}} & E^{36}_{\tau s} & E^{36}_{\tau s_{,x}} & (E^{33}_{\tau s} - \sigma^0_{yy}E_{\tau s}) & E^{13}_{\tau s_{,z}} & 0 \\ E^{45}_{\tau s_{,z}} & 0 & E^{55}_{\tau s_{,z}} & 0 & E^{45}_{\tau s_{,x}} & (E^{55}_{\tau s} - \sigma^0_{yy}E_{\tau s}) \end{bmatrix} \tag{7.12}$$

For a given expansion order, the natural boundary conditions can be obtained in the form of Eq. (7.13) by expanding $\mathbf{B}^{\tau s}$ in order to have

$$\mathbf{P} = \mathbf{B}\hat{\mathbf{U}} \tag{7.13}$$

In the particular case of composite laminates, the matrices **L** and **B** are evaluated for each layer; global matrices are then obtained by summing the contribution of each lamina.

7.1.3 Buckling analysis

In the case of buckling analysis, the inertial terms do not appear in the governing equations. Thus, the assumption of harmonic motion is not necessary. In this case, the governing equations in Eq. (4.35) can be written in the following compact form:

$$\delta\mathbf{u}_\tau : \quad \mathbf{L}^{\tau s}\tilde{\mathbf{u}}_s = 0 \tag{7.14}$$

where

$$\tilde{\mathbf{u}}_s = \left\{ \begin{array}{ccccccccc} u_{xs} & u_{xs_{,y}} & u_{xs_{,yy}} & u_{ys} & u_{ys_{,y}} & u_{ys_{,yy}} & u_{zs} & u_{zs_{,y}} & u_{zs_{,yy}} \end{array} \right\}^T \tag{7.15}$$

The components of matrix $\mathbf{L}^{\tau s}$ are

$$
\begin{aligned}
&L^{\tau s}_{(11)} = E^{22}_{\tau_{,x} s_{,x}} + E^{44}_{\tau_{,z} s_{,z}}, \quad L^{\tau s}_{(12)} = E^{26}_{\tau_{,x} s} - E^{26}_{\tau s_{,x}}, \quad L^{\tau s}_{(13)} = \sigma^0_{yy} E_{\tau s} - E^{66}_{\tau s} \\
&L^{\tau s}_{(14)} = E^{26}_{\tau_{,x} s_{,x}} + E^{45}_{\tau_{,z} s_{,z}}, \quad L^{\tau s}_{(15)} = E^{23}_{\tau s_{,x}} - E^{66}_{\tau s_{,x}}, \quad L^{\tau s}_{(16)} = -E^{36}_{\tau s} \\
&L^{\tau s}_{(17)} = E^{12}_{\tau_{,x} s_{,z}} + E^{44}_{\tau_{,z} s_{,x}}, \quad L^{\tau s}_{(18)} = E^{45}_{\tau_{,z} s} - E^{16}_{\tau s_{,z}}, \quad L^{\tau s}_{(19)} = 0 \\
&L^{\tau s}_{(21)} = E^{26}_{\tau_{,x} s_{,x}} + E^{45}_{\tau_{,z} s_{,z}}, \quad L^{\tau s}_{(22)} = E^{66}_{\tau_{,x} s} - E^{23}_{\tau s_{,x}}, \quad L^{\tau s}_{(23)} = -E^{36}_{\tau s} \\
&L^{\tau s}_{(24)} = E^{66}_{\tau_{,x} s_{,x}} + E^{55}_{\tau_{,z} s_{,z}}, \quad L^{\tau s}_{(25)} = E^{36}_{\tau_{,x} s} - E^{36}_{\tau s_{,x}}, \quad L^{\tau s}_{(26)} = \sigma^0_{yy} E_{\tau s} - E^{33}_{\tau s} \\
&L^{\tau s}_{(27)} = E^{16}_{\tau_{,x} s_{,z}} + E^{45}_{\tau_{,z} s_{,x}}, \quad L^{\tau s}_{(28)} = E^{55}_{\tau_{,z} s} - E^{13}_{\tau s_{,z}}, \quad L^{\tau s}_{(29)} = 0 \\
&L^{\tau s}_{(31)} = E^{44}_{\tau_{,x} s_{,z}} + E^{12}_{\tau_{,z} s_{,x}}, \quad L^{\tau s}_{(32)} = E^{16}_{\tau_{,z} s_{,x}} - E^{45}_{\tau s_{,z}}, \quad L^{\tau s}_{(33)} = 0 \\
&L^{\tau s}_{(34)} = E^{45}_{\tau_{,x} s_{,z}} + E^{16}_{\tau_{,z} s_{,x}}, \quad L^{\tau s}_{(35)} = E^{13}_{\tau_{,z} s} - E^{55}_{\tau s_{,z}}, \quad L^{\tau s}_{(36)} = 0 \\
&L^{\tau s}_{(37)} = E^{44}_{\tau_{,x} s_{,x}} + E^{11}_{\tau_{,z} s_{,z}}, \quad L^{\tau s}_{(38)} = E^{45}_{\tau_{,x} s} - E^{45}_{\tau s_{,x}}, \quad L^{\tau s}_{(39)} = \sigma^0_{yy} E_{\tau s} - E^{55}_{\tau s}
\end{aligned}
\tag{7.16}
$$

Again, given the order of expansion and the class of the selected beam theory, $\mathbf{L}^{\tau s}$ is expanded to give the final system of matrix equation as

$$\mathbf{L}\,\tilde{\mathbf{u}} = 0 \tag{7.17}$$

In a similar manner, the natural boundary conditions in Eq. (4.36) can be handled to give

$$\delta \mathbf{u}_\tau : \quad \mathbf{P}_s = \mathbf{B}^{\tau s}\, \hat{\mathbf{u}}_s \tag{7.18}$$

where $\mathbf{B}^{\tau s}$ is the same as in Eq. (7.12) and

$$\hat{\mathbf{u}}_s = \left\{ \begin{array}{cccccc} u_{xs} & u_{xs_{,y}} & u_{ys} & u_{ys_{,y}} & u_{zs} & u_{zs_{,y}} \end{array} \right\}^T \tag{7.19}$$

The expanded natural boundary conditions are

$$\mathbf{P} = \mathbf{B}\,\hat{\mathbf{u}} \tag{7.20}$$

7.2 Solution of the differential equations

Because of CUF and since the derivatives are taken as variables, it is clear that each of Eqs. (7.4), (7.10) and (7.17) is a system of ODEs of second order in y with constant coefficients. The procedure to solve a system of ordinary differential equations of second order with constant coefficients is shown in Appendix B once the matrices $\tilde{\mathbf{S}}$ (Eq. (B.3)) and $\mathbf{S}$ (Eq. (B.7)) are formulated. As explained in Appendix B, a change of variables to reduce the second order system to a first order system is first needed. In the case of free vibrations of beams and beam-columns, the following change of variables is needed:

$$\begin{gathered}\mathbf{Z} = \left\{ \begin{array}{cccc} Z_1 & Z_2 & \dots & Z_n \end{array} \right\}^T = \hat{\mathbf{U}} = \\ \left\{ \begin{array}{ccccccccccccc} U_{x1} & U_{x1,y} & U_{y1} & U_{y1,y} & U_{z1} & U_{z1,y} & \dots & U_{xM} & U_{xM,y} & U_{yM} & U_{yM,y} & U_{zM} & U_{zM,y} \end{array} \right\}^T\end{gathered} \tag{7.21}$$

where $\hat{\mathbf{U}}$ is the expansion of $\hat{\mathbf{U}}_s$ for a given theory order, M is the number of expansion terms for the given beam theory, and $n = 6 \times M$ is the dimension of the unknown vector as well as the number of differential equations. On the other hand, in the case of buckling problems, one has similarly

$$\begin{gathered}\mathbf{Z} = \left\{ \begin{array}{cccc} Z_1 & Z_2 & \dots & Z_n \end{array} \right\}^T = \hat{\mathbf{u}} = \\ \left\{ \begin{array}{ccccccccccccc} u_{x1} & u_{x1,y} & u_{y1} & u_{y1,y} & u_{z1} & u_{z1,y} & \dots & u_{xM} & u_{xM,y} & u_{yM} & u_{yM,y} & u_{zM} & u_{zM,y} \end{array} \right\}^T\end{gathered} \tag{7.22}$$

where $\hat{\mathbf{u}}$ is the expansion of $\hat{\mathbf{u}}_s$. For the sake of simplicity, no distinctions are made between $\hat{\mathbf{U}}$ and $\hat{\mathbf{u}}$ in the following.

The main problem now is to find an algorithm to transform the expanded $\mathbf{L}$ matrix of Eqs. (7.4), (7.10) and (7.17) into the matrix $\mathbf{S}$ of the following differential problem:

$$\mathbf{Z}_{,y}(y) = \mathbf{S}\mathbf{Z}(y) \tag{7.23}$$

In fact, by looking at Eq. (B.2), see Appendix B, it could be seen that there are only second derivatives on the left hand side (LHS) of the differential equations whereas by looking, for example, at Eq (4.33), it is clear that for each equation more than one second derivative appears. In order to obtain the matrix $\tilde{\mathbf{S}}$ from the $\mathbf{L}$ matrix, decoupling between the second derivatives can be done line by line so that only one second derivative remains on each line. Moreover, for each line, the coefficient of the second order derivative which is left, has to be set as -1 by means of a factorization. By performing the above procedure on the $\mathbf{L}$ matrix and by removing the columns which contain the coefficient -1 of the second order derivative, the matrix of the coefficients of the differential equations is formulated in the form of the matrix $\tilde{\mathbf{S}}$ as it appears in Appendix B. The procedure to transform the matrix $\mathbf{L}$ into the matrix $\tilde{\mathbf{S}}$ consists of performing a number of Gauss eliminations. This procedure is discussed in Appendix C. Subsequently, the matrix $\mathbf{S}$ of Eq. (7.23) can be obtained from $\tilde{\mathbf{S}}$ by adding rows with 0's and 1's in order to account for the change of variables (see Appendix B, Eqs. (B.3) and (B.7)). Once the matrix $\tilde{\mathbf{S}}$ (Eq. (B.3)) is obtained, and subsequently transformed into $\mathbf{S}$ (Eq. (B.7)), by following the procedure in Appendix B, the solution can be written in matrix form as follows:

$$\begin{bmatrix} Z_1 \\ Z_2 \\ \vdots \\ Z_n \end{bmatrix} = \begin{bmatrix} \delta_{11} & \delta_{21} & \dots & \delta_{n1} \\ \delta_{12} & \delta_{22} & \dots & \delta_{n2} \\ \vdots & \vdots & \ddots & \vdots \\ \delta_{1n} & \delta_{2n} & \dots & \delta_{nn} \end{bmatrix} \begin{bmatrix} C_1 \mathrm{e}^{\lambda_1 y} \\ C_2 \mathrm{e}^{\lambda_2 y} \\ \vdots \\ C_n \mathrm{e}^{\lambda_n y} \end{bmatrix} \tag{7.24}$$

where λ_i is the i-th eigenvalue of the $\mathbf{S}$ matrix, δ_{ij} is the j-th element of the i-th eigenvector of the $\mathbf{S}$ matrix and C_i are the integration constants which need to be determined by using the boundary conditions. The above equation can be written in a matrix form as follows:

$$\mathbf{Z} = \delta \mathbf{C} \mathrm{e}^{\lambda y} \tag{7.25}$$

Vector $\mathbf{Z}$ contains not only the displacements but also their first derivatives. If only the displacements are needed, according to Eqs. (7.21) and (7.22), only the lines $1,3,5,\dots,n-1$ should be taken into account, giving a solution in the following form:

$$\begin{aligned} U_{x1}(y) &= C_1\delta_{11}\mathrm{e}^{\lambda_1 y} + C_2\delta_{21}\mathrm{e}^{\lambda_2 y} + \dots + C_n\delta_{n1}\mathrm{e}^{\lambda_n y} \\ U_{y1}(y) &= C_1\delta_{13}\mathrm{e}^{\lambda_1 y} + C_2\delta_{23}\mathrm{e}^{\lambda_2 y} + \dots + C_n\delta_{n3}\mathrm{e}^{\lambda_n y} \\ U_{z1}(y) &= C_1\delta_{15}\mathrm{e}^{\lambda_1 y} + C_2\delta_{25}\mathrm{e}^{\lambda_2 y} + \dots + C_n\delta_{n5}\mathrm{e}^{\lambda_n y} \\ &\vdots \\ U_{zM}(y) &= C_1\delta_{1(n-1)}\mathrm{e}^{\lambda_1 y} + C_2\delta_{2(n-1)}\mathrm{e}^{\lambda_2 y} + \dots + C_n\delta_{n(n-1)}\mathrm{e}^{\lambda_n y} \end{aligned} \tag{7.26}$$

Once the displacements are known, the boundary conditions are obtained by substituting the solution of Eq. (7.25) into the boundary conditions (Eq. (7.8)). In fact, it should be noted that $\hat{\mathbf{U}}$ is equal to $\mathbf{Z}$ (Eq. (7.21)) which eventually leads to

$$\mathbf{P} = \mathbf{B}\delta\mathbf{C}\mathrm{e}^{\lambda y} = \mathbf{\Lambda}\mathbf{C}e^{\lambda y} \tag{7.27}$$

where $\mathbf{\Lambda} = \mathbf{B}\delta$. The boundary conditions can be written in explicit form as follows:

$$\begin{aligned}
P_{x1}(y) &= C_1\Lambda_{11}\mathrm{e}^{\lambda_1 y} + C_2\Lambda_{12}\mathrm{e}^{\lambda_2 y} + \ldots + C_n\Lambda_{1n}\mathrm{e}^{\lambda_n y} \\
P_{y1}(y) &= C_1\Lambda_{21}\mathrm{e}^{\lambda_1 y} + C_2\Lambda_{22}\mathrm{e}^{\lambda_2 y} + \ldots + C_n\Lambda_{2n}\mathrm{e}^{\lambda_n y} \\
P_{z1}(y) &= C_1\Lambda_{31}\mathrm{e}^{\lambda_1 y} + C_2\Lambda_{32}\mathrm{e}^{\lambda_2 y} + \ldots + C_n\Lambda_{3n}\mathrm{e}^{\lambda_n y} \\
&\vdots \\
P_{zM}(y) &= C_1\Lambda_{n1}\mathrm{e}^{\lambda_1 y} + C_2\Lambda_{n2}\mathrm{e}^{\lambda_2 y} + \ldots + C_n\Lambda_{nn}\mathrm{e}^{\lambda_n y}
\end{aligned} \tag{7.28}$$

Although resorting to the **L** matrix seems extremely convoluted and complicated, it is in fact the simplest and most effective way to solve the problem. The matrix $\mathbf{L}^{\tau s}$ is simply a different way to write the differential equations but the greatest advantage is that it allows for automatic formulation of the differential equations of any order beam theories in a systematic way. In sharp contrast to the structural problems illustrated in the literature and those methods outlined in the previous chapters, where the system becomes algebraic, here by using **L** the differential equations can be written automatically, thus allowing the solution for any-order theory possible with relative ease.

7.3 Dynamic stiffness matrix

Once the closed form analytical solution of the differential equations of motion of the structural element in free vibration has been sought, a number of general boundary conditions - which are usually the nodal displacements and forces - equal to twice the number of integration constants in algebraic form needs to be applied (see Fig. 7.2).

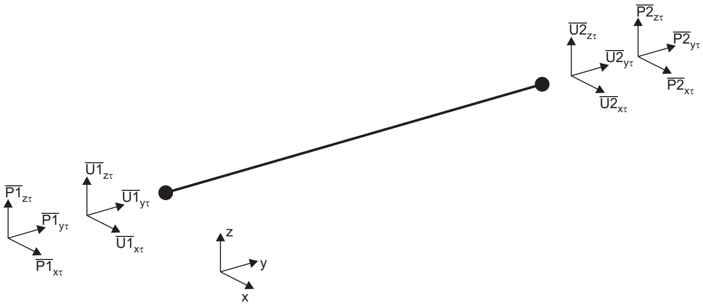
$\overline{P2}_{z\tau}$
$\overline{U2}_{z\tau}$
$\overline{P2}_{y\tau}$
$\overline{U2}_{y\tau}$
$\overline{P2}_{x\tau}$
$\overline{U2}_{x\tau}$
$\overline{U1}_{z\tau}$
$\overline{P1}_{z\tau}$
$\overline{U1}_{y\tau}$
$\overline{P1}_{y\tau}$
$\overline{U1}_{x\tau}$
$\overline{P1}_{x\tau}$
z
y
x

Figure 7.2 Boundary conditions of the beam element and sign conventions.

Starting from the displacements, the boundary conditions can be written as

$$
\begin{aligned}
\text{At}\quad & y = 0: \\
& U_{x1}(0) = -\overline{U}1_{x1} \\
& U_{y1}(0) = -\overline{U}1_{y1} \\
& U_{z1}(0) = -\overline{U}1_{z1} \\
& \vdots \\
& U_{zM}(0) = -\overline{U}1_{zM}
\end{aligned}
\tag{7.29}
$$

$$
\begin{aligned}
\text{At}\quad & y = L: \\
& U_{x1}(L) = \overline{U}2_{x1} \\
& U_{y1}(L) = \overline{U}2_{y1} \\
& U_{z1}(L) = \overline{U}2_{z1} \\
& \vdots \\
& U_{zM}(L) = \overline{U}2_{zM}
\end{aligned}
\tag{7.30}
$$

By evaluating Eq. (7.26) at $y = 0$ and $y = L$ and applying the boundary conditions of Eqs. (7.29) and (7.30), the following matrix relation for the nodal generalized displacements is obtained:

$$
\begin{Bmatrix}
\overline{U}1_{x1} \\
\overline{U}1_{y1} \\
\overline{U}1_{z1} \\
\vdots \\
\overline{U}1_{zM} \\
\overline{U}2_{x1} \\
\overline{U}2_{y1} \\
\overline{U}2_{z1} \\
\vdots \\
\overline{U}2_{zM}
\end{Bmatrix}
=
\begin{bmatrix}
-\delta_{11} & -\delta_{21} & \dots & -\delta_{n1} \\
-\delta_{13} & -\delta_{23} & \dots & -\delta_{n3} \\
-\delta_{15} & -\delta_{25} & \dots & -\delta_{n5} \\
\vdots & \vdots & \ddots & \vdots \\
-\delta_{1(n-1)} & -\delta_{2(n-1)} & \dots & -\delta_{n(n-1)} \\
\delta_{11}e^{\lambda_1 L} & \delta_{21}e^{\lambda_2 L} & \dots & \delta_{n1}e^{\lambda_n L} \\
\delta_{13}e^{\lambda_1 L} & \delta_{23}e^{\lambda_2 L} & \dots & \delta_{n3}e^{\lambda_n L} \\
\delta_{15}e^{\lambda_1 L} & \delta_{25}e^{\lambda_2 L} & \dots & \delta_{n5}e^{\lambda_n L} \\
\vdots & \vdots & \ddots & \vdots \\
\delta_{1(n-1)}e^{\lambda_1 L} & \delta_{2(n-1)}e^{\lambda_2 L} & \dots & \delta_{n(n-1)}e^{\lambda_n L}
\end{bmatrix}
\begin{Bmatrix}
C_1 \\
C_2 \\
C_3 \\
\vdots \\
C_{\frac{n}{2}} \\
C_{\frac{n}{2}+1} \\
C_{\frac{n}{2}+2} \\
C_{\frac{n}{2}+3} \\
\vdots \\
C_n
\end{Bmatrix}
\tag{7.31}
$$

The above equation can be written in a more compact form as

$$
\overline{\mathbf{U}} = \mathbf{AC}
\tag{7.32}
$$

Similarly, boundary conditions for generalized nodal forces are as follows:

$$\begin{aligned}
&\text{At} \quad y = 0: \\
&\quad P_{x1}(0) = -\overline{P}1_{x1} \\
&\quad P_{y1}(0) = -\overline{P}1_{y1} \\
&\quad P_{z1}(0) = -\overline{P}1_{z1} \\
&\quad \vdots \\
&\quad P_{zM}(0) = -\overline{P}1_{zM}
\end{aligned} \tag{7.33}$$

$$\begin{aligned}
&\text{At} \quad y = L: \\
&\quad P_{x1}(L) = \overline{P}2_{x1} \\
&\quad P_{y1}(L) = \overline{P}2_{y1} \\
&\quad P_{z1}(L) = \overline{P}2_{z1} \\
&\quad \vdots \\
&\quad P_{zM}(L) = \overline{P}2_{zM}
\end{aligned} \tag{7.34}$$

By evaluating Eq. (7.28) in $y = 0$ and $y = L$ and applying the boundary conditions of Eqs. (7.33) and (7.34), the following matrix relation for the nodal forces is obtained:

$$\left\{\begin{array}{c}
\overline{P}1_{x1} \\ \overline{P}1_{y1} \\ \overline{P}1_{z1} \\ \vdots \\ \overline{P}1_{zM} \\ \overline{P}2_{x1} \\ \overline{P}2_{y1} \\ \overline{P}2_{z1} \\ \vdots \\ \overline{P}2_{zM}
\end{array}\right\} = \left[\begin{array}{cccc}
-\Lambda_{11} & -\Lambda_{12} & \ldots & -\Lambda_{1n} \\
-\Lambda_{21} & -\Lambda_{22} & \ldots & -\Lambda_{2n} \\
-\Lambda_{31} & -\Lambda_{32} & \ldots & -\Lambda_{3n} \\
\vdots & \vdots & \ddots & \vdots \\
-\Lambda_{n1} & -\Lambda_{n2} & \ldots & -\Lambda_{nn} \\
\Lambda_{11}e^{\lambda_1 L} & \Lambda_{12}e^{\lambda_2 L} & \ldots & \Lambda_{1n}e^{\lambda_n L} \\
\Lambda_{21}e^{\lambda_1 L} & \Lambda_{22}e^{\lambda_2 L} & \ldots & \Lambda_{2n}e^{\lambda_n L} \\
\Lambda_{31}e^{\lambda_1 L} & \Lambda_{32}e^{\lambda_2 L} & \ldots & \Lambda_{3n}e^{\lambda_n L} \\
\vdots & \vdots & \ddots & \vdots \\
\Lambda_{n1}e^{\lambda_1 L} & \Lambda_{n2}e^{\lambda_2 L} & \ldots & \Lambda_{nn}e^{\lambda_n L}
\end{array}\right] \left\{\begin{array}{c}
C_1 \\ C_2 \\ C_3 \\ \vdots \\ C_{\frac{n}{2}} \\ C_{\frac{n}{2}+1} \\ C_{\frac{n}{2}+2} \\ C_{\frac{n}{2}+3} \\ \vdots \\ C_n
\end{array}\right\} \tag{7.35}$$

The above equation can be written in a more compact form as

$$\overline{\mathbf{P}} = \mathbf{RC} \tag{7.36}$$

The integration constants in vector **C** from Eqs. (7.32) and (7.36) can now be eliminated by relating the harmonically varying amplitudes of the generalized nodal forces to the

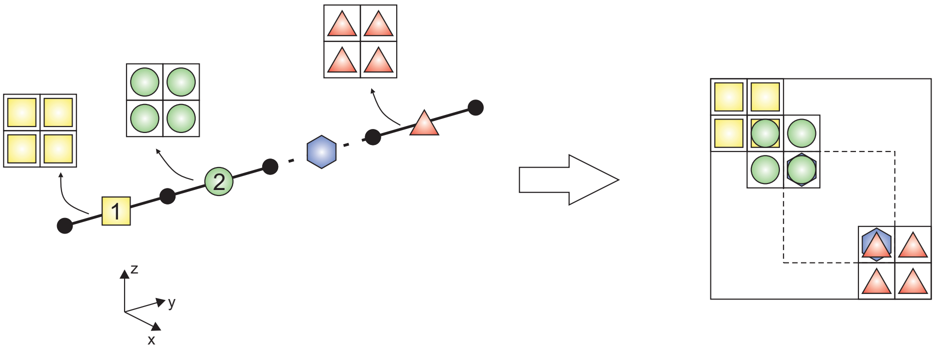

Figure 7.3 Assembly of dynamic stiffness matrices.

corresponding amplitudes of the generalized displacements to give the DS matrix of one beam element as follows:

$$\overline{\mathbf{P}} = \mathscr{K}\overline{\mathbf{U}} \tag{7.37}$$

where

$$\mathscr{K} = \mathbf{R}\mathbf{A}^{-1} \tag{7.38}$$

is the required DS matrix.

The DS matrix given by Eq. (7.38) is the basic building block to compute the exact natural frequencies or critical buckling loads of a higher-order beam. The global DS matrix can be obtained by assembling elemental matrices as in the classical way similar to FEM, see Fig. 7.3. As far as the boundary conditions are concerned, they can be applied by using the well-known penalty method (often used in FEM) or by simply removing rows and columns of the dynamic stiffness matrix corresponding to the degrees of freedom which are zeroes. In this thesis, the penalty method is used to suppress the unnecessary degrees of freedom [56].

7.4 The Wittrick-Williams algorithm

The analytical, closed form-solution and the collocation method discussed in the previous chapters lead to algebraic or linear eigenvalue problems. By contrast, the DSM leads to a transcendental (non-linear) eigenvalue problem for which the Wittrick-Williams algorithm [49] is generally used. In the case of free vibration analysis, the basic working principle of the algorithm is briefly summarised as follows:

(i) A trial frequency ω^* is chosen to compute the DS matrix $\mathscr{K}^*$ of the final structure;

(ii) $\mathscr{K}^*$ is reduced to its upper triangular form by the usual form of Gauss elimination to obtain $\mathscr{K}^{*\triangle}$ and the number of negative terms on the leading diagonal of $\mathscr{K}^{*\triangle}$ is counted: this is known as the sign count $s(\mathscr{K}^*)$ of the algorithm;

(iii) The number, j, of natural frequencies (ω) of the structure which lie below the trial frequency (ω^*) is given by:

$$j = j_0 + s(\mathscr{K}^*) \tag{7.39}$$

where j_0 is the number of natural frequencies of all individual elements with clamped-clamped boundary conditions on their opposite sides which still lie below the trial frequency ω^*.

The procedure in the case of buckling analysis is analogous. The main difference is that, in this case, the DS matrix depends on the axial load, whose critical trial value is $-\sigma_{yy}^0 = \lambda^*$. Note that, in the procedure above, j_0 is required because the DSM allows for an infinite number of natural frequencies to be accounted for when all the nodes of the structure are fully clamped so that one or more individual elements of the structure can still vibrate or buckle on their own between the nodes. Thus j_0 corresponds to $\overline{\mathbf{U}} = 0$ modes of Eq. (7.37) when $\overline{\mathbf{P}} = 0$. Assuming that j_0 is known (it can be calculated by exact formula or by subdividing members), and $s(\mathscr{K}^*)$ can be obtained by counting the number of negative terms in $\mathscr{K}^{*\triangle}$, a suitable procedure can be devised, for example the bi-section method, to bracket any natural frequency between an upper and lower bound of the trial frequency ω^* to any desired accuracy.

7.5 Eigenvalues and eigenmodes calculation

Once the natural frequency or the critical buckling load has been computed and the related global DS matrix is evaluated, the corresponding nodal generalized displacements giving the mode shapes can be obtained by using a random force vector $\overline{\mathbf{P}}$ in Eq. (7.37) or by solving the associated homogeneous system. Then, by utilizing the nodal generalized displacements $\overline{\mathbf{U}}$, the integration constants $\mathbf{C}$ of the element can be computed with the help of Eq. (7.32). In this way, by using Eq. (7.26), the unknown generalized displacements are computed as a function of y. Finally, by using Eqs. (6.3) and (3.7), the complete displacement field can be generated as a function of x, y, z and the time t (if an animated plot is needed). Clearly, the plot of the required mode can be visualised on a fictitious 3D mesh. By following this procedure, it is possible to compute the exact free vibratory mode shapes or buckling modes by using just one single element, which is impossible in weak-form solutions such as in FEM or in other numerical methods.

Chapter 8

Numerical Results

Based on the theories presented in previous chapters, this chapter presents some practical applications with illustrative examples of metallic and composite beam and plate structures. Solid and thin-walled cross-section beams made of isotropic and composite materials are considered. Two principal aims are given preference when obtaining the results: (i) The validation of the refined CUF structural models; and (ii) The investigation about the different exact and numerical approaches for the solutions of the strong-form governing equations. A wide range of problems are addressed, including static analysis, free vibrations of unstressed and pre-stressed structures, and linearized buckling.

8.1 Static analysis

Closed-form analytical solutions for static analysis of composite beams by LE models are addressed in this section. With regard to closed-form solutions of TE CUF theories as applied to metallic structures, the readers are referred to the works by Giunta *et al.* [129] and Catapano *et al.* [130] as supplements.

8.1.1 Composite beams subjected to sinusoidal pressure load

In order to test the validity and accuracy of the present method, a well-known test case is now presented. It is a beam problem and the beam considered has simply supported boundary conditions and has a square cross-section. Three different cross-ply laminations schemes are used to define the cross-section. These are [0°], [0°/90°], and [0°/90°/0°]. Each layer has the same thickness. The coordinate system, the geometry and the loading are shown in Fig. 8.1 for the illustrative case of the two-layer [0°/90°] beam. The material is carbon/epoxy

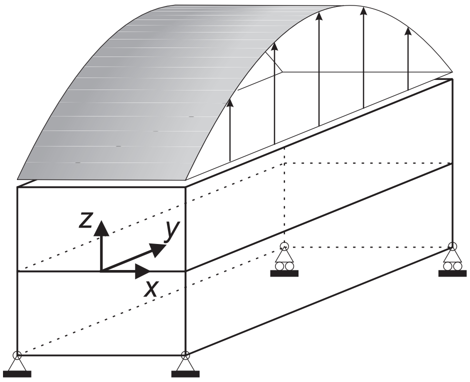

Figure 8.1 Simply supported composite beam of two-layer square cross-section subjected to sinusoidal pressure load.

composite and the material properties are such that the following relations are satisfied:

$$\frac{E_L}{E_T} = 25, \quad \frac{G_{TT}}{E_T} = 0.2, \quad \frac{G_{LT}}{E_T} = 0.5, \quad \nu_{LT} = \nu_{TT} = 0.25 \tag{8.1}$$

where the subscripts “L” and “T” stand for the direction parallel to the fibers and the transverse direction, respectively. In the analysis addressed in this section, the composite beam undergoes a transverse sinusoidal loading $q(x) = q_0 \sin\frac{\pi y}{L}$ on the top surface (see Fig. 8.1).

Pagano [131] was amongst the first few who discussed similar problems when he developed the Exact Solution for the Cylindrical Bending of Plates (ESCBP) in 1969, providing exact solutions for the problem under consideration. Subsequently, Lu and Liu [132], Vinayak *et al.* [133], Manjunatha and Kant [134, 135] used Higher order Shear Deformation Theories (HSDT) to solve the same problem. By contrast, Maiti and Sinha [136] studied those cross-ply beams with the First-order Shear Deformation Theory (FSDT). A Layer-wise Trigonometric Shear Deformation Theory (LTSDT) was discussed in [137, 138], whereas Tahani [139] employed the Beam Layer-Wise Theory (BLWT) in his investigation. Interestingly, Catapano *et al.* [140] addressed the same problem with different CUF-TE analytical solutions.

The results obtained from the theories developed in this thesis for axial and transverse displacements as well as axial and transverse stresses are presented using the following

Table 8.1 Maximum non-dimensional transverse displacement, $\bar{u}_z(0, L/2, -h/2)$, of the simply-supported composite beam under sinusoidal surface loading.

	[0°]		[0°/90°]			[0°/90°/0°]	
Model	$S=10$	$S=40$	$S=4$	$S=10$	$S=100$	$S=10$	$S=40$
Reference solutions							
ESCBP [131]	0.710	0.510	4.320	2.920	2.620	0.920	0.510
HSDT [132]	–	–	4.777	3.000	–	–	–
HSDT [134]	–	–	4.283	2.899	–	–	–
FSDT [136]	–	–	4.790	–	–	–	–
HSDT [133]	–	–	4.790	–	–	–	–
LTSDT [137]	–	–	4.743	2.974	–	–	–
LTSDT [138]	–	–	4.744	2.974	–	–	–
BLWT [139]	–	–	–	–	–	0.900	0.520
EBBM [140]	–	–	2.627	2.626	2.625	–	–
TE (N=5) [140]	–	–	4.671	2.626	2.627	–	–
Present LE models							
1×2 L4	0.697	0.505	4.430	2.904	2.615	–	–
1×6 L4	0.728	0.508	4.593	2.939	2.626	0.928	0.538
2×6 L4	0.728	0.508	4.594	2.939	2.626	0.928	0.538
1×2 L9	0.730	0.508	4.512	2.925	2.627	–	–
1×6 L9	0.733	0.508	4.703	2.960	2.628	0.933	0.538
2×6 L9	0.733	0.508	4.702	2.960	2.628	0.933	0.538
1×2 L16	0.733	0.508	4.705	2.960	2.628	–	–
1×3 L16	0.733	0.508	–	–	–	0.934	0.538
1×6 L16	0.733	0.508	4.706	2.960	2.628	0.934	0.538
2×6 L16	0.733	0.508	4.706	2.960	2.628	0.934	0.538

non-dimensional parameters

$$\begin{aligned} \bar{u}_i &= \frac{E_T}{q_0 h} u_i \quad \text{with} \quad i = x, y; \quad \bar{u}_z = 100 \frac{E_T h^3}{q_0 L^4} u_z \\ \bar{\sigma}_{ij} &= \frac{\sigma_{ij}}{q_0} \quad \text{with} \quad i = x, y, z; \quad S = \frac{L}{h}; \quad \bar{z} = \frac{z}{h} \end{aligned} \tag{8.2}$$

Tables 8.1 and 8.2 show some selected values of the transverse and axial displacement components using various theories, including LE models developed in this thesis solved. The present LE models make use of a Navier-type solution. The through-thickness distributions of the same quantities are also given in graphical form in Figs. 8.2 and 8.3. Various LE models have been considered and they have been referred to as $\xi \times \zeta\,\mathrm{L}\psi$, where ξ and ζ are the number of Lagrange polynomials along x and z directions, respectively, and ψ is the polynomial order. Clearly excellent agreement is found with L9 and L16 models in terms of displacements. For the short beam with $S = 4$, the results from the current analysis show some errors, but they are less than 3% when compared with the exact solution by

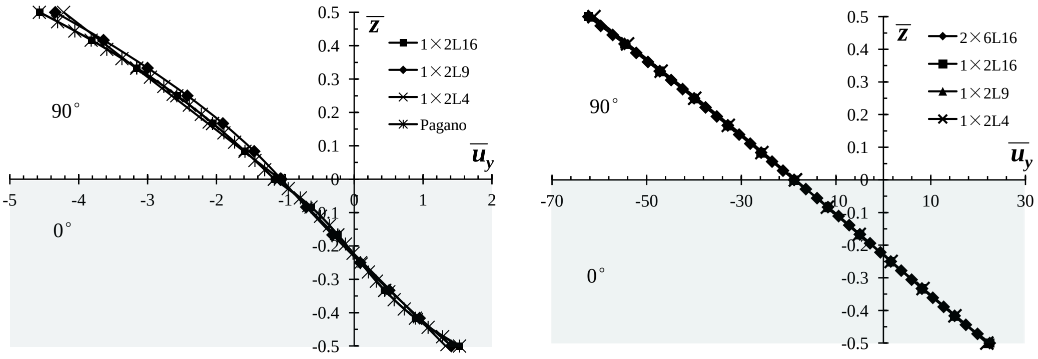

(a) $[0°/90°], S = 4$ (b) $[0°/90°], S = 10$

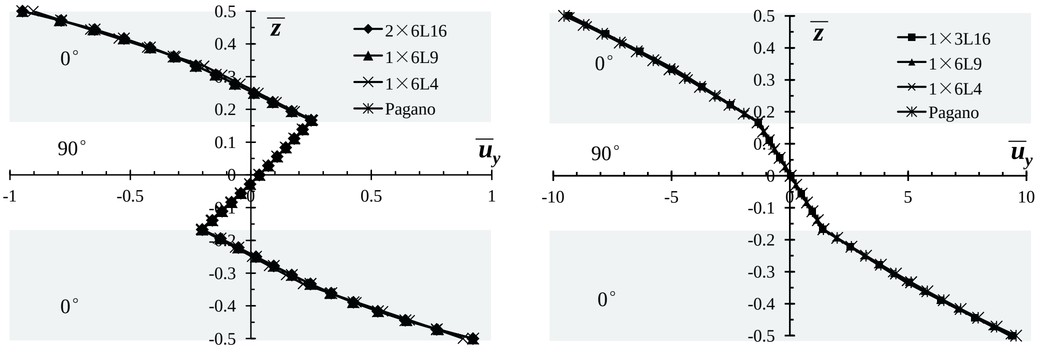

(c) $[0°/90°/0°], S = 4$ (d) $[0°/90°/0°], S = 10$

Figure 8.2 Distribution of normalized axial displacement $\bar{u}_y$ along $\bar{z}$ and at $(x,y) = (0,0)$; simply-supported composite beam under sinusoidal surface loading.

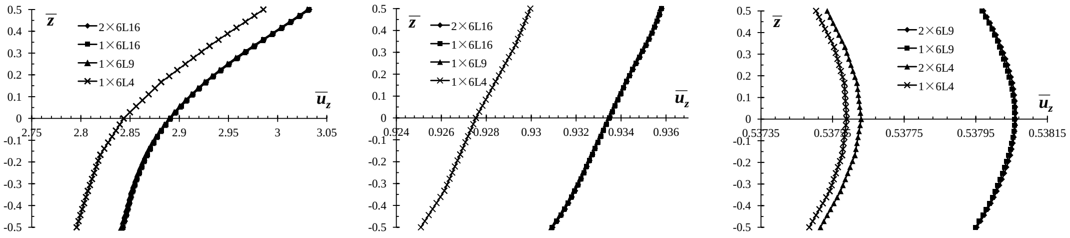

(a) $[0°/90°/0°], S = 4$ (b) $[0°/90°/0°], S = 10$ (c) $[0°/90°/0°], S = 40$

Figure 8.3 Distribution of normalized transverse displacement $\bar{u}_z$ along $\bar{z}$ and at $(x,y) = (0,L/2)$; simply-supported composite beam under sinusoidal surface loading.

Table 8.2 Non-dimensional axial displacement, $\bar{u}_y(0,0,-h/2)$, of the simply-supported composite beam under sinusoidal surface loading.

	[0°/90°]			[0°/90°/0°]	
Model	$S=4$	$S=10$	$S=100$	$S=4$	$S=10$
Reference solutions					
ESCBP [131]	-4.500	-61.667	-60143.00	-0.920	-9.300
HSDT [135]	-4.861	–	–	–	
HSDT [132]	-4.714	-61.667	–	–	–
LTSDT [137]	-5.057	-63.379	–	–	–
LTSDT [138]	-5.035	-63.305	–	–	–
EBBM [140]	-3.858	-60.273	-60273.000	–	–
TE (N=5) [140]	-4.575	-62.296	-60253.000	–	–
Present LE models					
1×2 L4	-4.218	-61.118	-59961.972	–	–
1×6 L4	-4.433	-61.841	-60220.324	-0.902	-9.253
2×6 L4	-4.434	-61.847	-60225.598	-0.906	-9.253
1×2 L9	-4.340	-62.518	-60249.211	–	–
1×6 L9	-4.562	-62.288	-60269.474	-0.947	-9.349
2×6 L9	-4.562	-62.289	-60270.461	-0.946	-9.349
1×2 L16	-4.565	-62.295	-60267.719	–	–
1×3 L16	–	–	–	-0.948	-9.350
1×6 L16	-4.566	-62.299	-60271.585	-0.948	-9.350
2×6 L16	-4.566	-62.301	-60272.647	-0.948	-9.350

Pagano [131]. In the case of slender bodies, i.e. $S = 10$, all the CUF LE models match perfectly to simulate the kinematics of the beam under consideration accurately.

The proposed analytical LE models are further validated by investigating the stress distributions within the beam. Tables 8.3 to 8.5 show some sample values of the axial $\bar{\sigma}_{yy}$, transverse normal $\bar{\sigma}_{zz}$, and transverse shear $\bar{\sigma}_{yz}$ stress components, respectively. The distributions of the same quantities through the thickness of the beam are shown in Figs. 8.4 to 8.6 for various length-to-height ratios and stacking sequences. Classical models, such as EBBM [140], provide inaccurate results for short beams, as expected. On the other hand, Lagrange-based LE models are more accurate than TE models and yet with reduced computational costs. In fact, it is easy to verify that the number of DOFs for the 2×6 L16 model is just 399. The layer-wise capabilities of the LE models are clearly evident from these results. The present models are able to satisfy correctly the conditions related to the zig-zag distribution of the axial stresses and to the interlaminar continuity of the transverse stresses if L9 and L16 discretizations are employed. It should be underlined that, although the displacements and stresses due to a sinusoidal pressure load have been analysed in this section, any other type of loading condition can be treated using the theory proposed by considering a Fourier series representation of the load.

Table 8.3 Non-dimensional axial stress, $\bar{\sigma}_{yy}$, at various z coordinates and $(x,y) = (0, L/2)$; simply-supported composite beam under sinusoidal surface loading.

Model	[0°]				[0°/90°]						[0°/90°/0°]			
	$S=4$		$S=10$		$S=4$		$S=10$		$S=100$		$S=4$		$S=10$	
	$z=-h/2$	$z=h/2$	$z=-h/2$	$z=h/2$	$z=-h/2$	$z=h/2$	$z=-h/2$	$z=h/2$	$z=-h/2$	$z=h/2$	$z=-h/2$	$z=h/2$	$z=-h/2$	$z=h/2$
ESCBP [131]	-13.200	14.200	-65.200	65.300	-30.029	3.836	-175.000	20.000	-17442.000	1894.400	-18.000	18.800	-73.200	73.200
HSDT [132]	–	–	–	–	-30.000	3.571	-175.000	20.000	–	–	–	–	–	–
HSDT [134]	–	–	–	–	-27.050	3.749	-173.000	19.710	–	–	–	–	–	–
FSDT [136]	–	–	–	–	-29.114	3.151	–	–	–	–	–	–	–	–
HSDT [133]	–	–	–	–	-27.000	4.000	–	–	–	–	–	–	–	–
LTSDT [137]	–	–	–	–	-30.298	3.965	-176.870	19.900	–	–	–	–	–	–
LTSDT [138]	–	–	–	–	-30.565	3.955	-177.149	19.888	–	–	–	–	–	–
BLWT [139]	–	–	–	–	-29.000	3.500	–	–	–	–	-18.500	18.800	–	–
EBBM [140]	–	–	–	–	-27.904	3.030	-174.400	18.935	-17440.000	1893.500	–	–	–	–
TE (N=7) [140]	–	–	–	–	-29.908	3.836	-176.440	19.826	-17449.000	1894.200	–	–	–	–
1×2 L4	-9.404	9.984	-60.732	60.872	-26.074	3.621	-172.331	19.887	-17433.381	1928.303	–	–	–	–
1×6 L4	-12.854	13.697	-64.866	65.051	-28.594	3.765	-175.186	19.837	-17453.136	1907.051	-17.308	17.987	-72.970	72.998
2×6 L4	-12.862	13.757	-64.872	65.066	-28.607	3.765	-175.163	19.838	-17447.558	1907.196	-17.316	18.046	-72.971	73.009
1×2 L9	-13.041	13.943	-65.195	65.392	-27.678	3.672	-173.976	19.577	-17420.076	1891.707	–	–	–	–
1×6 L9	-13.558	14.487	-65.524	65.721	-30.015	3.836	-176.524	19.819	-17441.291	1893.421	-18.104	18.853	-73.650	73.687
2×6 L9	-13.554	14.480	-65.523	65.720	-30.010	3.836	-176.534	19.820	-17441.730	1893.562	-18.103	18.843	-73.652	73.684
1×2 L16	-13.546	14.474	-65.528	65.725	-30.075	3.842	-176.633	19.842	-17447.267	1895.396	–	–	–	–
1×3 L16	-13.562	14.492	-65.525	65.722	–	–	–	–	–	–	-18.123	18.868	-73.654	73.686
1×6 L16	-13.562	14.494	-65.524	65.723	-30.040	3.838	-176.551	19.827	-17442.416	1894.053	-18.117	18.869	-73.651	73.689
2×6 L16	-13.588	14.492	-65.522	65.726	-30.038	3.841	-176.566	19.830	-17442.289	1894.096	-18.117	18.867	-73.654	73.696

Table 8.4 Non-dimensional transverse normal stress, $\bar{\sigma}_{zz}$, at $(x,y,z) = (0,L/2,h/2)$; simply-supported composite beam under sinusoidal surface loading.

	[0°]		[0°/90°]		[0°/90°/0°]	
Model	$S=4$	$S=10$	$S=4$	$S=10$	$S=4$	$S=10$
ESCBP [131]	1.000	1.000	1.000	1.000	1.000	–
HSDT [134]	–	–	1.000	1.000	–	–
HSDT [133]	–	–	1.000	–	–	–
LTSDT [137]	–	–	0.980	0.990	–	–
LTSDT [138]	–	–	1.000	1.000	–	–
EBBM [140]	–	–	1.000	1.000	–	–
TE (N=7) [140]	–	–	0.999	1.164	–	–
1×2 L4	0.784	1.062	1.226	2.709	–	–
1×6 L4	1.000	1.110	1.131	1.629	1.176	1.152
2×6 L4	0.996	1.101	1.132	1.629	1.116	1.140
1×2 L9	1.073	1.089	1.006	1.002	–	–
1×6 L9	1.022	1.018	1.005	1.001	1.026	1.022
2×6 L9	1.023	1.020	1.009	1.002	1.027	1.021
1×2 L16	1.025	1.022	1.002	1.006	–	–
1×3 L16	1.012	1.008	–	–	1.015	0.996
1×6 L16	1.007	1.008	1.001	1.002	1.001	1.001
2×6 L16	1.002	1.002	1.001	1.000	1.002	1.002

Table 8.5 Non-dimensional transverse shear stress, $\bar{\sigma}_{yz}$, at $(x,y,z) = (0,0,-h/4)$; simply-supported composite beam under sinusoidal surface loading.

	[0°]		[0°/90°]			[0°/90°/0°]	
Model	$S=4$	$S=10$	$S=4$	$S=10$	$S=100$	$S=4$	$S=10$
ESCBP [131]	1.410	–	2.700	7.220	73.360	1.500	4.100
HSDT [132]	–	–	2.793	7.300	–	–	–
HSDT [134]	–	–	1.927	4.913	–	–	–
FSDT [136]	–	–	2.847	–	–	–	–
HSDT [133]	–	–	2.750	–	–	–	–
LTSDT [137]	–	–	2.989	7.695	–	–	–
LTSDT [138]	–	–	2.990	7.695	–	–	–
BLWT [139]	–	–	2.750	–	–	1.550	–
TE (N=13) [140]	–	–	2.707	7.235	73.376	–	–
1×2 L4	1.254	3.181	2.008	5.179	52.127	–	–
1×6 L4	1.421	3.565	2.663	7.033	71.165	1.529	3.721
2×6 L4	1.416	3.558	2.654	7.012	70.960	1.527	3.714
1×2 L9	1.248	3.177	2.422	5.190	52.190	–	–
1×6 L9	1.411	3.545	2.626	6.992	70.902	1.522	3.702
2×6 L9	1.411	3.545	2.628	6.996	70.935	1.523	3.703
1×2 L16	1.437	3.595	2.731	7.240	73.352	–	–
1×3 L16	1.431	3.589	–	–	–	1.563	3.747
1×6 L16	1.429	3.589	2.698	7.211	73.184	1.569	3.763
2×6 L16	1.429	3.589	2.700	7.214	73.209	1.569	3.763

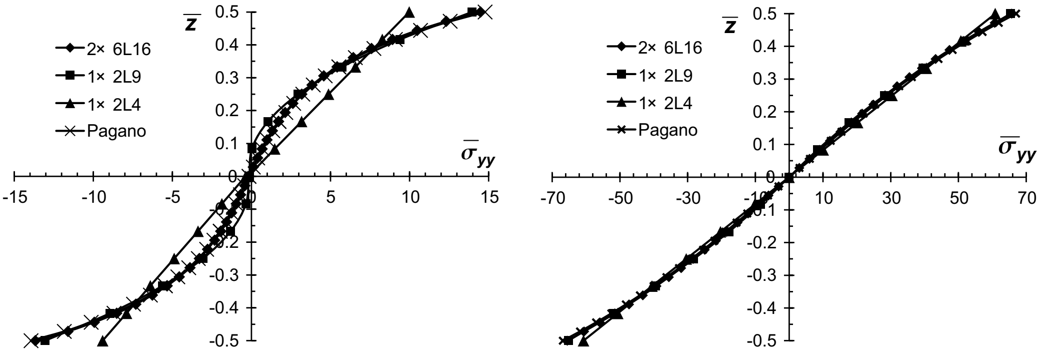

(a) $[0°], S = 4$ (b) $[0°], S = 10$

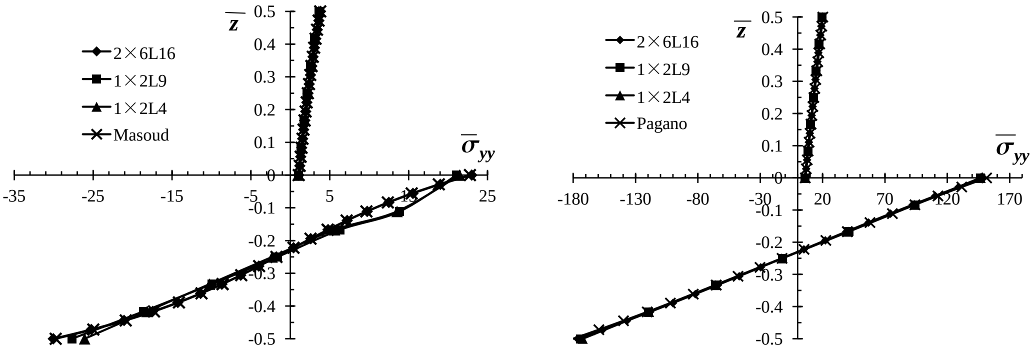

(c) $[0°/90°], S = 4$ (d) $[0°/90°], S = 10$

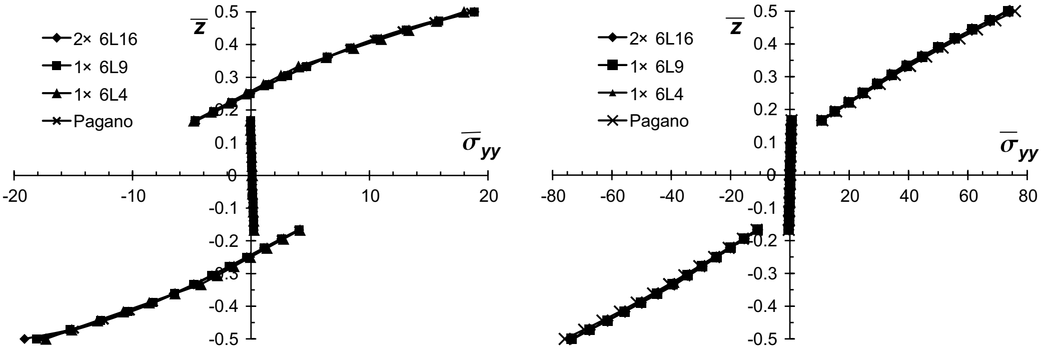

(e) $[0°/90°/0°], S = 4$ (f) $[0°/90°/0°], S = 10$

Figure 8.4 Distribution of normalized axial stress, $\bar{\sigma}_{yy}$, along $\bar{z}$ and at $(x, y) = (0, L/2)$; simply-supported composite beam under sinusoidal surface loading.

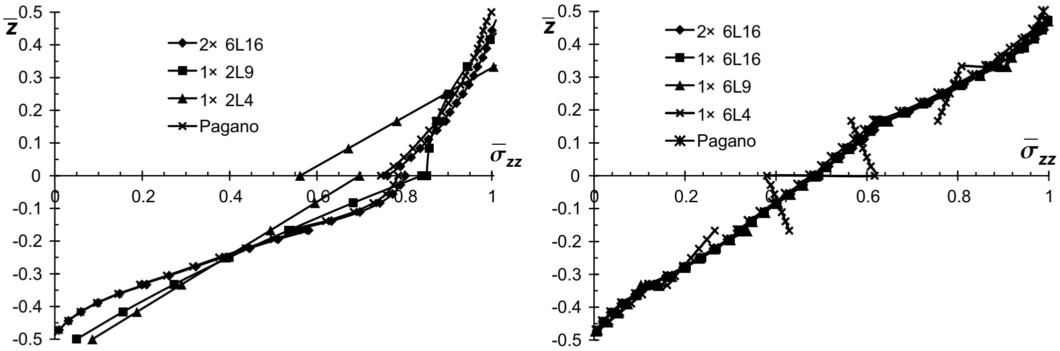

(a) $\lceil 0^\circ/90^\circ \rceil, S = 4$ (b) $\lceil 0^\circ/90^\circ/0^\circ \rceil, S = 4$

Figure 8.5 Distribution of normalized axial stress, $\bar{\sigma}_{zz}$, along $\bar{z}$ and at $(x,y) = (0, L/2)$; simply-supported composite beam under sinusoidal surface loading.

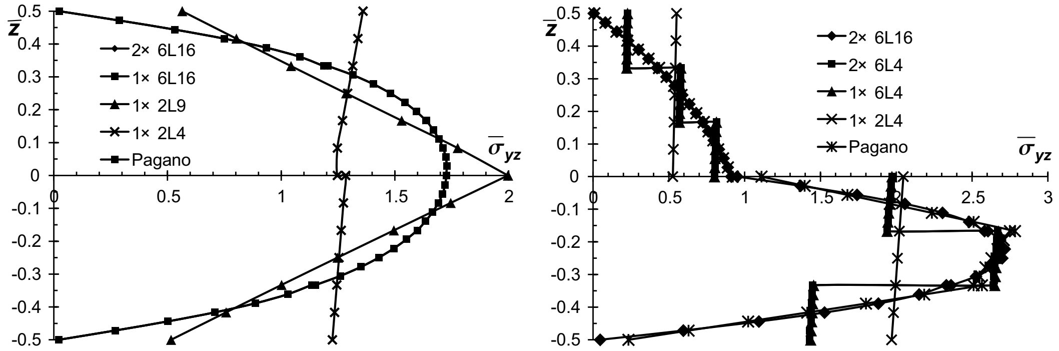

(a) $\lceil 0^\circ \rceil, S = 4$ (b) $\lceil 0^\circ/90^\circ \rceil, S = 4$

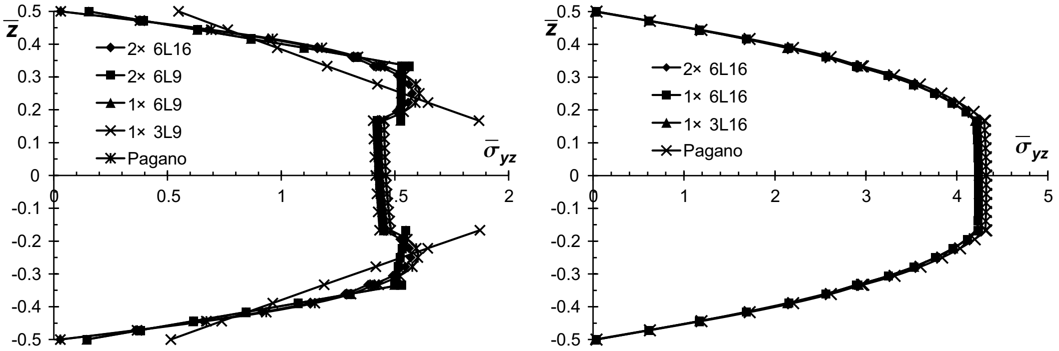

(c) $\lceil 0^\circ/90^\circ/0^\circ \rceil, S = 4$ (d) $\lceil 0^\circ/90^\circ/0^\circ \rceil, S = 10$

Figure 8.6 Distribution of normalized axial stress, $\bar{\sigma}_{yz}$, along $\bar{z}$ and at $(x,y) = (0,0)$; simply-supported composite beam under sinusoidal surface loading.

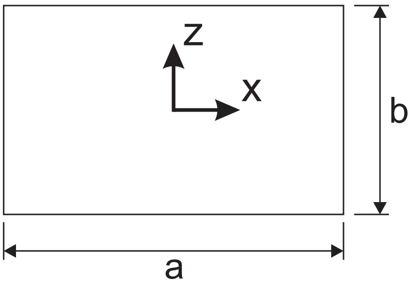

Figure 8.7 Solid rectangular cross-section.

8.2 Free vibration analysis

Closed-form solutions of CUF 1D models are available only for simply supported beam structures and cross-ply laminates. These are no doubt restrictive, but the limitations can be overcome if numerical solutions of strong-form governing equations are employed, such as the use of DSM or RBFs. In this section, particular emphasis is placed on these two methodologies (i.e., DSM and RBFs) and comparisons of results with those from the literature and, wherever possible, with those from closed-form CUF solutions are made. From the analyses, the power and strength of the DSM with particular reference to the Wittrick-Williams algorithm, which allows the solutions of transcendental (nonlinear) eigenvalue problems within any desired accuracy, will be demonstrated.

8.2.1 Metallic, rectangular cross-section beams

A metallic beam with a solid rectangular cross-section such as the one shown in Fig. 8.7 is considered first. For illustrative purposes, it is assumed that the beam has a square cross-section ($a = b$), with $b = 0.2$ m and length L such that $L/b = 10$. The material data are: Young modulus, $E = 75$ GPa, Poisson ratio, $\nu = 0.33$, material density, $\rho = 2700\ \mathrm{kg/m^3}$.

Table 8.6 shows the first four bending natural frequencies in non-dimensional form ($\omega^* = \frac{\omega L^2}{b}\sqrt{\frac{\rho}{E}}$) for a simply-supported (SS) square beam using both the present DSM and finite element (FEM) solutions based on TE models. Approximate higher-order TE FEM results were retrieved from [56]. These approximate solutions were obtained by using various FE mesh sizes and shape function polynomial approximations (i.e., $p = 1,2,3$). Classical beam theories (TBM), linear ($N = 1$), quadratic ($N = 2$), cubic ($N = 3$) and fourth-order ($N = 4$) TE models are considered in the table. It is clearly shown that, as far as FEM solutions of CUF higher-order models are concerned, the number of beam elements that are necessary to obtain accurate results (provided by the DSM) increases as natural frequencies as well as beam theory order increase.

Table 8.6 First to fourth non-dimensional bending frequencies $\omega^* = \frac{\omega L^2}{b}\sqrt{\frac{\rho}{E}}$ for the SS square beam; $L/b = 10$.

No. Elem.	p	EBBM	TBM	$N=1$	$N=2$	$N=3$	$N=4$
Bending mode I							
FEM [56]							
10	1	2.873	2.842	2.842	2.847	2.843	2.843
20	1	2.846	2.816	2.816	2.818	2.813	2.813
40	1	2.840	2.809	2.809	2.810	2.806	2.806
10	2	2.838	2.807	2.807	2.808	2.803	2.803
20	2	2.838	2.807	2.807	2.808	2.803	2.803
Present DSM solution							
		2.838	2.807	2.807	2.808	2.803	2.803
Bending mode II							
FEM [56]							
10	1	11.775	11.292	11.292	11.378	11.304	11.304
20	1	11.350	10.904	10.904	10.931	10.864	10.863
40	1	11.247	10.810	10.810	10.823	10.758	10.757
10	2	11.216	10.782	10.782	10.791	10.726	10.725
20	2	11.213	10.779	10.779	10.788	10.723	10.722
40	2	11.213	10.779	10.779	10.787	10.723	10.722
10	3	11.213	10.779	10.779	10.787	10.723	10.722
Present DSM solution							
		11.213	10.779	10.779	10.787	10.723	10.722
Bending mode III							
FEM [56]							
10	1	27.587	25.209	25.209	25.611	25.266	25.260
20	1	25.409	23.409	23.409	23.526	23.245	23.241
40	1	24.905	22.988	22.988	23.042	22.775	22.771
10	2	24.777	22.881	22.881	22.916	22.653	22.649
20	2	24.743	22.852	22.852	22.886	22.623	22.619
40	2	24.740	22.850	22.850	22.884	22.621	22.617
10	3	24.740	22.850	22.850	22.884	22.621	22.617
20	3	24.740	22.849	22.849	22.884	22.621	22.617
40	3	24.740	22.849	22.849	22.884	22.621	22.617
Present DSM solution							
		24.742	22.849	22.849	22.884	22.621	22.617
Bending mode IV							
FEM [56]							
10	1	51.823	44.543	44.543	45.676	44.680	44.647
20	1	44.865	39.400	39.400	39.707	38.995	38.975
40	1	43.339	38.236	38.237	38.371	37.713	37.697
10	2	43.038	38.006	38.005	38.097	37.448	37.432
20	2	42.860	37.868	37.868	37.950	37.309	37.292
40	2	42.848	37.859	37.859	37.940	37.300	37.283
10	3	42.849	37.860	37.860	37.941	37.301	37.284
Present DSM solution							
		42.853	37.858	37.858	37.939	37.298	37.282

Table 8.7 Comparison between TE and LE CUF models; non-dimensional natural frequencies $\omega^* = \frac{\omega L^2}{b}\sqrt{\frac{\rho}{E}}$ for the SS square beam ($L/b = 10$).

Model	Bending I	Bending II	Bending III	Bending IV
1 L9 LE	2.808	10.784	22.869	37.902
1 L16 LE	2.803	10.722	22.618	37.291
$N = 4$ TE	2.803	10.722	22.617	37.282

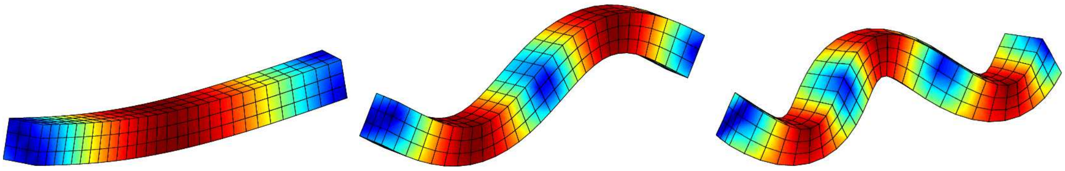
(a) (b) (c)

Figure 8.8 First (a), second (b) and third (c) bending modes for a SS square beam ($L/b = 10$); DSM $N = 4$ TE model.

A comparison between TE and LE models is shown in Table 8.7. In this table, the DSM TE solution is, in fact, compared to exact Navier-type solutions of two different LE models. In the 1 L9 LE model, the beam cross-section is discretized with one single L9 element. Similarly, the 1 L16 LE makes use of a single L16 element on the cross-section.

Figure 8.8 shows the first three bending modes of the beam with SS boundary conditions obtained from the DSM analysis when using a $N = 4$ TE model. It should be emphasized that DSM results are mesh independent and the mesh used in Fig. 8.8 is merely a plotting grid for convenience.

One of the most important features of the DSM is that it provides exact solutions for any kind of boundary conditions. Moreover, TE higher-order theories are able to take into account several non-classical effects such as warping, in-plane deformations, shear effects and bending-torsion couplings as demonstrated in [108]. In Table 8.8, the first two bending modes and the first two torsional modes for a clamped-free (CF) short ($L/b = 10$) square beam are shown. In this table, RBFs solutions of classical and higher-order TE models are compared to exact solutions by DSM. RBFs results are obtained by considering 37 collocation points and a shape parameter $c = \frac{2.4}{L}$ (see Chapter 6). Results obtained by 3D FEM models using MSC Nastran [141] are also shown in Table 8.8. The generic three-dimensional FEM solution is herein referred to as "Solid". In the results shown in Table 8.8, Solid is built by using 8-node CHEXA Nastran elements. Figure 8.9 shows some representative modal shapes by DSM for the fifth-order TE model of the CF beam. Some comments are relevant:

Table 8.8 Non-dimensional natural periods $\omega^* = \frac{\omega L^2}{b}\sqrt{\frac{\rho}{E}}$ for the CF square beam; $L/b = 10$.

Model	Bending I	Bending II	Torsional I	Torsional II
		MSC Nastran model		
Solid	1.016	6.088	8.852	26.516
		Classical and refined TE, DSM solutions		
$N=5$	1.013	6.069	8.868	26.603
$N=4$	1.013	6.070	8.871	26.619
$N=3$	1.014	6.075	9.631	28.893
$N=2$	1.015	6.107	9.631	28.893
TBM	1.008	6.069	-*	-
		Classical and refined TE, RBFs solutions		
$N=5$	1.011	6.075	8.872	26.605
$N=4$	1.012	6.078	8.875	26.623
$N=3$	1.013	6.081	9.634	28.895
$N=2$	1.014	6.115	9.634	28.895
TBM	1.007	6.076	-	-

*: not provided by the model

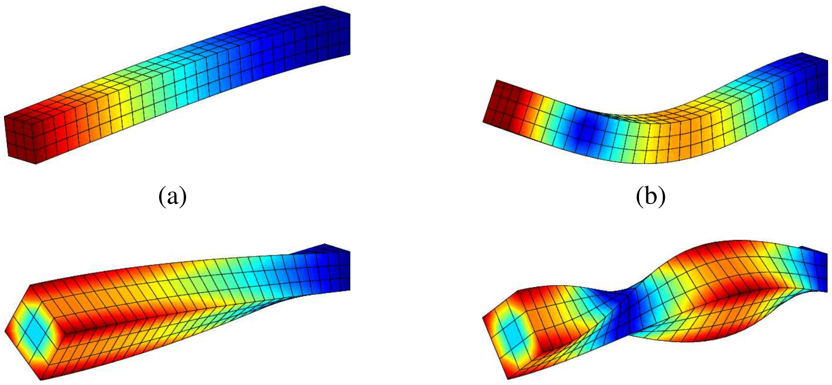

Figure 8.9 First bending (a), second bending (b), first torsional (c) and second torsional (d) modes for a CF square cross-section beam ($L/b = 10$); DSM $N = 5$ TE model.

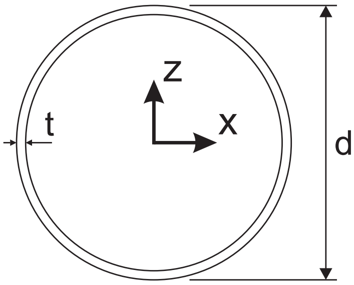

Figure 8.10 Cross-section of the thin-walled cylinder.

- According to 3D MSC Nastran solution and exact LE models, the present lower-order TE models are able to characterize the bending behaviour of solid cross-section beams.
- DSM provides exact solutions unlike FEM and RBFs methods which give inexact, but reliable results when applied to CUF refined beam models of compact cross-section beams.
- A fourth-order ($N = 4$) TE model is necessary to correctly detect torsional frequencies.

8.2.2 Thin-walled cylinder

A thin-walled cylinder is considered to highlight further the higher-order capabilities of the present formulation. Particular attention is focused on the comparison between RBFs and DSM solutions of higher-order TE models. The cross-section geometry is shown in Fig. 8.10. The cylinder has an outer diameter $d = 2$ m, thickness $t = 0.02$ m, and length $L = 20$ m. The structure is made of the same metallic material as in the previous example.

Table 8.9 shows the natural frequencies of the thin-walled cylinder for different boundary conditions (BCs). In particular, free-free (FF), clamped-free (CF), clamped-clamped (CC), as well as simply-supported (SS) ends are considered. Both classical TBM and higher-order CUF beam model results are shown in Table 8.9, where the natural frequencies of the RBFs-based method are compared with those from the exact DSM higher-order TE beam models and MSC Nastran 2D FE (Shell) solutions obtained by using CQUAD4 elements. In the case of RBFs, a number of centres equal to 31 and a shape parameter $c = \frac{2.4}{L}$ were used. It is shown that classical and lower-order beam models are able to capture bending and torsional modes, whereas 1D higher-order theories are mandatory in order to detect local shell-like modes in accordance with 2D solutions.

Figure 8.11 shows the percentage error between the present RBFs method and exact reference solution from DSM. In this figure the first bending, torsional, and shell-like modes for different expansion orders N and boundary conditions are considered. It is shown that,

Table 8.9 Natural frequencies (Hz) of the thin-walled cylinder for different boundary conditions; Comparison of RBFs and DSM solutions.

BCs	Model	I Bending	II Bending	I Shell-like	II Shell-like	I Torsional	II Torsional
SS	Shell	13.978	51.366	14.913	22.917	80.415	160.810
	$N = 5$, DSM	14.022	51.503	18.405	25.460	80.786	161.573
	$N = 5$, RBFs	14.294	51.567	18.608	25.574	80.639	162.551
	$N = 3$, DSM	14.022	51.520	34.935	61.300	80.787	161.572
	$N = 3$, RBFs	14.295	51.583	35.049	61.353	80.847	161.712
	TBM, DSM	14.182	53.542	-*	-	-	-
	TBM, RBFs	14.459	53.604	-	-	-	-
CC	Shell	28.498	68.960	17.396	30.225	80.415	160.810
	$N = 5$, DSM	28.576	69.110	20.484	32.222	80.786	161.573
	$N = 5$, RBFs	28.354	69.096	20.463	31.974	80.838	161.596
	$N = 3$, DSM	28.605	69.199	38.690	70.333	80.787	161.572
	$N = 3$, RBFs	28.259	68.921	38.889	70.056	80.838	161.596
	TBM, DSM	30.302	76.443	-	-	-	-
	TBM, RBFs	30.435	76.489	-	-	-	-
CF	Shell	5.059	29.001	14.235	17.435	40.209	120.620
	$N = 5$, DSM	5.076	29.088	17.805	20.580	40.394	121.181
	$N = 4$, DSM	5.077	29.090	23.069	25.239	40.393	121.181
	$N = 4$, RBFs	5.047	29.002	23.003	24.979	40.431	121.203
	$N = 3$, DSM	5.079	29.104	26.882	49.252	40.393	121.181
	$N = 3$, RBFs	5.059	28.953	26.934	49.356	40.431	121.203
	TBM, DSM	5.108	30.237	-	-	-	-
	TBM, RBFs	5.060	30.312	-	-	-	-
FF	Shell	30.829	76.806	14.129	14.171	80.415	160.810
	$N = 5$, DSM	30.932	77.041	17.709	17.777	80.788	161.576
	$N = 4$, DSM	30.932	77.043	22.987	23.053	80.789	161.577
	$N = 4$, RBFs	30.945	77.052	22.864	23.048	80.787	161.592
	$N = 3$, DSM	30.935	77.090	22.987	34.700	80.789	161.576
	$N = 3$, RBFs	31.121	77.099	23.043	34.678	80.787	161.592
	TBM, DSM	31.338	80.275	-	-	-	-
	TBM, RBFs	31.341	80.286	-	-	-	-

*: not provided by the model

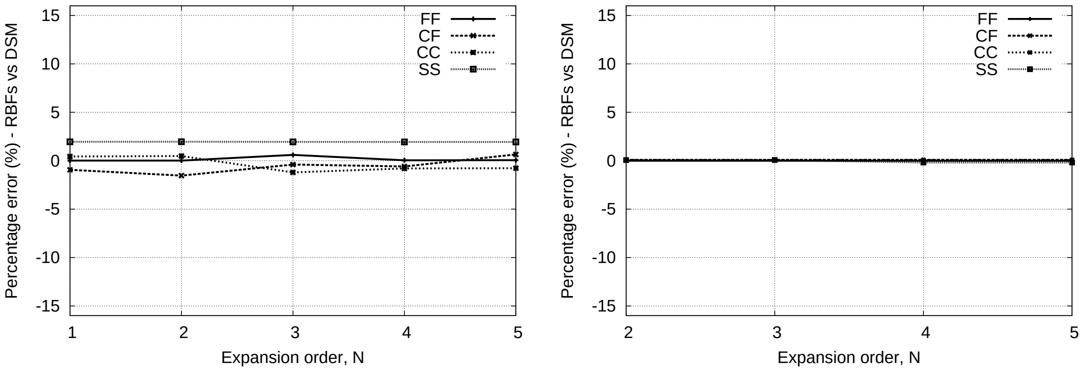

(a) Bending I (b) Torsional I

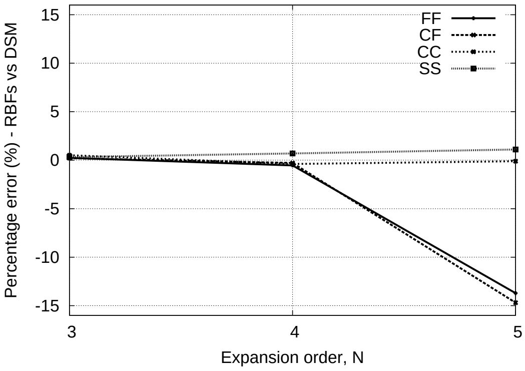

(c) Shell-like mode I

Figure 8.11 Percentage error between the RBFs and exact DSM solutions for various expansion orders and boundary conditions; Thin-walled cylinder.

for fixed values of the parameters *c* and number of centres *n*, bending and torsional modes exhibit a good convergence for all the boundary conditions and theory order considered. On the other hand, shell-like modes become instable if higher than fourth-order ($N = 4$) models and CF or FF boundary conditions are examined. This is the reason why in Table 8.9 only up to $N = 4$ models were considered for those boundary conditions in the case of RBFs.

Figure 8.12 shows the important modes of the cylinder for CC boundary condition by the fifth-order ($N = 5$) TE DSM model. The following comments arise:

- Only the flexural modes are provided by the classical beam theories.

- Torsional modes are correctly detected by the linear TE ($N = 1$) model in the case of axisymmetric structures.

- 1D higher-order model are necessary to detect shell-like modes as evident from the 2D FEM solutions provided by MSC Nastran. Classical beam theories would not predict these results.

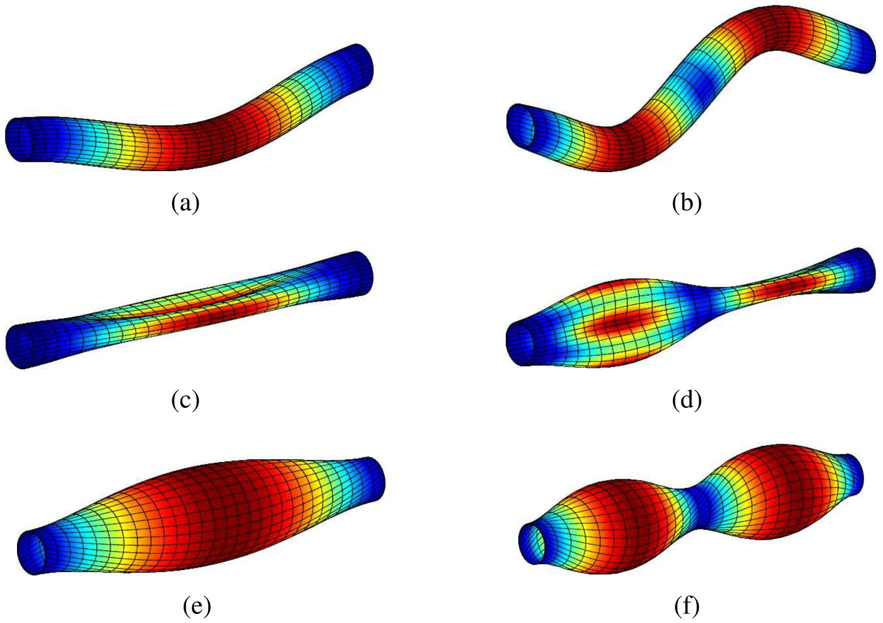

Figure 8.12 First flexural (a), second flexural (b), first shell-like (c), second shell-like (d), first torsional (e) and second torsional (f) modes for a CC thin-walled cylinder; DSM $N = 5$ TE model.

- Instabilities may occur in the case of RBFs when thin-walled structures are considered.

8.2.3 Four- and two-layer composite beams

The capabilities of the proposed methodology when applied to free vibration analysis of laminated composite structures is further verified. The beam has a solid square cross-section and a length-to-side ratio, L/h, equal to 15 with $h = 25.4$ mm. The material adopted is a AS4/3501-6 graphite/epoxy composite in accordance with [142].

Table 8.10 shows the first nine non-dimensional natural frequencies ($\omega^* = \frac{\omega L^2}{b}\sqrt{\frac{\rho}{E_1}}$) for a $[+45°/-45°/+45°/-45°]$ antisymmetric angle-ply lamination scheme in the case of clamped-clamped (CC) boundary conditions. The results by classical and refined beam theories from the present CUF method by both DSM and RBFs are compared with those from the literature. In the case of RBFs solutions, a uniform grid of 40 centres and a shape parameter $c = 4 \times 10^{-3}$ were used. It is clear that torsional and coupled axial/shear modes are captured by the presents models if a sufficiently higher-order kinematics is adopted.

To show the capability of the present models to deal with arbitrary laminations, Fig. 8.13 shows the effect of increasing the angle of orientation θ on the fundamental natural frequencies of two lamination schemes $[\theta/-\theta]$ and $[0/\theta]$. The present fourth-order ($N = 4$)

Table 8.10 Non-dimensional natural frequencies, $\omega^* = \frac{\omega L^2}{b}\sqrt{\frac{\rho}{E_{11}}}$, of a CC $[+45/-45/+45/-45]$ antisymmetric angle-ply beam.

	DSM				RBFs				References	
	TBM	$N=2$	$N=4$	$N=6$	TBM	$N=2$	$N=4$	$N=6$	Ref. [143]	Ref. [144]
Mode 1[a]	1.993	2.112	1.987	1.962	1.993	2.123	1.995	1.976	1.845	1.981
Mode 2[b]	2.067	2.144	2.084	2.045	2.067	2.153	2.103	2.071	-*	-
Mode 3[a]	5.261	5.577	5.188	5.134	5.261	5.579	5.206	5.164	4.987	5.217
Mode 4[b]	5.641	5.852	5.687	5.579	5.641	5.878	5.738	5.647	-	-
Mode 5[c]	-*	10.627	9.241	9.131	-	10.633	9.265	9.169	-	-
Mode 6[a]	9.793	10.342	9.553	9.474	9.793	10.344	9.579	9.516	9.539	9.691
Mode 7[b]	10.898	11.319	10.990	10.782	10.898	11.369	11.089	10.920	-	-
Mode 8[a]	15.278	16.088	14.756	14.663	15.278	16.088	14.785	14.719	13.474	10.535
Mode 9[d]	15.174	15.472	15.307	15.092	15.174	15.496	15.370	15.177	15.292	15.098

[a]: Flexural on plane *yz*; [b]: Flexural on plane *xy*; [c]: Torsional mode; [d]: Axial/shear (plane *xz*) mode

[*]: Mode not provided by the theory

CUF-DSM model is compared with the solution available from [144], where a 1D FE model based on a higher-order shear deformation theory was used. The same analysis is of course not possible by using a Navier-type solution.

Finally, Fig. 8.14 shows the effect of material anisotropy on the fundamental frequencies of composite beams. Also for this analysis case, the results by the present $N=4$ TE-DSM model are validated with those from the literature. It should be underlined that, in Fig. 8.14, the value of E_1 is varied, whereas the other elastic parameters are kept constant. It is clear that the angle-ply configuration tends to lower the frequencies more rapidly than the cross-ply beam.

8.2.4 Cross-ply laminated composite plates

The capability of the present beam models to deal with plate-like geometries is demonstrated in this section. Analyses of simply-supported (SS-F-SS-F-SS) square cross-ply laminates are, therefore, discussed in detail. The lamination scheme, i.e. the lay-up or stacking sequence, is taken as $[90°/0°/90°/0°/90°]_s$. Each lamina has the same thickness and it is made of an orthotropic material that satisfies the following relations:

$$\frac{E_1}{E_2} = 40, \ \frac{G_{12}}{E_2} = \frac{G_{13}}{E_2} = 0.6, \ \frac{G_{23}}{E_2} = 0.5, \ \nu_{12} = \nu_{13} = \nu_{23} = 0.25 \tag{8.3}$$

In Table 8.11, the natural frequencies for plates with different side-to-thickness ratio (a/h) are given in non-dimensional form of the frequency parameter

$$\omega^* = \omega \frac{a}{h}\sqrt{\frac{\rho}{E_2}} \tag{8.4}$$

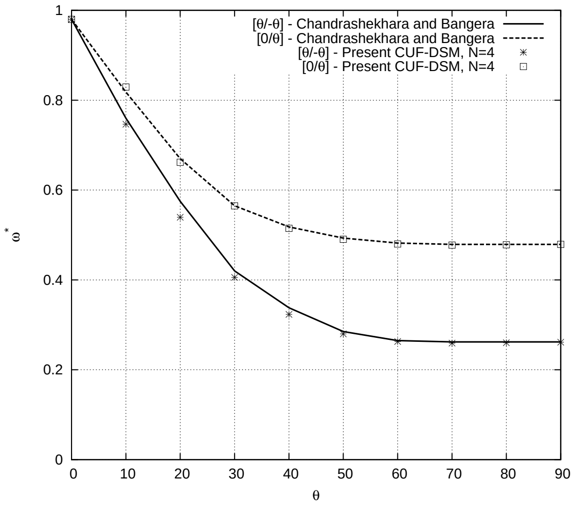

Figure 8.13 Effect of ply orientation angle on first flexural natural frequencies of two-layer CF beams; DSM $N = 4$ TE model versus [144].

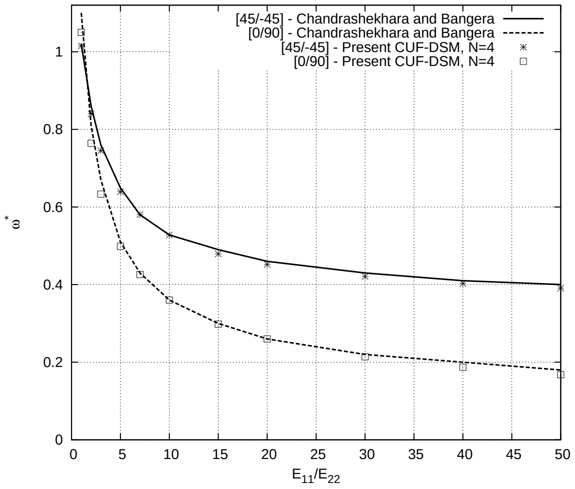

Figure 8.14 Effect of material anisotropy on the first flexural natural frequencies of angle-ply and cross-ply CF beams; DSM $N = 4$ TE model versus [144].

Table 8.11 Non-dimensional natural frequencies, $\omega^* = \omega\frac{a}{h}\sqrt{\frac{\rho}{E_2}}$, for the cross-ply SS-F-SS-F plate.

a/h	Model	Mode 1	Mode 2	Mode 3	Mode 4
5	HSDT [47]	7.263	7.909	18.113	18.113
	FSDT [47]	7.489	8.073	18.916	19.330
	$N = 6$	7.312	7.919	18.134	18.642
	$N = 5$	7.312	7.935	18.134	18.665
	$N = 4$	7.314	7.937	18.143	18.686
	$N = 3$	7.315	8.531	18.162	20.762
	$N = 2$	7.905	8.544	20.355	20.778
	TBM	7.902	–	20.351	–
10	HSDT [47]	9.939	10.248	29.017	29.054
	FSDT [47]	9.516	10.352	28.638	29.956
	$N = 6$	9.544	10.376	28.829	29.250
	$N = 5$	9.545	10.394	29.142	29.250
	$N = 4$	9.547	10.395	29.527	29.256
	$N = 3$	9.547	10.733	34.673	29.261
	$N = 2$	9.861	10.755	–	31.621
	TBM	9.855	–	–	31.607

The results from both TBM and higher-order beam models are given and compared with the results reported by Fazzolari *et al.* [47], in which both First-order Shear Deformation Theory (FSDT) and Higher-order Shear Deformation Theory (HSDT) were used in conjunction with the DSM to carry out the free vibration analysis of the composite plate assemblies. The results by EBBM are not shown in Table 8.11 for obvious reason because imprecise and inadequate results were inevitably produced by this theory. All the results presented in this section were obtained by using the DSM.

Figures 8.15 and 8.16 show the first four mode shapes of the cross-ply laminae by the present sixth-order ($N = 6$) CUF-DSM model for both $a/h = 5$ and $a/h = 10$, respectively. The proposed analysis shows the enhanced capabilities of the present beam formulation that is able to deal with 2D-like analysis of laminated structures.

8.2.5 Symmetric 32-layer composite plate

This illustrative example consists in a 32-layer rectangular thin plate. The plate has a total thickness $t = 6.17$ mm, width a equal to 296.5 mm and length $b = 599$ mm. The lamination scheme is $[(0^\circ/45^\circ/-45^\circ/90^\circ)_4]_s$ and each lamina has the same thickness and is made by an orthotropic material with the following data: $E_1 = 157430$ MPa, $E_2 = E_3 = 9430$ MPa,

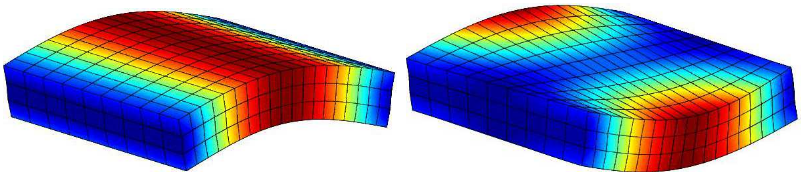

(a) Mode 1, $\omega^* = 7.312$ (b) Mode 2, $\omega^* = 7.919$

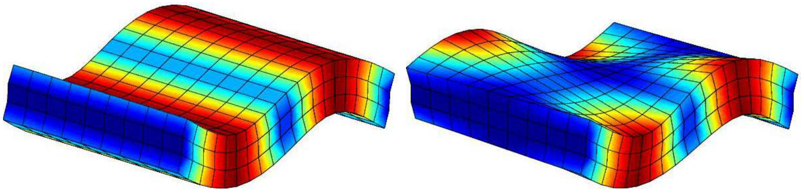

(c) Mode 3, $\omega^* = 18.134$ (d) Mode 4, $\omega^* = 18.642$

Figure 8.15 First four modes of the SS-F-SS-F cross-ply plate with $a/h = 5$, $N = 6$.

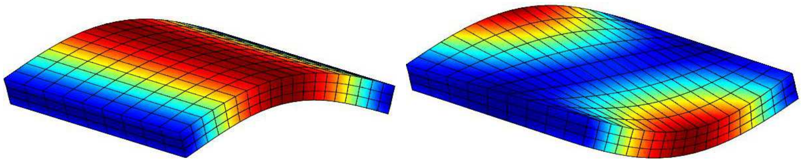

(a) Mode 1, $\omega^* = 9.544$ (b) Mode 2, $\omega^* = 10.376$

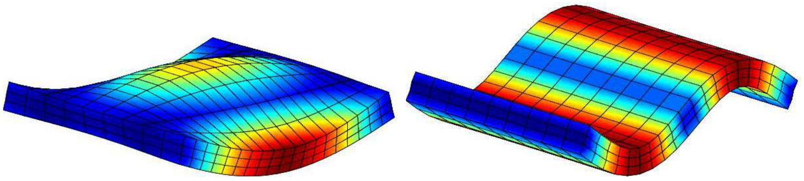

(c) Mode 3, $\omega^* = 28.829$ (d) Mode 4, $\omega^* = 29.250$

Figure 8.16 First four modes of the SS-F-SS-F cross-ply plate with $a/h = 10$, $N = 6$.

Table 8.12 Natural frequencies (Hz) of the FFFF symmetric 32-layer composite thin plate.

	Mode 1	Mode 2	Mode 3	Mode 4	Mode 5
			Reference solutions		
Plate FE model	112.3	138.8	302.2	313.4	479.3
Experimental	110.8	138.6	299.6	309.9	475.3
			Present 1D CUF - DSM solutions		
$N = 6$	112.4	139.7	303.6	314.3	480.4
$N = 5$	112.5	140.1	303.8	314.4	484.5
$N = 4$	112.5	140.5	305.6	315.3	484.8
$N = 3$	112.6	141.3	307.7	316.9	560.4
$N = 2$	113.4	141.6	311.2	326.9	564.8
$N = 1$	99.8	1484.3	2968.6	274.7	–
TBM	99.9	–	–	274.7	–
EBBM	99.9	–	–	275.3	–

$\nu_{12} = \nu_{13} = \nu_{13} = 0.4$, $G_{12} = G_{13} = G_{23} = 4520$ MPa, $\rho = 1644.18$ $\mathrm{Kg\,m^{-3}}$. Free edge boundary conditions are considered (FFFF).

The first five natural frequencies by the present DSM methodology are given in Table 8.12, where classical and refined 1D DSM-CUF TE models are compared to the reference solutions as shown. In particular, both the plate FEM solution from MSC Nastran meshed with 30×56 CQUAD4 elements and the results from experimental tests are shown in Table 8.12 for comparison purposes. The experimental setup is shown in Fig. 8.17.

The modal behaviour of the proposed plate is characterized by coupled bending/torsional modes on yz-plane (Modes 1 and 4), torsional modes (Modes 2 and 3), and a coupled bending/torsional mode on xy-plane (Mode 5). The first five mode shapes from the sixth-order ($N = 6$) TE model are shown in Fig. 8.18.

It should be noted that classical as well as linear TE ($N = 1$) beam models underestimate the natural frequencies of the 32-layer plate. In fact, these models do not predict torsional and coupling effects, therefore the natural frequencies by lower-order models that are shown in Table 8.12 are related to pure bending and do not capture coupled modes at all. The results actually show that at least a fourth-order ($N = 4$) TE beam model is necessary to detect coupled bending-torsional modes correctly in accordance to the reference solutions.

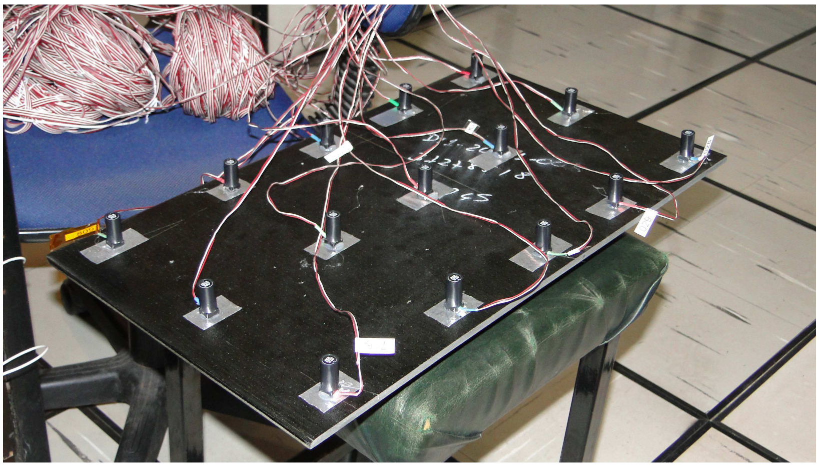

Figure 8.17 Experimental setup for the measurement of the natural frequencies, symmetric 32-layer plate.

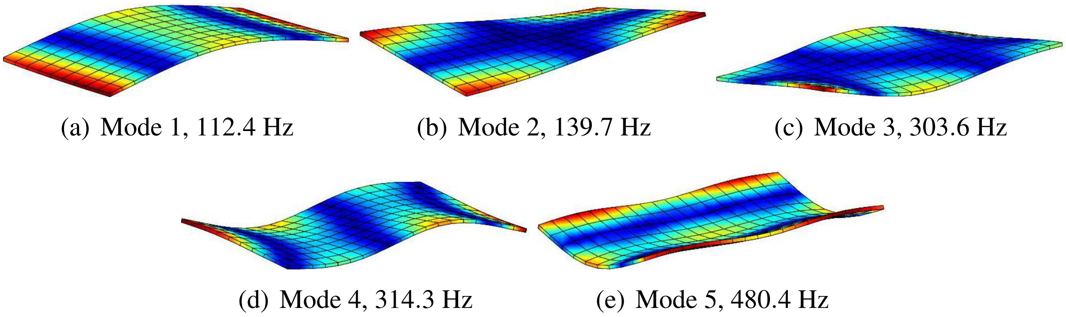

(a) Mode 1, 112.4 Hz (b) Mode 2, 139.7 Hz (c) Mode 3, 303.6 Hz

(d) Mode 4, 314.3 Hz (e) Mode 5, 480.4 Hz

Figure 8.18 First five modes of the FFFF symmetric 32-layer thin plate, $N = 6$.

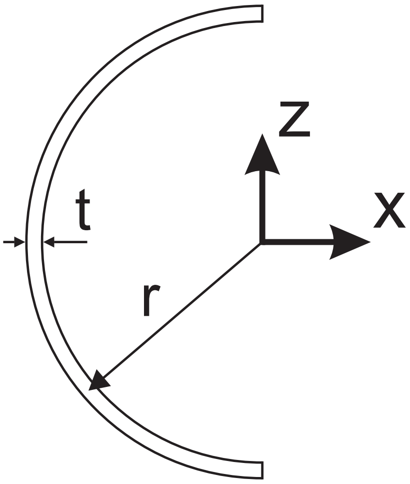

Figure 8.19 Semi-circular cross-section.

8.3 Free vibration of beam-columns

This section investigates the effect of an axial force on the free vibration characteristics of beams using refined models. Because of the clear superiority of the DSM, this solution method is preferred and used hereafter. The attention is focused on a thin-walled cross-section beam that is affected by high bending-torsional coupling and that is well documented in the literature. In this way, the enhanced capabilities of the present CUF formulation and its connectivity with the DSM will be clear from an easy comparison with readily available solutions in the literature.

8.3.1 Semi-circular cross-section beam

A thin-walled beam with the semi-circular cross-section shown in Fig. 8.19 is analyzed. The geometrical dimensions are taken from the literature [145–150] so that a direct and straightforward comparison of the results is possible. The radius, r, is assumed to be equal to 2.45×10^{-2} m, the thickness, t, is equal to 4×10^{-3} m, the length, L, of the beam is set to 0.82 m. The beam is made of aluminum with the Young modulus, E, equal to 68.9 GPa, the Poisson ratio, ν, equal to 0.3, and the density, ρ, equal to 2700 $\mathrm{Kg\,m^{-3}}$. The effect of boundary conditions and axial pre-stress (σ^0_{yy}) on the vibrations is evaluated in the analysis.

Table 8.13 shows the first eight natural frequencies ($\sigma^0_{yy} = 0$) for various boundary conditions and theories, including the present lower- to higher-order TE models. DSM is effectively used to carry out the analyses.

Tables 8.14 and 8.15 quote the vibration frequencies of the same structure undergoing compressive and tensile loadings, respectively. The superiority of the present DSM-CUF

Table 8.13 Natural frequencies (Hz) for the unloaded ($P = 0$) semi-circular cross-section beam.

		DSM-TE models								Reference solutions						
BCs	Frequency	EBBM	TBM	N=1	N=2	N=3	N=4	N=5	N=6	Ref. [149]	Ref. [151]	Ref. [145]	Ref. [146]	Ref. [147]	Ref. [150]	Ref. [148]
CF	1	31.88	31.87	31.87	31.96	31.88	31.88	31.88	31.88	31.81	-	31.80	-	-	31.80	-
	2	72.85	72.65	72.65	72.75	68.46	64.31	64.31	63.78	63.79	62.34	63.79	63.50	63.51	63.15	60.21
	3	199.57	198.85	198.85	198.94	177.96	139.97	139.97	137.09	137.70	129.87	137.68	137.38	137.39	137.66	128.30
	4	453.72	445.50	445.50	444.82	198.16	198.12	198.12	198.11	199.30	-	199.31	-	-	199.04	-
	5	557.72	553.02	553.02	551.15	348.68	282.66	282.66	276.52	278.40	259.26	278.35	275.81	275.82	276.04	257.90
	6	1089.87	1073.21	953.20	706.28	547.75	489.78	489.78	481.05	484.80	418.90	484.77	481.09	481.10	481.35	-
	7	1258.00	1207.36	1073.21	1063.81	591.58	547.39	547.39	547.34	558.10	-	558.09	-	-	-	-
	8	1536.22	1279.84	1207.36	1201.33	752.26	645.75	645.75	639.28	663.80	-	663.84	639.75	639.76	-	-
SS	1	89.15	89.06	89.06	88.98	88.93	88.86	87.72	89.27			89.27	-		89.23	
	2	204.25	203.10	203.10	202.90	190.32	176.13	152.94	150.28			150.44	149.66		149.74	
	3	352.00	350.45	350.43	348.77	343.79	356.19	320.87	316.60			320.32	317.25		317.78	
	4	766.40	755.28	754.25	723.95	478.99	381.61	354.31	353.91			357.11	-		356.44	
	5	811.66	794.15	794.15	791.22	508.48	483.01	374.31	365.33			365.81	364.02		364.31	
	6	1199.24	1108.70	1094.76	945.46	607.18	786.99	615.55	602.49			604.13	600.97		600.87	
	7	1584.68	1488.25	1480.12	1400.81	799.01	795.03	784.94	784.50			803.50	-		-	
	8	1806.64	1725.48	1725.48	1429.22	1039.69	1097.77	895.41	879.90			885.01	879.69		-	
CC	1	202.81	201.70	201.70	202.15	200.98	200.73	200.66	198.13			198.81	197.72		197.97	
	2	462.77	450.03	450.03	449.57	328.28	260.12	202.73	200.64			202.38	-		202.27	
	3	558.25	551.61	551.61	550.07	545.44	544.57	431.49	422.53			425.04	422.22		422.41	
	4	1091.92	1070.12	1070.12	1060.37	670.26	554.02	544.11	544.05			557.87	589.20		556.43	
	5	1266.11	1194.57	1194.57	1188.13	718.51	610.75	590.48	588.91			618.09	-		589.86	
	6	1799.44	1746.11	1746.11	1425.28	1047.87	881.69	698.59	686.43			695.63	687.15		687.16	
	7	2453.69	2236.51	1906.38	1717.13	1139.20	1045.77	999.41	985.40			999.31	991.51		-	
	8	2677.59	2559.47	2236.51	2213.76	1517.58	1232.01	1043.59	1043.35			1093.66	-		-	
FF	1	202.49	202.21	202.21	201.99	201.88	201.87	201.86	201.85			202.38	-			
	2	458.97	455.84	455.84	455.32	420.92	330.28	240.67	233.24			233.95	233.54			
	3	556.75	553.96	553.96	551.75	475.79	383.92	327.43	321.48			322.89	320.67			
	4	1087.85	1076.36	1076.36	1067.31	550.60	550.47	550.21	550.19			557.87	-			
	5	1248.92	1219.09	1219.09	1213.26	934.66	749.63	584.63	571.66			575.57	572.11			
	6	1790.88	1758.90	1758.90	1401.37	1011.99	782.99	675.30	668.13			684.22	669.44			
	7	2408.47	2295.73	1906.40	1733.89	1062.38	1061.88	863.28	846.48			857.91	850.63			
	8	2662.17	2559.51	2295.73	2274.85	1425.49	1106.07	1060.19	1060.05			1093.66	-			

Table 8.14 Natural frequencies (Hz) for the semi-circular cross-section beam undergoing a compression load ($P = 1790$ N).

		DSM-TE models								Reference solutions			
BCs	Frequency	EBBM	TBM	N=1	N=2	N=3	N=4	N=5	N=6	Ref. [149]	Ref. [151]	Ref. [145]	Ref. [150]
CF	1	25.11	25.10	25.10	25.19	25.13	25.11	25.11	25.11	25.01	-	25.01	25.01
	2	70.21	70.02	70.02	70.12	68.09	65.93	61.84	61.31	61.28	59.97	61.31	65.15
	3	192.89	192.17	192.17	192.25	191.61	176.87	138.50	135.57	136.00	128.10	136.15	138.98
	4	450.85	442.62	442.62	441.94	242.40	191.48	191.43	191.43	192.40	-	192.62	192.35
	5	552.11	547.39	547.39	545.51	402.38	345.95	279.39	273.19	274.90	256.00	275.03	276.53
	6	1084.58	1067.88	953.09	706.14	542.60	542.10	484.58	475.69	478.50	413.10	479.40	482.49
	7	1255.54	1204.87	1067.88	1058.44	726.84	587.95	541.74	541.70	550.70	-	552.47	-
	8	1536.16	1279.76	1204.87	1198.83	952.93	749.92	643.37	636.88	654.80	-	661.37	-
SS	1	84.60	84.50	84.50	84.41	84.37	84.30	83.59	84.69			84.69	84.66
	2	202.29	201.12	201.12	200.93	188.21	173.85	150.31	147.60			147.77	150.82
	3	347.59	346.03	346.01	344.35	339.64	351.71	319.63	315.34			319.07	318.44
	4	762.30	751.27	750.27	720.69	507.69	380.56	349.79	349.37			352.62	351.96
	5	809.69	792.14	792.14	789.20	604.55	479.70	370.03	360.93			361.42	364.75
	6	1196.89	1106.96	1093.10	943.53	794.57	782.42	609.69	596.50			598.16	601.16
	7	1581.64	1484.61	1476.40	1400.52	1036.23	790.50	780.35	779.91			799.02	-
	8	1804.66	1723.40	1723.40	1424.93	1232.42	1096.32	888.26	872.62			877.78	-
CC	1	200.34	199.22	199.22	199.67	198.50	198.25	198.18	195.86			196.55	198.18
	2	461.68	448.94	448.94	448.47	326.95	258.44	200.54	198.16			199.91	199.79
	3	554.89	548.24	548.24	546.68	542.05	541.17	427.44	418.39			420.89	422.63
	4	1088.24	1066.40	1066.40	1056.62	669.48	550.92	540.71	540.65			554.53	553.09
	5	1264.62	1193.03	1193.03	1186.59	716.16	609.87	589.43	587.84			616.77	590.51
	6	1795.56	1742.16	1742.16	1424.99	1044.10	877.43	693.24	681.00			690.47	687.26
	7	2452.03	2234.76	1906.17	1713.12	1135.96	1041.99	992.61	978.50			992.45	-
	8	2673.58	2559.31	2234.76	2212.00	1514.25	1226.59	1039.81	1039.57			1090.00	-
FF	1	454.66	451.53	192.09	191.87	191.76	191.75	191.73	191.73			192.23	
	2	548.83	546.02	451.53	451.00	416.46	328.91	238.80	231.31			232.02	
	3	1080.95	1069.41	546.02	543.79	474.81	379.24	322.13	316.10			317.53	
	4	1245.50	1215.62	1069.41	1060.33	542.63	542.51	542.25	542.23			549.93	
	5	1784.52	1752.46	1215.62	1209.79	930.65	744.72	578.24	565.11			569.08	
	6	2405.47	2292.63	1752.46	1401.07	1009.89	780.23	671.75	664.50			680.40	
	7	2656.15	2559.34	1906.19	1727.39	1055.38	1054.88	856.04	839.10			850.78	
	8	3072.31	2585.12	2292.63	2271.74	1421.17	1100.42	1053.18	1053.04			1086.74	

Table 8.15 Natural frequencies (Hz) for the semi-circular cross-section beam undergoing a traction load ($P = -1790$ N).

		DSM-TE models								Reference solutions	
BCs	Frequency number	EBBM	TBM	N=1	N=2	N=3	N=4	N=5	N=6	Ref. [151]	Ref. [150]
CF	1	37.19	37.17	37.17	37.26	37.19	37.18	37.17	37.18	-	37.11
	2	75.37	75.17	75.17	75.26	73.13	70.87	66.65	66.11	64.59	61.77
	3	206.00	205.29	205.29	205.38	204.73	179.03	141.40	138.55	131.57	136.32
	4	456.58	448.37	448.37	447.68	244.16	204.60	204.55	204.55	-	205.47
	5	563.28	558.59	558.59	556.73	407.40	351.40	285.89	279.84	262.45	275.57
	6	1095.14	1078.51	953.30	706.43	553.84	553.34	494.92	486.33	424.63	480.20
	7	1260.45	1209.84	1078.51	1069.14	732.19	595.18	552.98	552.93	-	-
	8	1536.29	1279.93	1209.84	1203.81	956.66	754.59	648.10	641.64	-	-
SS	1	93.49	93.40	93.40	93.32	93.28	93.19	100.72	93.63		93.60
	2	206.20	205.05	205.05	204.86	192.40	178.38	155.53	152.91		148.64
	3	356.36	354.82	354.80	353.14	347.86	360.62	322.12	317.86		317.13
	4	770.47	759.26	758.20	727.16	509.26	382.65	358.79	358.39		360.87
	5	813.62	796.16	796.16	793.23	609.80	486.30	378.55	369.67		363.85
	6	1201.57	1110.43	1096.42	947.41	803.43	791.54	621.35	608.41		600.57
	7	1587.73	1491.90	1483.84	1401.09	1043.13	799.53	789.50	789.06		-
	8	1808.63	1727.56	1727.56	1433.51	1235.00	1099.22	902.50	887.12		-
CC	1	205.25	204.14	204.14	204.59	203.43	203.18	203.11	200.34		197.74
	2	463.85	451.13	451.13	450.66	329.61	261.79	204.90	203.09		204.71
	3	561.58	554.96	554.96	553.43	548.81	547.94	435.50	426.63		422.19
	4	1095.59	1073.83	1073.83	1064.11	671.04	557.10	547.48	547.42		559.75
	5	1267.61	1196.10	1196.10	1189.67	720.86	611.63	591.50	589.96		589.19
	6	1803.31	1750.05	1750.05	1425.57	1051.63	885.93	703.91	691.84		687.04
	7	2455.36	2238.25	1906.59	1721.13	1142.43	1049.53	1006.15	992.24		-
	8	2681.60	2559.64	2238.25	2215.52	1520.86	1237.40	1047.35	1047.12		-
FF	1	212.08	211.81	211.81	211.59	211.48	211.47	211.45	211.45		
	2	463.23	460.11	460.11	459.59	425.32	331.65	242.52	235.14		
	3	564.55	561.77	561.77	559.58	476.77	388.54	332.63	326.77		
	4	1094.71	1083.26	1083.26	1074.24	558.44	558.31	558.05	558.03		
	5	1252.34	1222.55	1222.55	1216.71	938.66	754.52	590.95	578.12		
	6	1797.22	1765.31	1765.31	1401.67	1014.07	785.73	678.79	671.69		
	7	2411.47	2298.83	1906.61	1740.36	1069.33	1068.84	870.48	853.81		
	8	2668.18	2559.67	2298.83	2277.96	1429.81	1111.69	1067.15	1067.01		

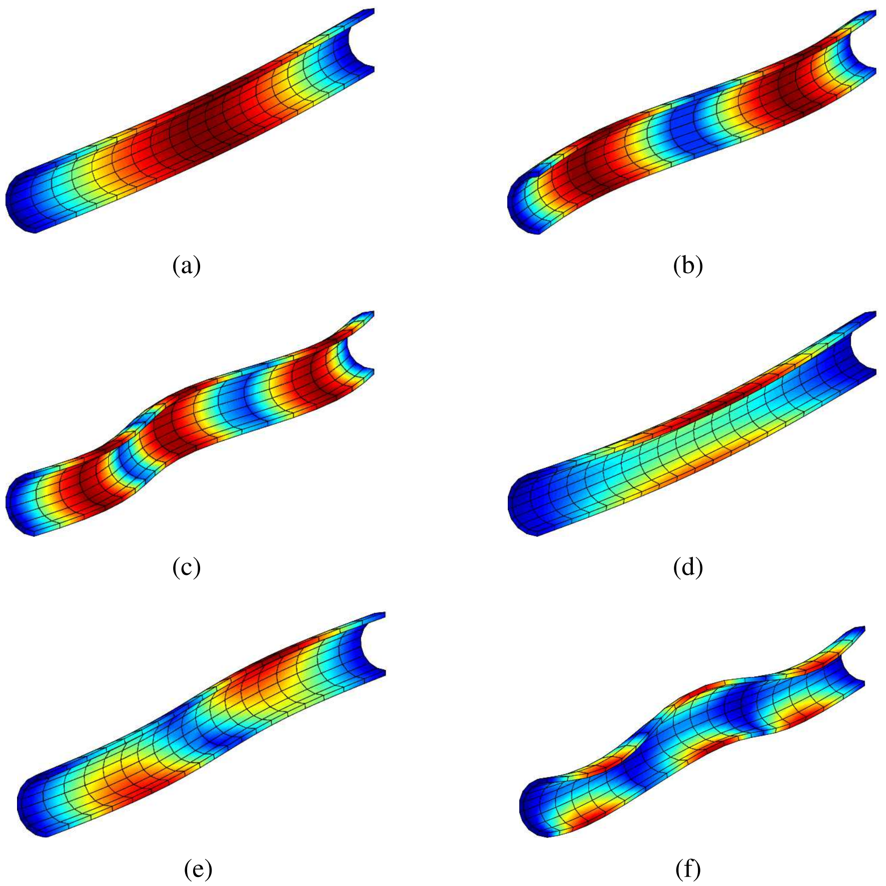
(a) (b) (c) (d) (e) (f)

Figure 8.20 Uncoupled (a, b, c) and coupled (d, e, f) modal shapes for the unloaded ($P = 0$) SS semi-circular beam; DSM-TE $N = 6$ model.

models is clearly evident from the comparison with other theories.

Figure 8.20 shows both the uncoupled and coupled modal shapes for the SS semi-circular beam. Some comments arise from the analysis.

- Classical and lower-order CUF models can only detect the first uncoupled modes. Refined models are necessary to describe the higher modes and the coupling behaviour of the structure.

- As a consequence of compressive axial load, obviously, the natural frequencies of the coupled beam decrease. By contrast, by applying a tensile load, the natural frequencies increase as expected. The effects of coupling as well the axial load are correctly taken into account by the present approach which is in accord with the solutions from the literature.

Table 8.16 First three non-dimensional buckling loads ($P_{cr}^* = \frac{P_{cr}L^2}{\pi^2 EI}$) of the metallic beam, $L/h = 20$.

Mode	Euler	Matsunaga [152]	TBM		N=1		N=2		N=3	
			FEM [153]	DSM	FEM [153]	DSM	FEM [153]	DSM	FEM [153]	DSM
1	1.000	0.992	0.990	0.993	0.993	0.993	0.993	0.993	0.992	0.992
2	4.000	3.873	3.875	3.886	3.884	3.886	3.885	3.887	3.873	3.874
3	9.000	8.387	8.422	8.444	8.437	8.444	8.444	8.451	8.387	8.391

8.4 Buckling analysis

As an interesting, but demanding set of problems, linearized buckling analyses are carried out. Solid and thin-walled cross-section columns made of isotropic and composite materials are addressed. Here, again, DSM is used in this context to solve the strong-form equations of CUF beam theories.

8.4.1 Metallic rectangular cross-section column

A simply-supported metallic column is analysed as illustrative example. The same structure was addressed by Matsunaga [152] and Ibrahim *et al.* [153]. The results given by these authors are quoted later for comparison purposes. The beam-column has a solid rectangular cross-section as shown in Fig. 8.7 and the material is aluminium alloy with elastic modulus $E = 71.7$ GPa and Poisson's ratio $\nu = 0.3$.

Table 8.16 shows the first three critical buckling loads for a length-to-height ratio, L/h, equal to 20. Although only the first critical buckling load is of practical significance, the other two critical buckling loads are given for benchmarking comparison purposes. Critical loads are given in non-dimensional form as follows:

$$P_{cr}^* = \frac{P_{cr}L^2}{\pi^2 EI} \tag{8.5}$$

where I is the moment of inertia, $I = \frac{bh^3}{12}$. The second column of Table 8.16 shows the n-th non-dimensional critical buckling load from the Euler buckling formula give by

$$P_{cr_{Euler}}^* = n^2 \tag{8.6}$$

In column 3 the results by Matsunaga [152] are given, whereas columns 4 to 7 report the results by classical and refined models based on DSM TE CUF models of the present thesis.

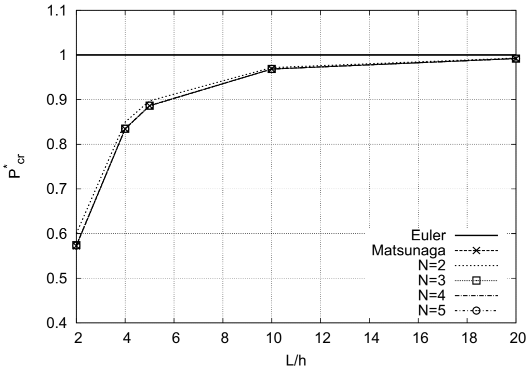

Figure 8.21 First non-dimensional critical buckling load ($P^*_{cr} = \frac{P_{cr}L^2}{\pi^2 EI}$) versus length-to-height ratio, L/h, for the rectangular metallic beam.

Table 8.17 First non-dimensional buckling load ($P^*_{cr} = \frac{P_{cr}L^2}{\pi^2 EI}$) of the metallic beam for different length-to-height ratios L/h.

L/h	Euler	Matsunaga [152]	Present CUF-DSM			
			N=2	N=3	N=4	N=5
2	1.000	0.5723	0.5999	0.5741	0.5733	0.5730
4	1.000	0.8342	0.8497	0.8350	0.8349	0.8348
5	1.000	0.8860	0.8973	0.8866	0.8866	0.8865
10	1.000	0.9683	0.9718	0.9685	0.9685	0.9685
20	1.000	0.9919	0.9930	0.9919	0.9919	0.9919

The exact solutions by the present DSM are compared to those from FEM, which were used in [153].

Figure 8.21 shows the variation of the first non-dimensional critical buckling load versus the length-to-height ratio, L/h, for different higher-order beam models by applying the present approach and the results are compared with those reported in [152] and also with those obtained from classical Euler theory. For benchmarking reasons, the results are given in tabular form in Table 8.17.

The following comments arise from the analysis:

- Refined theories are mandatory when dealing with buckling analysis of short beam-columns.
- The Euler buckling formula overestimates the critical loads of the beam-columns, even though when a high slenderness ratio is considered. This is dangerous from a design point of view.

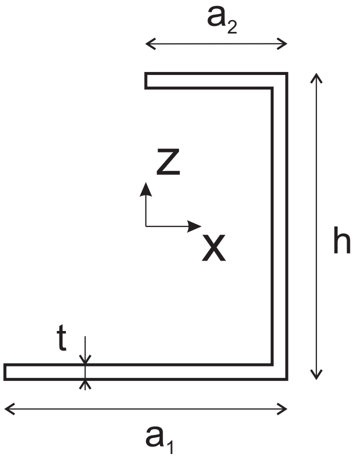

Figure 8.22 Cross-section of the C-shaped beam.

Table 8.18 Flexural-torsional buckling loads [N] for the axially compressed C-section beam.

Mode	Present CUF-DSM							ABAQUS [154]	Kim et al. [154]	Vo and Lee [155]
	$N=2$	$N=3$	$N=4$	$N=5$	$N=6$	$N=7$	$N=8$			
1	14.227	14.227	14.178	14.178	14.111	14.111	13.875	14.001	13.789	12.977
2	127.805	127.242	125.076	122.885	120.428	119.034	117.375	113.100	111.840	113.440
3	212.883	212.086	209.810	206.955	203.568	201.510	199.125	190.080	191.160	190.567
4	350.977	348.070	332.065	315.729	298.065	289.034	280.125	256.670	255.100	263.999
5	679.430	666.727	606.728	551.271	498.744	475.502	454.875	408.530	406.280	–

- Higher-order CUF theories are effective in refining the solution and the results are in good agreement with those available in the literature.

- The critical buckling load becomes lower as the expansion order for TE CUF models increases. This is significant because other theories give unconservative estimates of critical buckling loads, which can be dangerous.

- The exact solutions provided with the DSM are slightly higher then those by FEM. This is unusual and may be due to numerical problems inherent in FEM.

8.4.2 Thin-walled symmetric and non-symmetric cross-sections

A cantilever beam-column with unequal channel section shown in Fig. 8.22 is now considered. The main dimensions of the cross-section are $a_1 = 4$ cm, $a_2 = 2$ cm, $h = 10$ cm and $t = 0.5$ cm. The beam has a length $L = 2$ m and is made of homogeneous isotropic material with elastic modulus $E = 3 \times 10^4$ N/cm^2 (0.3 GPa) and shear modulus $G = 1.15 \times 10^4$ N/cm^2 (0.115 GPa).

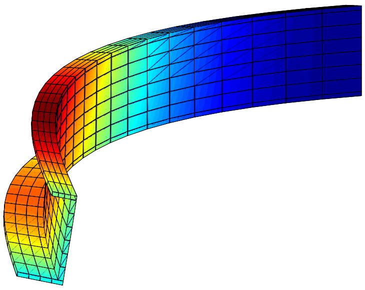

Figure 8.23 Second flexural-torsional buckling mode of the C-shaped section beam by the seventh-order ($N = 7$) CUF model.

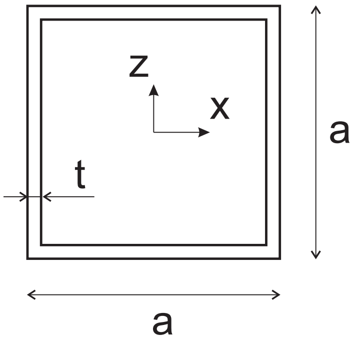

Figure 8.24 Cross-section of the box beam.

Table 8.18 shows the first three critical buckling loads by higher-order beam models by the present CUF-DSM methodology. The results are compared with those given by Vo and Lee [155], who developed an analytical model based on the shear deformable beam theory, and also with those presented by Kim *et al.* [154], where a general formulation for spatial free vibration and stability analysis of non-symmetric thin-walled DS space frame members considering the effects of shear deformations was presented. A FEM solution from ABAQUS is also provided in Ref. [154]. Figure 8.23 shows the second buckling mode by the seventh-order ($N = 7$) CUF-DSM model. The figure clearly shows that the present method can predict the flexural-torsional buckling load accurately. The analysis highlights that

- Relatively higher-order kinematics are needed to detect flexural-torsional buckling modes of axially loaded thin-walled structures accurately.
- The results by the proposed CUF-DSM models are in good agreement with the results found in the literature.

A hollow square cross-section beam is considered next. The cross-section, which is shown in Fig. 8.24, has each side equal to $a = 0.1$ m and the uniform thickness $t = a/20$.

Table 8.19 Critical buckling loads [MPa] for various length-to-side ratio, L/a, of the SS square box beam.

L/a	3D FEM [156]	$N=4$		$N=3$		$N=2$		TBM		EBBM	
		Ref. [156]	DSM	Ref. [156]	DSM	Ref. [156]	DSM	Ref. [156]	DSM	Ref. [156]	DSM
100	10.651	10.664	10.664	10.664	10.664	10.668	10.668	10.668	10.668	10.672	10.672
50	42.497	42.551	42.551	42.551	42.551	42.605	42.604	42.604	42.604	42.669	42.669
20	261.040	261.340	261.341	261.340	261.343	263.360	263.359	263.320	263.320	265.850	265.850
15	457.010	457.310	457.305	457.320	457.318	463.510	463.509	463.400	463.400	471.260	471.260

The whole structure is made of the same aluminium alloy as in the case of the rectangular solid cross-section beam-column. The critical buckling loads for various length-to-side ratios, L/a, are shown in Table 8.19, where the results by the present CUF-DSM methodology are compared with those from Giunta *et al.* [156], who adopted Navier-type solutions for simply-supported (SS) TE CUF beams and 3D FE models by ANSYS. It is clear that DSM can provide analytical solutions for CUF models, which exhibit 3D capabilities as the expansion order N is increased. Table 8.20 shows the first four buckling modes for the slender configuration, $L/a = 100$. The i-th mode is characterized by having i half-waves in the axial direction of the beam. In is intended that in the proposed analyses, the first critical buckling load is of practical importance. Higher critical buckling loads are given in this thesis so that the results can be used as an aid to validate FEM and other methods. It is clear from the analysis that, in the case of the slender beams, classical theories yield acceptable results for this problem unless higher buckling modes are required. In the case of short beams (e.g. $L/a = 15$), refined beam models are indeed necessary to obtain a 3D-like solution.

8.4.3 Cross-ply laminated beams

In this section a number of cross-ply laminated beam-columns are addressed and their stability characteristics are investigated. First, simply supported (SS) composite beam-columns with symmetric cross-ply $[0^\circ/90^\circ/0^\circ]$ and anti-symmetric cross-ply $[0^\circ/90^\circ]$ stacking sequences are considered. Each lamina has the same thickness and two different sets of material properties are considered as follows:

$$\text{Material set I:} \qquad E_1/E_2 = 10,\ G_{12} = G_{13} = 0.6E_2,\ G_{23} = 0.5E_2,\ \nu_{12} = 0.25$$

$$\text{Material set II:} \qquad E_1/E_2 = 10,\ G_{12} = G_{13} = 0.5E_2,\ G_{23} = 0.2E_2,\ \nu_{12} = 0.25$$

Table 8.20 First four buckling loads [MPa] of the SS square box beam for $L/a = 100$.

Model	Mode 1	Mode 2	Mode 3	Mode 4
Giunta et al. [156]				
3D FEM	10.651	42.443	95.008	167.780
$N = 4$	10.664	42.551	95.339	168.500
$N = 3$	10.664	42.551	95.339	168.500
$N = 2$	10.668	42.604	95.607	169.340
TBM	10.668	42.603	95.602	169.330
EBBM	10.672	42.669	95.934	170.370
Present CUF-DSM				
$N = 4$	10.664	42.551	95.339	168.507
$N = 3$	10.664	42.551	95.339	168.507
$N = 2$	10.668	42.604	95.607	169.340
TBM	10.668	42.603	95.603	169.327
EBBM	10.672	42.669	95.935	170.373

The critical buckling loads from the present higher-order TE CUF-DSM refined beam theories are shown in Table 8.21 and they are given in the following non-dimensional form:

$$P^*_{cr} = \frac{P_{cr}L^2}{E_2bh^3} \tag{8.7}$$

In Table 8.21 the proposed solutions are compared with those available in the literature, see Vo and Thai [159] and Aydogdu [158]. The former [159] used FEM in conjunction with both a first-order beam theory (FSDT) and a higher-order beam theory (HSDT) accounting for the parabolic variation of shear strains through the thickness. The latter [158] is based on a three-degree-of-freedom shear deformable beam theory and the Ritz method was used to carry out stability analyses. The following comments are noteworthy:

- The present formulation can deal with the linearized stability analysis of composite laminated beam-columns.
- The solutions from both first- and higher-order beam models from the literature can be improved by the present CUF-DSM theories, especially when short beams and softer materials (e.g. Material set II) are considered.

The last illustrative example is a rectangular beam with symmetric cross-ply $[(0°/90°)_2]_s$ arrangements. The laminate is made of eight identical graphite/epoxy plies. The material has the following characteristics: $E_1 = 1.344 \times 10^5$ MPa, $E_2 = E_3 = 1.034 \times 10^4$ MPa,

Table 8.21 Effect of length-to-height ratio, L/h , on the non-dimensional critical buckling loads ($P_{cr}^{*} = \frac{P_{cr}L^2}{E_2 bh^3}$) of symmetric and anti-symmetric cross-ply SS laminated beams.

L/h	Present CUF-DSM				Vo and Thai [157]		Aydogdu [158]
	$N=2$	$N=3$	$N=4$	$N=5$	FSDT	HSDT	
			Material set I - [0°/90°/0°]				
5	4.992	4.668	4.667	4.666	4.752	4.709	4.726
10	6.937	6.751	6.750	6.749	6.805	6.778	–
20	7.677	7.618	7.618	7.617	7.630	7.620	7.666
50	7.917	7.904	7.904	7.903	7.897	7.896	–
			Material set I - [0°/90°]				
5	1.856	1.831	1.820	1.816	1.883	1.910	1.919
10	2.140	2.130	2.126	2.125	2.148	2.156	–
20	2.226	2.223	2.222	2.222	2.226	2.228	2.241
50	2.252	2.252	2.252	2.252	2.249	2.249	–
			Material set II - [0°/90°/0°]				
5	4.319	3.666	3.666	3.560	4.069	3.717	3.728
10	6.600	6.126	6.126	6.033	6.420	6.176	–
20	7.570	7.403	7.402	7.366	7.503	7.416	7.459
50	7.896	7.868	7.868	7.862	7.875	7.860	–
			Material set II - [0°/90°]				
5	1.745	1.711	1.710	1.705	1.605	1.758	1.765
10	2.100	2.086	2.086	2.084	1.876	2.104	–
20	2.215	2.211	2.211	2.210	1.958	2.214	2.226
50	2.252	2.252	2.252	2.252	1.983	2.247	–

Table 8.22 Critical buckling loads [N] of the 8-layer cross-ply rectangular beam for different boundary conditions.

BCs	Present CUF-DSM					Chattopadhyay and Radu [160]		
	EBBM	$N=2$	$N=3$	$N=4$	$N=5$	CLPT	FSDT	HSDT
CF	16696	15752	15615	15607	15606	16344	15772	15364
CC	261957	163934	151256	151137	151132	261623	165644	152179

$G_{12} = G_{13} = 4.999 \times 10^3$ MPa, $G_{23} = 1.999 \times 10^3$ MPa, $\nu_{12} = \nu_{13} = \nu_{23} = 0.33$. The beam-column has a length $L = 127$ mm, width $b = 12.7$ mm, and thickness $h = 10.16$ mm. Table 8.22 shows the critical buckling loads of this beam-column for both clamped-free (CF) and clamped-clamped (CC) boundary conditions. Classical EBBM and up to the fifth-order ($N = 5$) CUF-DSM beam models are used for the results given in Table 8.22, which are compared to those provided by Chattopadhyay and Radu [160], who used the Classical Lamination Plate Theory (CLPT), the First-order Shear Deformation Theory (FSDT), and a Higher-order Shear Deformation Theory (HSDT) to carry out reasonably detailed instability analyses of composite plates [161]. The results from the present theory clearly demonstrate the capability of the CUF-DSM theory on beam-column modelling, which is able to reproduce and in many ways refine the solutions from 2D plate models.

Chapter 9

Summary of Principal Contributions

9.1 Work summary

Application of mathematical theory of elasticity and advanced kinematics in the development of refined beam theories have been thoroughly explored in this thesis. The main novelty of the work lies in developing the governing differential equations and seeking their solutions in concise, compact and unified forms. This has been possible by employing the Carrera Unified Formulation (CUF), which allows for a systematic approximation of the 3D problems to 1D ones with desired accuracy.

Chapter 1 gives a brief overview of the existing beam theories. Attention in the chapter is focused on both classical (e.g., Euler-Bernoulli and Timoshenko models) and refined theories, including those coming from the shear correction, the Variational Asymptotic Method (VAM), the Generalized Beam Theories (GBT), and the Proper Generalized Decomposition (PGD) method. An outline of some numerical methods adopted for the resolution of strong-form governing equations has also been given in Chapter 1. In particular, the conditions that a structure should satisfy in order to obtain closed-form analytical solutions have been reviewed and critically examined. The Dynamic Stiffness Method (DSM) and collocations schemes (such as Radial Basis Functions, RBFs, method) have also been introduced in this chapter as practical, but effective numerical methods for exact as well as approximate solutions for beam problems.

Beam theories and related displacement field have been discussed in detail in Chapter 2. Classical beam models have been given extensive coverage, including a commentary on the limitations they are affected by (e.g., the violation of the homogeneous condition of transverse stress components at the unloaded edges of the beam). The use of the shear correction factors has been described as an approximate, but ad-hoc attempt to take into account the actual distribution of the shear stress field. Advanced models have been described subsequently. The main idea behind Chapter 2 has been the fact that due recognition should be given to complex physics and kinematics which demand richer displacement fields. This aspect has been elaborately discussed by considering many of the well-know refined beam theories.

In Chapter 3 the constitutive equations and the displacement-strain relations have been introduced and exemplificated. Next, beam theories have been formulated using CUF, which has been extensively applied in the domain of solid-mechanics for plate/shell and beam problems. This is accomplished by expressing the 3D displacement field as an N^{th}-order truncated expansion series of the generalized unknowns (i.e. displacements and displacement derivatives) to obtain variable kinematic beam models. The resulting beam models have been referred to as TE (Taylor Expansion) because Taylor-series polynomials are the basic origin of the displacement field. Classical beam models and many other higher-order models (e.g., the Vlasov-Reddy third-order model) are captured as degenerate cases of the TE. Pure displacement variables have also been used in the same chapter to create beam models and they have been referred to as LE (Lagrange Expansion) models. LE refined models are developed within the framework of CUF by interpolating the cross-sectional unknowns with bi-linear, quadratic or cubic Lagrange polynomials or a combination of them.

The governing differential equations have been derived using a variational approach in Chapter 4 particularly by employing the principle of virtual work. The variations of virtual works of the strain energy, the external loadings, the inertial loads and the axial pre-stresses are written in terms of fundamental nuclei. The main characteristic of the fundamental nuclei is that their formal expression does not depend on the order of the beam model. Therefore, by suitably expanding the nuclei depending on the beam theory and order, the governing differential equations of the generic beam model can be automatically formulated. The investigation is focused on static analysis, free vibration of beam and beam-columns, and buckling analysis.

Chapters 5 to 7 have been devoted to analytical and numerical solutions of the strong-form governing differential equations of generic refined beam theories. Chapter 5, in particular, discusses closed-form analytical solutions, which are generally available for the case of simply-supported beams of metallic constructions or cross-ply laminated structures. Chapter 6 shows how to avoid the limitations of conventional theories by employing a collocation method based on RBFs. Collocation methods, generally, suffer from numerical instabilities, and therefore, in Chapter 7, a numerically exact method based on DSM has been introduced. This chapter represents one of the most innovative aspects of the thesis, since it allows, for the first time in the literature, the resolution of arbitrarily chosen refined beam assemblies in an exact manner. In fact, by exploiting CUF, the transcendental dynamic stiffness matrix is written in the form of a fundamental nucleus, whose expression does not change regardless of the mathematical structure of the 1D model. This remarkable achievement has been possible due to the application of the Wittrick-Williams algorithm, which allows for the iterative resolution of non-linear eigenvalue problems in an exact manner.

Selective, but important numerical results have been illustrated in Chapter 8. Attention here is focused on closed-form static analyses of laminated structures; free vibration of metallic, thin-walled and composite beams; vibrations of metallic and composite beam-columns; and buckling analyses of slender structures. Wherever possible, the results have been compared with those available in the literature and also by using commercial codes and experiments. Some interesting conclusions and remarks based on the numerical investigations are briefly summarized in the following chapter.

9.2 Main contributions

The main novelties and important contributions resulting from the present research can be briefly summarized as in the following:

- By using the principle of virtual work and the recursive notation of CUF, the differential form of the equations of motion of axially loaded beams have be written in terms of a fundamental nucleus.

- For the first time, the strong form governing equations for buckling and free vibration analysis of beams and beam-columns have been solved by using RBFs method and DSM. The resulting formulation has been implemented in a Matlab code able to deal with general geometries and boundary conditions.

- The main achievement has been surely the extension of DSM to refined CUF models, which has resulted in an innovative and powerful tool able to reproduce exactly the mechanical behaviour of beam and plate structures. As an example, exact free vibration characteristics of free-edge composite plates have been analysed and benchmark results have been given for future investigations and assessments. In fact, closed-form solutions of free and unconstrained plate structures were not available with conventional methods.

- Closed-form analytical results from the stress analysis of composite structures with layer-wise accuracy have been obtained by imposing a Navier-type solution to LE-CUF models.

Chapter 10

Conclusions and scope for future work

10.1 Conclusions

The following major, but general conclusions can be drawn from the investigation carried out in this thesis:

- LE models provide accurate solutions for the static analysis of metallic and composite structures. In fact, LE beam theory is able to describe correctly the interlaminar continuity of the shear stresses as well as the zig-zag behaviour of the axial stresses.
- Other theories from the literature, including TE, cannot ensure the same degree of accuracy as LE models, if accurate stress analysis is required.
- The layer-wise capabilities of LE can be significantly enhanced by refining the beam theory at local level.
- Both TE and LE CUF models are effective in modal and buckling analyses of metallic and composite beam structures.
- TE models are particularly effective for the free vibration analysis of thin-walled structures.
- Analytical closed-form solutions are preferred if possible, but in the case of generic boundary conditions and stacking sequences, DSM is strongly suggested as the best candidate because it can provide exact solutions with low computational efforts. RBFs and, in general, collocation methods may be sometimes computationally more convenient, but they can be affected by numerical inconsistencies if ad-hoc strategies and mathematical filters are not employed. As a general guideline, the use of RBFs in the

framework of CUF is rather discouraged, because numerical problems can be more acute when the order of the theory is increased. By contrast, DSM is an extremely robust method. For this reason, it has been employed for most of the analyses carried out in this thesis.

- If compared with available numerical methods based on weak-form formulation (such as FEM), the proposed DSM-CUF method presents several advantage both in terms of accuracy and efficiency. In fact, one single DS element is sufficient, in principle, for acquiring the vibration characteristics of structures in the entire frequency band of interest, making sure that the value of j_0 is known.
- As in FEM, exact DSM elements can be assembled and used to analyse complex structures. This characteristic has not been fully investigated in the present work and will be the subject of future research although.
- Pre-stress loads play very important roles in free vibration analyses of beam-columns. The models presented describe accurately the effects of pre-stresses, particularly due to axial loads. Those effects are much more pronounced when the order of the theory is increased, especially in the case for which mechanical couplings are present.
- The beam models developed in this thesis have demonstrated excellent accuracy and computational efficiencies in all cases, including the investigation of buckling. Of particular interest is the application related to composite beams and thin-walled box structures, which provides added confidence for future research in advanced aerospace structures.

10.2 Scope for future work

This thesis has answered several questions, but it has opened up potential possibilities and has given new prospectives in elastodynamic fields of study that may be the subjects of future research. DSM employs the exact wave solutions of the governing differential equations to formulate structural element properties that deal with the continuous mass and stiffness distributions exactly. Assemblies of DS elements can, thus, depict the correct free vibration behaviour of complex structures within any frequency range of interest. When coupled with CUF, the methodology proposed in this thesis can be extremely effective when extended to dynamic response analysis of metallic and composite structures because accurate solutions can only be obtained by capturing all necessary high frequency wave modes. For the same reason and due to the efficacy of CUF refined beam models in dealing with thin-walled structures, attention can also be focussed on acoustics applications with particular emphasis to aerospace constructions. Eventually, the effects of damping in the aforementioned problems need to be investigated. This task can be accomplished by DSM, because the DS matrix can be formulated by incorporating the stiffness, mass and damping characteristics of the structural element, but the Wittrick-Williams algorithm will require further enhancements.

Appendix A

Material coefficients

In the case of *orthotropic materials* (i.e., materials with three mutually perpendicular planes of elastic symmetry) the material constitutive law matrix has 9 independent coefficients. With respect to the material coordinate system the Hooke's law (Eq. 3.5) can be written as

$$\begin{Bmatrix} \sigma_{33} \\ \sigma_{22} \\ \sigma_{11} \\ \sigma_{21} \\ \sigma_{31} \\ \sigma_{23} \end{Bmatrix} = \begin{bmatrix} C_{33} & C_{23} & C_{13} & 0 & 0 & 0 \\ C_{23} & C_{22} & C_{12} & 0 & 0 & 0 \\ C_{13} & C_{12} & C_{11} & 0 & 0 & 0 \\ 0 & 0 & 0 & C_{44} & 0 & 0 \\ 0 & 0 & 0 & 0 & C_{55} & 0 \\ 0 & 0 & 0 & 0 & 0 & C_{66} \end{bmatrix} \begin{Bmatrix} \varepsilon_{33} \\ \varepsilon_{22} \\ \varepsilon_{11} \\ \varepsilon_{21} \\ \varepsilon_{31} \\ \varepsilon_{23} \end{Bmatrix} \tag{A.1}$$

Coefficients C_{ij} are defined in the usual notation as follows:

$$\begin{aligned} C_{11} &= \frac{E_1 (1 - \nu_{23}\nu_{32})}{\Delta}; \quad C_{12} = \frac{E_1 (\nu_{21} + \nu_{23}\nu_{31})}{\Delta}; \quad C_{13} = \frac{E_1 (\nu_{31} + \nu_{21}\nu_{32})}{\Delta}; \\ C_{22} &= \frac{E_2 (1 - \nu_{13}\nu_{31})}{\Delta}; \quad C_{23} = \frac{E_2 (\nu_{32} + \nu_{12}\nu_{31})}{\Delta}; \quad C_{33} = \frac{E_3 (1 - \nu_{12}\nu_{21})}{\Delta}; \\ C_{44} &= G_{21}; \qquad C_{55} = G_{31}; \qquad C_{66} = G_{23}; \end{aligned} \tag{A.2}$$

where:

$$\Delta = 1 - \nu_{12}\nu_{21} - \nu_{13}\nu_{31} - \nu_{23}\nu_{32} - \nu_{12}\nu_{23}\nu_{31} - \nu_{13}\nu_{21}\nu_{32} \tag{A.3}$$

The terms $\{E_i : i = 1, 2, 3\}$ are the Young moduli, $\{\nu_{ij} : i, j = 1, 2, 3\}$ are the Poisson ratios and $\{G_{ij} : i = 2, 3; j = 1, 3\}$ are the shear moduli in the *material coordinate system*. The Poisson ratios are defined as:

$$\nu_{ij} = -\frac{\varepsilon_{jj}}{\varepsilon_{ii}} \qquad i, j = 1, 2, 3 \qquad i \neq j \tag{A.4}$$

In Eq. (A.1) the material constitutive relationship has been referred to the material coordinate system $(1, 2, 3)$, which has been graphically illustrated in Fig. 3.1. This system is supposed to be aligned with the fibres in a unidirectionally reinforced lamina that lies in the $2-3$ plane. In general, the material coordinate system is different from the physical coordinate system (x, y, z). Thus, one may want to write the constitutive law with respect to (x, y, z) by employing coordinate transformation equations. The stress vector $\boldsymbol{\sigma} = \left\{\sigma_{yy}\ \sigma_{xx}\ \sigma_{zz}\ \sigma_{xz}\ \sigma_{yz}\ \sigma_{xy}\right\}^T$ in physical coordinates can be obtained in terms of the stress vector $\boldsymbol{\sigma}_m = \{\sigma_{33}\ \sigma_{22}\ \sigma_{11}\ \sigma_{21}\ \sigma_{31}\ \sigma_{23}\}^T$ in material coordinates as follows:

$$\boldsymbol{\sigma} = \mathbf{T}\boldsymbol{\sigma}_m \tag{A.5}$$

where $\mathbf{T}$ is the following 6×6 transformation matrix:

$$\mathbf{T} = \begin{bmatrix} \cos^2\theta & \sin^2\theta & 0 & 0 & 0 & 2\sin\theta\cos\theta \\ \sin^2\theta & \cos^2\theta & 0 & 0 & 0 & -2\sin\theta\cos\theta \\ 0 & 0 & 1 & 0 & 0 & 0 \\ 0 & 0 & 0 & \cos\theta & -\sin\theta & 0 \\ 0 & 0 & 0 & \sin\theta & \cos\theta & 0 \\ -\sin\theta\cos\theta & \sin\theta\cos\theta & 0 & 0 & 0 & \cos^2\theta - \sin^2\theta \end{bmatrix} \tag{A.6}$$

The physical strain vector can be related to the strain vector in the material coordinate in a similar way,

$$\boldsymbol{\varepsilon}_m = \mathbf{T}^T\boldsymbol{\varepsilon} \tag{A.7}$$

By substituting Eqs. (A.1) and (A.7) into Eq. (A.5), a *transformed constitutive relationship* $\widetilde{\mathbf{C}}$ is obtained as follows:

$$\widetilde{\mathbf{C}} = \mathbf{T}\mathbf{C}_m\mathbf{T}^T \tag{A.8}$$

The transformed constitutive law described by the matrix $\widetilde{\mathbf{C}}$ contains the elastic coefficients referred to the physical coordinate system. The stress-strain relations referred to the physical coordinate system (cf. Eqs. (3.5) and (3.6)) can then be written as follows:

$$\begin{Bmatrix} \sigma_{yy} \\ \sigma_{xx} \\ \sigma_{zz} \\ \sigma_{xz} \\ \sigma_{yz} \\ \sigma_{xy} \end{Bmatrix} = \begin{bmatrix} \widetilde{C}_{33} & \widetilde{C}_{23} & \widetilde{C}_{13} & 0 & 0 & \widetilde{C}_{36} \\ \widetilde{C}_{23} & \widetilde{C}_{22} & \widetilde{C}_{12} & 0 & 0 & \widetilde{C}_{26} \\ \widetilde{C}_{13} & \widetilde{C}_{12} & \widetilde{C}_{11} & 0 & 0 & \widetilde{C}_{16} \\ 0 & 0 & 0 & \widetilde{C}_{44} & \widetilde{C}_{45} & 0 \\ 0 & 0 & 0 & \widetilde{C}_{45} & \widetilde{C}_{55} & 0 \\ \widetilde{C}_{36} & \widetilde{C}_{26} & \widetilde{C}_{16} & 0 & 0 & \widetilde{C}_{66} \end{bmatrix} \begin{Bmatrix} \varepsilon_{yy} \\ \varepsilon_{xx} \\ \varepsilon_{zz} \\ \varepsilon_{xz} \\ \varepsilon_{yz} \\ \varepsilon_{xy} \end{Bmatrix} \tag{A.9}$$

Carrying out the matrix multiplications in Eq. (A.8) for the orthotropic case, the elastic coefficients of the transformed matrix $\widetilde{\mathbf{C}}$ are expressed as a function of the coefficients of the material stiffness matrix $\mathbf{C}$ and the ply angle θ. The elements of the $\widetilde{\mathbf{C}}$ matrix are given as follows:

$$\begin{aligned}
\widetilde{C}_{33} &= C_{33}\cos^4\theta + 2\left(C_{23}+2C_{66}\right)\sin^2\theta\cos^2\theta + C_{22}\sin^4\theta \\
\widetilde{C}_{23} &= C_{23}\left(\sin^4\theta+\cos^4\theta\right) + \left(C_{33}+C_{22}-4C_{66}\right)\sin^2\theta\cos^2\theta \\
\widetilde{C}_{13} &= C_{13}\cos^2\theta + C_{12}\sin^2\theta \\
\widetilde{C}_{36} &= \left(-C_{33}+C_{23}+2C_{66}\right)\sin\theta\cos^3\theta + \left(C_{22}-C_{23}-2C_{66}\right)\sin^3\theta\cos\theta \\
\widetilde{C}_{22} &= C_{22}\cos^4\theta + 2\left(C_{23}+2C_{66}\right)\sin^2\theta\cos^2\theta + C_{33}\sin^4\theta \\
\widetilde{C}_{12} &= C_{12}\cos^2\theta + C_{13}\sin^2\theta \\
\widetilde{C}_{26} &= \left(-C_{33}+C_{23}+2C_{66}\right)\sin^3\theta\cos\theta + \left(C_{22}-C_{23}-2C_{66}\right)\sin\theta\cos^3\theta \\
\widetilde{C}_{11} &= C_{11} \\
\widetilde{C}_{16} &= \left(C_{12}-C_{13}\right)\sin\theta\cos\theta \\
\widetilde{C}_{44} &= C_{44}\cos^2\theta + C_{55}\sin^2\theta \\
\widetilde{C}_{45} &= \left(C_{44}-C_{55}\right)\sin\theta\cos\theta \\
\widetilde{C}_{55} &= C_{55}\cos^2\theta + C_{44}\sin^2\theta \\
\widetilde{C}_{66} &= \left(C_{33}+C_{22}-2C_{23}-2C_{66}\right)\sin^2\theta\cos^2\theta + C_{66}\left(\sin^4\theta+\cos^4\theta\right)
\end{aligned} \tag{A.10}$$

Appendix B

Solution of a system of second order differential equations

A system of differential equations of the second order in x can be written as

$$\frac{d^2\mathbf{y}(x)}{dx^2} = \mathbf{y}_{,xx}(x) = f\left(\mathbf{y}(x), \mathbf{y}_{,x}(x)\right) \tag{B.1}$$

where $\mathbf{y}(x) = [y_1, y_2, ..., y_n]^T$ are the n unknown functions. Thus $\mathbf{y}_{,x}(x)$ can be written in matrix form as

$$\mathbf{y}_{,x}(x) = \tilde{\mathbf{S}} \left\{ y_1 \; y_{1,x} \; y_2 \; y_{2,x} \; \dots \; y_n \; y_{n,x} \right\}^T \tag{B.2}$$

where $\tilde{\mathbf{S}}$ is the matrix of coefficient whose dimension is $n \times 2n$ and which can be written as:

$$\tilde{\mathbf{S}} = \begin{bmatrix} S_{11} & S_{12} & S_{13} & S_{14} & \dots & S_{1(2n-1)} & S_{1(2n)} \\ S_{21} & S_{22} & S_{23} & S_{24} & \dots & S_{2(2n-1)} & S_{2(2n)} \\ \vdots & \vdots & \vdots & \vdots & \ddots & \vdots & \vdots \\ S_{n1} & S_{n2} & S_{n3} & S_{n4} & \dots & S_{n(2n-1)} & S_{n(2n)} \end{bmatrix} \tag{B.3}$$

With a simple change of variables, the system of second order differential equations can be transformed into a system of first order differential equations. The change of variables is

$$\begin{aligned} & Z_1(x) = y_1(x) \,,\; Z_2(x) = y_{1,x}(x) \\ & Z_3(x) = y_2(x) \,,\; Z_4(x) = y_{2,x}(x) \\ & \vdots \\ & Z_{(2n-1)}(x) = y_n(x) \,,\; Z_{(2n)}(x) = y_{n,x}(x) \end{aligned} \tag{B.4}$$

In this way, a number of first order differential equations, such as $Z_{1_{,x}} = Z_2$, $Z_{3_{,x}} = Z_4$ and $Z_{n-1_{,x}} = Z_n$, will be added to the system of Eq. (B.1) - and consequently to Eq. (B.2) - which becomes a first order differential system. If the differential system is linear and the coefficients are constant, the set of equations can be re-written in matrix form as

$$\mathbf{Z}_{,x}(x) = \mathbf{S}\mathbf{Z}(x) \tag{B.5}$$

where the unknown functions are now:

$$\mathbf{Z} = \{Z_1\ Z_2\ Z_3\ Z_4\ \dots\ Z_{2n-1}\ Z_{2n}\}^T = \left\{y_1\ y_{1_{,x}}\ y_2\ y_{2_{,x}}\ \cdots\ y_n\ y_{n_{,x}}\right\}^T \tag{B.6}$$

and the new matrix of coefficients $\mathbf{S}$, whose dimension now is $2n \times 2n$ can be written as:

$$\mathbf{S} = \begin{bmatrix} 0 & 1 & 0 & 0 & \dots & 0 & 0 \\ S_{11} & S_{12} & S_{13} & S_{14} & \dots & S_{1(2n-1)} & S_{1(2n)} \\ 0 & 0 & 0 & 1 & \dots & 0 & 0 \\ S_{21} & S_{22} & S_{23} & S_{24} & \dots & S_{2(2n-1)} & S_{2(2n)} \\ \vdots & \vdots & \vdots & \vdots & \ddots & \vdots & \vdots \\ 0 & 0 & 0 & 0 & \dots & 0 & 1 \\ S_{n1} & S_{n2} & S_{n3} & S_{n4} & \dots & S_{n(2n-1)} & S_{n(2n)} \end{bmatrix} \tag{B.7}$$

The solution of first order differential equations of Eq. (B.5) can be written as

$$Z_i = \sum_{j=1}^{2n} C_j \delta_{ji} e^{\lambda_j x} \tag{B.8}$$

where C_j are the constants of integration, λ_j is the j-th eigenvalue of the matrix $\mathbf{S}$ and δ_{ji} is i-th value in the j-th eigenvector of the matrix $\mathbf{S}$. For the sake of simplicity, the solution for Z_1, i.e. y_1 (see Eq. (B.4)) is given in explicit form

$$y_1(x) = C_1\delta_{11}e^{\lambda_1 x} + C_2\delta_{21}e^{\lambda_2 x} + \ldots + C_{2n}\delta_{(2n)1}e^{\lambda_{2n} x} \tag{B.9}$$

if the eigenvectors are written as a matrix δ in the following form:

$$\delta = \begin{bmatrix} \delta_{11} & \delta_{21} & \dots & \delta_{(2n)1} \\ \delta_{12} & \delta_{22} & \dots & \delta_{(2n)2} \\ \vdots & \vdots & \ddots & \vdots \\ \delta_{1(2n)} & \delta_{2(2n)} & \dots & \delta_{(2n)(2n)} \end{bmatrix} \tag{B.10}$$

where, for δ_{ji}, j is the eigenvector number and i is the position in the eigenvector, and the eigenvalues with the constants are written in the following form:

$$\mathbf{Ce}^{\lambda\mathbf{x}} = \left\{ C_1 e^{\lambda_1 x} \; C_2 e^{\lambda_2 x} \; \ldots \; C_{2n} e^{\lambda_{2n} x} \right\}^T \tag{B.11}$$

then the solution of Eq. (B.8) can be written in a more compact matrix form as

$$\mathbf{Z} = \delta \mathbf{Ce}^{\lambda\mathbf{x}} \tag{B.12}$$

Appendix C

Forward and backward Gauss elimination

In this appendix, the procedure to transform the matrix **L** (Eq. (7.3)) into $\tilde{\mathbf{S}}$ (Eq. (B.3)) is described in details. In matrix **L**, the coefficients of the second derivatives are located in the columns which are multiple of 3. In order to decouple the equations, the first row should have -1 in the third column and zero below it, the second row should have -1 in the sixth column and zeros above and below that and so on. This matrix has been referred to as $\hat{\mathbf{L}}$. Let us examine a 3 by 9 **L** matrix which is fully populated. The algorithm can easily be extended to a matrix of N by $N \times 3$ dimension. The matrix $\hat{\mathbf{L}}$ and subsequently the matrix $\tilde{\mathbf{S}}$ (see Eq. (B.3)) can be obtained by following four steps.

$$\mathbf{L} = \begin{bmatrix} l_{11} & l_{12} & l_{13} & l_{14} & l_{15} & l_{16} & l_{17} & l_{18} & l_{19} \\ l_{21} & l_{22} & l_{23} & l_{24} & l_{25} & l_{26} & l_{27} & l_{28} & l_{29} \\ l_{31} & l_{32} & l_{33} & l_{34} & l_{35} & l_{36} & l_{37} & l_{38} & l_{39} \end{bmatrix} \tag{C.1}$$

(i) Forward Gauss elimination. Gauss elimination is carried out on entries below l_{13}, l_{26}. This is achieved by the following algorithm for the third column

$$\begin{aligned} l_{2i} &= l_{2i} - \frac{l_{23}}{l_{13}} l_{1i} \quad \text{for} \quad i = 1, \ldots, 9 \\ l_{3i} &= l_{3i} - \frac{l_{33}}{l_{13}} l_{1i} \quad \text{for} \quad i = 1, \ldots, 9 \end{aligned} \tag{C.2}$$

and for the sixth column[1]

$$l_{3i} = l_{3i} - \frac{l_{36}}{l_{26}} l_{2i} \quad \text{for} \quad i = 1, \ldots, 9 \tag{C.3}$$

note that the name of the new element has not been changed for sake of simplicity. The results would be a new **L** matrix in the following form

$$\mathbf{L} = \begin{bmatrix} l_{11} & l_{12} & l_{13} & l_{14} & l_{15} & l_{16} & l_{17} & l_{18} & l_{19} \\ l_{21} & l_{22} & 0 & l_{24} & l_{25} & l_{26} & l_{27} & l_{28} & l_{29} \\ l_{31} & l_{32} & 0 & l_{34} & l_{35} & 0 & l_{37} & l_{38} & l_{39} \end{bmatrix} \tag{C.4}$$

(ii) Backward Gauss Elimination. As before but starting from the third row, ninth column and eliminating everything that is above that element in order to obtain the following new **L** matrix

$$\mathbf{L} = \begin{bmatrix} l_{11} & l_{12} & l_{13} & l_{14} & l_{15} & 0 & l_{17} & l_{18} & 0 \\ l_{21} & l_{22} & 0 & l_{24} & l_{25} & l_{26} & l_{27} & l_{28} & 0 \\ l_{31} & l_{32} & 0 & l_{34} & l_{35} & 0 & l_{37} & l_{38} & l_{39} \end{bmatrix} \tag{C.5}$$

(iii) Factorisation. It is required to have -1 on the coefficient corresponding to the second derivative so to imply that if that coefficient were to be moved on the other side of the differential equation, its value would be 1. In order to do that the first row is divided by $-l_{13}$, the second by $-l_{26}$and the third by $-l_{39}$. in this way, the matrix $\hat{\mathbf{L}}$ can be obtained and it has the following form

$$\hat{\mathbf{L}} = \begin{bmatrix} l_{11} & l_{12} & -1 & l_{14} & l_{15} & 0 & l_{17} & l_{18} & 0 \\ l_{21} & l_{22} & 0 & l_{24} & l_{25} & -1 & l_{27} & l_{28} & 0 \\ l_{31} & l_{32} & 0 & l_{34} & l_{35} & 0 & l_{37} & l_{38} & -1 \end{bmatrix} \tag{C.6}$$

(iii) Eliminate the columns. By eliminating the columns corresponding to the position 3 and it multiples, is equivalent to moving the term containing the second derivatives to the other side of the equations and giving the matrix of coefficients associated with the second order differential equation. This matrix has been called $\tilde{\mathbf{S}}$ (see Eq. (B.3)) and following the notation in Eq. (C.6) it can be written as

---

[1] this algorithm can be generalised for any matrix dimension in a couple of lines

$$\tilde{\mathbf{S}} = \begin{bmatrix} l_{11} & l_{12} & l_{14} & l_{15} & l_{17} & l_{18} \\ l_{21} & l_{22} & l_{24} & l_{25} & l_{27} & l_{28} \\ l_{31} & l_{32} & l_{34} & l_{35} & l_{37} & l_{38} \end{bmatrix} \tag{C.7}$$

Appendix D

A list of publications arising from the research

Journal publications

E. Carrera, **A. Pagani**, J.R. Banerjee (2016) “Linearized buckling analysis of isotropic and composite beam-columns by Carrera Unified Formulation and Dynamic Stiffness Method”, Mechanics of Advanced Material and Structures, Vol. 23 no. 9, pp. 1092–1103. DOI: `10.1080/15376494.2015.1121524`.

A. Pagani, E. Carrera, A.J.M. Ferreira (2016) “Higher-order Theories and Radial Basis Functions Applied to Vibration of Thin-Walled Beams”, Mechanics of Advanced Material and Structures, Vol. 23 no. 9, pp. 1080–1091.
DOI: `10.1080/15376494.2015.1121555`.

M. Dan, **A. Pagani**, E. Carrera (2016) “Free vibration analysis of simply supported beams with solid and thin-walled cross-sections using higher-order theories based on displacement variables”, Thin-Walled Structures, Vol. 98, pp. 478–495. DOI: `10.1016/j.tws.2015.10.012`.

A. Pagani, E. Carrera, J.R. Banerjee, P.H. Cabral, G. Caprio, A. Prado (2014) “Free vibration analysis of composite plates by higher-order 1D dynamic stiffness elements and experiments”, Composite Structures, Vol. 118, pp. 654–663. DOI: `10.1016/j.compstruct.2014.08.020`.

A. Pagani, E. Carrera, M. Boscolo, J. R. Banerjee (2014) “Refined Dynamic Stiffness Elements Applied to Free Vibration Analysis of Generally Laminated Composite

Beams with Arbitrary Boundary Conditions”, Composite Structures, Vol. 110, pp. 305–316. DOI: `10.1016/j.compstruct.2013.12.010`.

A. Pagani, M. Boscolo, J. R. Banerjee, E. Carrera (2013) “Exact Dynamic Stiffness Elements based on One-Dimensional Higher-Order Theories for the Free Vibration Analysis of Compact and Thin-Walled Structures”, Journal of Sound and Vibration, Vol. 332 n. 23, pp. 6104-6127.
DOI: `10.1016/j.jsv.2013.06.023`.

Conference publications

A. Pagani, E. Carrera, J.R. Banerjee (2014) “Buckling of Beams by Refined Theories and Dynamic Stiffness Method”, In: *12th International Conference on Computational Structures Technology (CST2014)*, Napoli, Italy, 2-5 September, 2014.

A. Pagani, E. Carrera, A.J.M. Ferreira (2014) “Vibration of laminated composite beams via Carrera Unified Formulation and radial basis functions”, In: *1st International Conference on Mechanics of Composites (MECHCOMP2014)*, Stony Brook, Long Island (NY), USA, 8-12 June, 2014.

A. Pagani, E. Carrera, M. Boscolo, J.R. Banerjee (2013) “Exact Dynamic Stiffness Elements Using 1D Higher-Order Theories: Application to Sandwich Beams”, In: *17th International Conference on Composite Structures (ICCS17)*, Porto (Portugal), June 17-21, 2013.

A. Pagani, E. Carrera, M. Boscolo, J.R. Banerjee (2013) “Exact Dynamic Stiffness Elements Using 1D Higher-Order Theories: Application to Laminated Composites”, In: *17th International Conference on Composite Structures (ICCS17)*, Porto (Portugal), June 17-21, 2013.

E. Carrera, A.J.M. Ferreira, **A. Pagani**, M. Petrolo (2013) “Free Vibrations of Beams accounting for Refined Theories and Radial Basis Functions”, In: *9th International Symposium on Vibrations of Continuous Systems (ISVCS9)*, Courmayeur (Italy), July 22-26, 2013.

Bibliography

[1] L. Da Vinci. *Codex Madrid*, volume I. 1493.

[2] D. Bernoulli. *De vibrationibus et sono laminarum elasticarum.* Commentarii Academiae Scientiarum Imperialis Petropolitanae. Petropoli, 1751.

[3] L. Euler. *Methodus Inveniendi Lineas Curvas Maximi Minimive Proprietate Gaudentes, Sive Solutio Problematis Isoperimetrici Lattissimo Sensu Accept.* De curvis elasticis. Bousquet, 1744.

[4] A. J.-C. B. de Saint-Venant. Mèmoire sur la flexion des prismes, sur les glissement trans- versaux et longitudinaux qui l'accompagnent lorquelle ne sopére pas uniformément ou en arc de cercle, et sur la forme coubre effectée alors par leurs sections transversales primitivement planes. *Journal de Mathèmatiques pures et appliquèes de Liouville*, II(1):88–189, 1856.

[5] S. P. Timoshenko. On the corrections for shear of the differential equation for transverse vibrations of prismatic bars. *Philosophical Magazine*, 41:744–746, 1922.

[6] S. P. Timoshenko. On the transverse vibrations of bars of uniform cross section. *Philosophical Magazine*, 43:125–131, 1922.

[7] D.T. Mucichescu. Bounds for stiffness of prismatic beams. *Journal of Structural Engineering*, 110:1410–1414, 1984.

[8] V. V. Novozhilov. *Theory of Elasticity*. Pergamon Press, New York, 1961.

[9] S.P. Timoshenko and J.N. Goodier. *Theory of elasticity*. McGraw-Hill, New York, 1970.

[10] I. S. Sokolnikoff. *Mathematical Theory of Elasticity*. McGraw-Hill, New York, 1956.

[11] G.R. Cowper. The shear coefficient in Timoshenko's beam theory. *Journal of Applied Mechanics*, 33(2):335–340, 1966.

[12] J. Lubliner. *Plasticity Theory*. Macmillan Publishers, London, 1990.

[13] P. Ladevéze and J. Simmonds. New concepts for linear beam theory with arbitrary geometry and loading. *European Journal of Mechanics - A/Solids*, 17(3):377–402, 1998.

[14] A.A. Umanskij. *Kručenije i izgib tonkostennykh aviokon-strukcij*. Oborongiz, Moskva, 1939.

[15] V. Z. Vlasov. *Thin-walled elastic beams*. National Science Foundation, Washington, 1961.

[16] S. Benscoter. A theory of torsion bending for multicell beams. *Journal of Applied Mechanics*, 21(1):25–34, 1954.

[17] P. Ladevéze and J. Simmonds. De nouveaux concepts en théorie des poutres pour des charges et des géométries quelconques. *Comptes Rendus de l'Académie des Sciences de Paris*, 332:445–462, 1996.

[18] P. Ladevéze. *Nonlinear Computational Structural Mechanics*. Springer Verlag, New York, 1998.

[19] B. Bognet, F. Bordeu, F. Chinesta, A. Leygue, and A. Poitou. Advanced simulation of models defined in plate geometries: 3D solutions with 2D computational complexity. *Computer Methods in Applied Mechanics and Engineering*, 201–204:1–12, 2012.

[20] B. Bognet, A. Leygue, and F. Chinesta. Separated representations of 3D elastic solutions in shell geometries. *Advanced Modeling and Simulation in Engineering Sciences*, 1(1):1–34, 2014.

[21] P. Vidal, L. Gallimard, and O. Polit. Composite beam finite element based on the proper generalized decomposition. *Computers & Structures*, 102–103:76–86, 2012.

[22] V.L. Berdichevsky. Equations of the theory of anisotropic inhomogeneous rods. *Soviet Physics - Doklady*, 21(5):286–288, 1976.

[23] V.L. Berdichevsky, E. Armanios, and A. Badir. Theory of anisotropic thin-walled closed-cross-section beams. *Composites Engineering*, 2(5-7):411–432, 1992.

[24] V.V. Volovoi, D.H. Hodges, V.L. Berdichevsky, and V.G. Sutyrin. Asymptotic theory for static behavior of elastic anisotropic I-beams. *International Journal of Solids and Structures*, 36(7):1017–1043, 1999.

[25] R. Schardt. Eine erweiterung der technischen biegetheorie zur berechnung prismatischer faltwerke. *Der Stahlbau*, 35:161–171, 1966.

[26] R. Schardt. *Verallgemeinerte technische biegetheorie*. Springer Verlag, Berlin, 1989.

[27] R. Schardt. Generalized beam theory-an adequate method for coupled stability problems. *Thin-Walled Structures*, 19:161–180, 1994.

[28] N. Silvestre and D. Camotim. First-order generalised beam theory for arbitrary orthotropic materials. *Thin-Walled Structures*, 40(9):791–820, 2002.

[29] K. Washizu. *Variational Methods in Elasticity and Plasticity*. Pergamon, Oxford, 1968.

[30] K.R. Kapania and S. Raciti. Recent advances in analysis of laminated beams and plates, part I: Shear effects and buckling. *AIAA Journal*, 27(7):923–935, 1989.

[31] K.R. Kapania and S. Raciti. Recent advances in analysis of laminated beams and plates, part II: Vibrations and wave propagation. *AIAA Journal*, 27(7):935–946, 1989.

[32] L. Librescu and O. Song. On the static aeroelastic tailoring of composite aircraft swept wings modelled as thin-walled beam structures. *Composites Engineering*, 2:497–512, 1992.

[33] Z. Qin and L. Librescu. On a shear-deformable theory of anisotropic thin-walled beams: further contribution and validations. *Composite Structures*, 56:345–358, 2002.

[34] E. Carrera and G. Giunta. Refined beam theories based on a unified formulation. *International Journal of Applied Mechanics*, 2(1):117–143, 2010.

[35] E. Carrera, A. Pagani, M. Petrolo, and E. Zappino. Recent developments on refined theories for beams with applications. *Mechanical Engineering Reviews*, 2(2):1–30, 2015.

[36] J. R. Banerjee. Dynamic stiffness formulation for structural elements: a general approach. *Computers & Structures*, 63(1):101–103, 1997.

[37] J. R. Banerjee. Coupled bending-torsional dynamic stiffness matrix for beam elements. *International Journal for Numerical Methods in Engineering*, 28:1283–1298, 1989.

[38] J. R. Banerjee. Free vibration analysis of a twisted beam using the dynamic stiffness method. *International Journal of Solids and Structures*, 38(38–39):6703–6722, 2001.

[39] J. R. Banerjee. Free vibration of sandwich beams using the dynamic stiffness method. *Computers & Structures*, 81(18–19):1915–1922, 2003.

[40] J. R. Banerjee. Development of an exact dynamic stiffness matrix for free vibration analysis of a twisted timoshenko beam. *Journal of Sound and Vibration*, 270(1–2):379–401, 2004.

[41] J. R. Banerjee, C. W. Cheung, R. Morishima, M. Perera, and J. Njuguna. Free vibration of a three-layered sandwich beam using the dynamic stiffness method and experiment. *International Journal of Solids and Structures*, 44(22–23):7543–7563, 2007.

[42] F. W. Williams and W. H. Wittrick. An automatic computational procedure for calculating natural frequencies of skeletal structures. *International Journal of Mechanical Sciences*, 12(9):781–791, 1970.

[43] W. H. Wittrick. A unified approach to initial buckling of stiffened panels in compression. *Aeronautical Quarterly*, 19(3):265–283, 1968.

[44] W. H. Wittrick and F. W. Williams. Buckling and vibration of anisotropic or isotropic plate assemblies under combined loadings. *International Journal of Mechanical Sciences*, 16(4):209–239, 1974.

[45] M. Boscolo and J. R. Banerjee. Dynamic stiffness formulation for composite Mindlin plates for exact modal analysis of structures. Part I: Theory. *Computers & Structures*, 96-97:61–73, 2012.

[46] M. Boscolo and J.R. Banerjee. Dynamic stiffness formulation for composite Mindlin plates for exact modal analysis of structures. Part II: Results and applications. *Computers & Structures*, 96-97:74–83, 2012.

[47] F.A. Fazzolari, M. Boscolo, and J.R. Banerjee. An exact dynamic stiffness element using a higher order shear deformation theory for free vibration analysis of composite plate assemblies. *Composite Structures*, 96:262–278, 2013.

[48] F. A. Fazzolari, J. R. Banerjee, and M. Boscolo. Buckling of composite plate assemblies using higher order shear deformation theory - an exact method of solution. *Thin-Walled Structures*, 71:18–34, 2013.

[49] W. H. Wittrick and F. W. Williams. A general algorithm for computing natural frequencies of elastic structures. *Quarterly Journal of mechanics and applied sciences*, 24(3):263–284, 1970.

[50] R. L. Hardy. Multiquadric equations of topography and other irregular surfaces. *Geophysical Research*, 176:1905–1915, 1971.

[51] R. L. Hardy. Theory and applications of the multiquadric-biharmonic method: 20 years of discovery. *Computers & Mathematics with Applications*, 19(8-9):163–208, 1990.

[52] E.J. Kansa. Multiquadrics - A scattered data approximation scheme with applications to computational fluid dynamics. I: Surface approximations and partial derivative estimates. *Computers & Mathematics with Applications*, 19(8-9):127–145, 1990.

[53] E.J. Kansa. Multiquadrics - A scattered data approximation scheme with applications to computational fluid dynamics. II: Solutions to parabolic, hyperbolic and elliptic partial differential equations. *Computers & Mathematics with Applications*, 19(8-9):147–161, 1990.

[54] A. J. M. Ferreira. A formulation of the multiquadric radial basis function method for the analysis of laminated composite plates. *Composite Structures*, 59(3):385–392, 2003.

[55] A. J. M. Ferreira. Thick composite beam analysis using a global meshless approximation based on radial basis functions. *Mechanics of Advanced Materials and Structures*, 10:271–284, 2003.

[56] A. Pagani, M. Boscolo, J. R. Banerjee, and E. Carrera. Exact dynamic stiffness elements based on one-dimensional higher-order theories for free vibration analysis of solid and thin-walled structures. *Journal of Sound and Vibration*, 332(23):6104–6127, 2013.

[57] A. Pagani, E. Carrera, M. Boscolo, and J. R. Banerjee. Refined dynamic stiffness elements applied to free vibration analysis of generally laminated composite beams with arbitrary boundary conditions. *Composite Structures*, 110:305–316, 2014.

[58] A. Pagani, E. Carrera, J. R. Banerjee, P. H. Cabral, G. Caprio, and A. Prado. Free vibration analysis of composite plates by higher-order 1D dynamic stiffness elements and experiments. *Composite Structures*, 118:654–663, 2014.

[59] E. Carrera, A. Pagani, and J. R. Banerjee. Linearized buckling analysis of isotropic and composite beam-columns by carrera unified formulation and dynamic stiffness method. *Mechanics of Advanced Materials and Structures*, 23(9):1092–1103, 2016.

[60] A. Pagani, E. Carrera, and A. J. M. Ferreira. Higher-order theories and radial basis functions applied to free vibration analysis of thin-walled beams. *Mechanics of Advanced Materials and Structures*, 23(9), 2016.

[61] F. Gruttmann and W. Wagner. Shear correction factors in Timoshenko's beam theory for arbitrary shaped cross-sections. *Computational Mechanics*, 27:199–207, 2001.

[62] C. Bach and R. Baumann. *Elastizität und Festigkeit*. Springer, Berlin, 1924.

[63] D. Stojek. Zur schubverformung im biegebalken. *Zeitschrift für Angewandte Mathematik und Mechanik*, 44(8-9):393–396, 1964.

[64] E. Carrera, M. Petrolo, and E. Zappino. Performance of CUF approach to analyze the structural behavior of slender bodies. *Journal of Structural Engineering*, 138(2):285–297, 2012.

[65] P.R. Heyliger and Reddy J. N. A higher order beam finite element for bending and vibration problems. *Journal of Sound and Vibration*, 126(2):309–326, 1988.

[66] R. Schardt and D. Heinz. *Vibrations of thin-walled prismatic structures under simultaneous static load using generalized beam theory*, pages 921–927. Structural Dynamics. Balkema, Rotterdam, 1991.

[67] J. M. Davies and P. Leach. First-order generalised beam theory. *Journal of Constructional Steel Research*, 31(2-3):187–220, 1994.

[68] J. M. Davies, P. Leach, and D. Heinz. Second-order generalised beam theory. *Journal of Constructional Steel Research*, 31(2-3):221–241, 1994.

[69] N. Silvestre. Second-order generalised beam theory for arbitrary orthotropic materials. *Thin-Walled Structures*, 40(9):791–820, 2002.

[70] R. Bebiano, N. Silvestre, and D. Camotim. Local and global vibration of thin-walled members subjected to compression and non-uniform bending. *Journal of Sound and Vibration*, 315:509–535, 2008.

[71] R. Bebiano, D. Camotim, and N. Silvestre. Dynamic analysis of thin-walled members using generalised beam theory (GBT). *Thin-Walled Structures*, 72(0):188 – 205, 2013.

[72] R. Schardt. Lateral torsional and distortional buckling of channel and hat-sections. *Journal of Constructional Steel Research*, 31:243–265, 1994.

[73] R. Goncalves and D. Camotim. GBT local and global buckling analysis of aluminium and stainless steel columns. *Computers & Structures*, 82:1473–1484, 2004.

[74] P. Dinis, D. Camotim, and N. Silvestre. GBT formulation to analyse the buckling behaviour of thin-walled members with arbitrarily “branched” open cross-sections. *Thin-Walled Structures*, 44(1):20–38, 2006.

[75] N. Silvestre. Generalised beam theory to analyse the buckling behaviour of circular cylindrical shells and tubes. *Thin-Walled Structures*, 45(2):185–198, 2007.

[76] C. Basaglia, D. Camotim, and N. Silvestre. Global buckling analysis of plane and space thin-walled frames in the context of GBT. *Thin-Walled Structures*, 46:79–101, 2008.

[77] P. Leach and J. M. Davies. An experimental verification of the generalized beam theory applied to interactive buckling problems. *Thin-Walled Structures*, 25(1):61 – 79, 1996.

[78] R. Goncalves and D. Camotim. Thin-walled member plastic bifurcation analysis using generalised beam theory. *Advances in Engineering Software*, 38:637–646, 2007.

[79] C. Basaglia, D. Camotim, and N. Silvestre. Local, distortional and global post-buckling analysis of frames using generalised beam theory. In *the Proceedings of the Tenth International Conference on Computational Structures Technology*, Valencia, Spain, 2010.

[80] M. Abambres, D. Camotim, and N. Silvestre. Physically non-linear GBT analysis of thin-walled members. *Computers & Structures*, 129(0):148–165, 2013.

[81] M. Abambres, D. Camotim, N. Silvestre, and K.J.R. Rasmussen. GBT-based structural analysis of elastic–plastic thin-walled members. *Computers & Structures*, 136(0):1–23, 2014.

[82] F. Gruttmann, R. Sauer, and W. Wagner. Theory and numerics of three-dimensional beams with elastoplastic material behaviour. *International Journal for Numerical Methods in Engineering*, 48(12):1675–1702, 2000.

[83] J.N. Reddy, C.M. Wang, and K.H. Lee. Relationships between bending solutions of classical and shear deformation theories. *International Journal of Solids and Structures*, 34(26):3373–3384, 1997.

[84] R. El Fatmi. A non-uniform warping theory for beams. *Comptes Rendus Mécanique*, 335(8):467–474, 2007.

[85] R. El Fatmi. Non-uniform warping including the effects of torsion and shear forces. Part I: A general beam theory. *International Journal of Solids and Structures*, 44(18-19):5912–5929, 2007.

[86] R. El Fatmi. Non-uniform warping including the effects of torsion and shear forces. Part II: Analytical and numerical applications. *International Journal of Solids and Structures*, 44(18-19):5930–5952, 2007.

[87] A. Prokić. Thin-walled beams with open and closed cross-sections. *Computers & Structures*, 47(6):1065–1070, 1993.

[88] A. Prokić. New warping function for thin-walled beams. I: Theory. *Journal of Structural Engineering*, 122(12):1437–1442, 1996.

[89] A. Prokić. New warping function for thin-walled beams. II: Finite element method and applications. *Journal of Structural Engineering*, 122(12):1443–1452, 1996.

[90] E.J. Sapountzakis and V.G. Mokos. Dynamic analysis of 3-D beam elements including warping and shear deformation effects. *International Journal of Solids and Structures*, 43(22-23):6707–6726, 2006.

[91] E.J. Sapountzakis and V.J. Tsipiras. Warping shear stresses in nonlinear nonuniform torsional vibrations of bars by BEM. *Engineering Structures*, 32(3):741–752, 2010.

[92] E.J. Sapountzakis. Solution of non-uniform torsion of bars by an integral equation method. *Computers & Structures*, 77(6):659–667, 2000.

[93] E.J. Sapountzakis and V.G. Mokos. Warping shear stresses in nonuniform torsion by BEM. *Computational Mechanics*, 30(2):131–142, 2003.

[94] E.J. Sapountzakis and V.M. Protonotariou. A displacement solution for transverse shear loading of beams using the boundary element method. *Computers & Structures*, 86(7-8):771–779, 2008.

[95] J. Wackerfuß and F. Gruttmann. A nonlinear Hu-Washizu variational formulation and related finite-element implementation for spatial beams with arbitrary moderate thick cross-sections. *Computer Methods in Applied Mechanics and Engineering*, 200(17-20):1671–1690, 2011.

[96] W. Wagner and F. Gruttmann. Finite element analysis of Saint-Venant torsion problem with exact integration of the elastic-plastic constitutive equations. *Computer Methods in Applied Mechanics and Engineering*, 190(29-30):3831–3848, 2001.

[97] H.H. Chen and K.M. Hsiao. Coupled axial-torsional vibration of thin-walled Z-section beam induced by boundary conditions. *Thin-Walled Structures*, 45(6):573–583, 2007.

[98] M.K. Ferradi, X. Cespedes, and M. Arquier. A higher order beam finite element with warping eigenmodes. *Engineering Structures*, 46:748–762, 2013.

[99] K. Yoon and P.-S. Lee. Modeling the warping displacements for discontinuously varying arbitrary cross-section beams. *Computers & Structures*, 131:56–69, 2014.

[100] P. Ladevéze, P. Sanchez, and J. Simmonds. Beamlike (Saint-Venant) solutions for fully anisotropic elastic tubes of arbitrary closed cross section. *Internatinal Journal of Solids and Structures*, 41(7):1925–1944, 2004.

[101] E. Carrera, M. Cinefra, M. Petrolo, and E. Zappino. *Finite Element Analysis of Structures through Unified Formulation*. John Wiley & Sons, New York, 2014.

[102] P. Cicala. *Systematic approximation approach to linear shell theory*. Levrotto & Bella, Torino, 1965.

[103] W. Yu, V.V. Volovoi, D.H. Hodges, and X. Hong. Validation of the variational asymptotic beam sectional analysis (VABS). *AIAA Journal*, 40(10):2105–2113, 2002.

[104] W. Yu and D.H. Hodges. Elasticity solutions versus asymptotic sectional analysis of homogeneous, isotropic, prismatic beams. *Journal of Applied Mechanics*, 71:15–23, 2004.

[105] W. Yu and D.H. Hodges. Generalized Timoshenko theory of the variational asymptotic beam sectional analysis. *Journal of the American Helicopter Society*, 50(1):46–55, 2005.

[106] Q. Wang and W. Yu. A variational asymptotic approach for thermoelastic analysis of composite beams. *Advances in Aircraft and Spacecraft Sciences*, 1(1):93–123, 2014.

[107] E. Carrera and S. Brischetto. Analysis of thickness locking in classical, refined and mixed multilayered plate theories. *Composite Structures*, 82(4):549–562, 2008.

[108] E. Carrera, G. Giunta, and M. Petrolo. *Beam Structures: Classical and Advanced Theories*. John Wiley & Sons, New York, 2011.

[109] E. Oñate. *Structural Analysis with the Finite Element Method: Linear Statics. Volume 1: Basis and Solids*. Springer, Barcelona, 2009.

[110] E. Carrera and M. Petrolo. Refined beam elements with only displacement variables and plate/shell capabilities. *Meccanica*, 47(3):537–556, 2012.

[111] E. Carrera, A. Pagani, M. Petrolo, and E. Zappino. A component-wise approach in structural analysis. Computational Methods for Engineering Science, chapter 4, pages 75–115. Saxe-Coburg Publications, 2012.

[112] C. Lanczos. *The variational principles of mechanics*. Univesity of Toronto Press, Toronto, 1970.

[113] S.P. Timoshenko and J.M. Gere. Theory of elastic stability. *McGrawHill-Kogakusha Ltd*, 1961.

[114] E. Carrera and G. Giunta. Hierarchical closed form solutions for plates bent by localized transverse loadings. *Journal of Zhejiang University-SCIENCE A (Applied Physics & Engineering)*, 8(7):1026–1037, 2007.

[115] E. Carrera and G. Giunta. Hierarchical models for failure analysis of plates bent by distributed and localized transverse loadings. *Journal of Zhejiang University-SCIENCE A (Applied Physics & Engineering)*, 9(5):600–613, 2008.

[116] A. J. M. Ferreira, C. M. C. Roque, and P. A. L. S. Martins. Analysis of composite plates using higher-order shear deformation theory and a finite point formulation based on the multiquadric radial basis function method. *Composites Part B: Engineering*, 34(7):627–636, 2003.

[117] S. Xiang, Z.-Y Bi, S.-X. Jiang, Y.-X. Jin, and M.-S. Yang. Thin plate spline radial basis function for the free vibration analysis of laminated composite shells. *Composite Structures*, 93(2):611–615, 2011.

[118] A. J. M. Ferreira, G. E. Fasshauer, R. C. Batra, and J. D. Rodrigues. Static deformations and vibration analysis of composite and sandwich plates using a layerwise theory and RBF-PS discretizations with optimal shape parameter. *Composite Structures*, 86(4):328–343, 2008.

[119] H. Wendland. Error estimates for interpolation by compactly supported radial basis functions of minimal degree. *Journal of Approximation Theory*, 93:258–296, 1998.

[120] C. M. C. Roque and A. J. M. Ferreira. Numerical experiments on optimal shape parameters for radial basis functions. *Numerical Methods for Partial Differential Equations*, 26(3):675–689, 2010.

[121] W. H. Press, S. A. Teukolsky, W. T. Vetterling, and B. P. Flannery. *Numerical Recipes: The Art of Scientific Computing*. Cambridge University Press, New York, 3rd edition, 2007.

[122] G. E. Fasshauer. Newton iteration with multiquadrics for the solution of nonlinear PDEs. *Computers & Mathematics with Applications*, 43:423–438, 2002.

[123] A. J. M. Ferreira and G. E. Fasshauer. Computation of natural frequencies of shear deformable beams and plates by a RBF-Pseudospectral method. *Computer Methods in Applied Mechanics and Engineering*, 196:134–146, 2006.

[124] R. Schaback. On the efficiency of interpolation by radial basis functions. Surface fitting and multiresolution methods, pages 309–328. Vanderbilt University Press, Nashville, Tennessee, 1997.

[125] N. Fantuzzi, F. Tornabene, E. Viola, and A. J. M. Ferreira. A strong formulation finite element method (SFEM) based on RBF and GDQ techniques for the static and dynamic analyses of laminated plates of arbitrary shape. *Meccanica*, 49(10):2503–2542, 2014.

[126] E. J. Kansa and Y. C. Hon. Circumventing the ill-conditioning problem with multiquadric radial basis functions. *Computers and Mathematics with Applications*, 39(7–8):123–137, 2000.

[127] F. Tornabene, N. Fantuzzi, E. Viola, and A. J. M. Ferreira. Radial basis function method applied to doubly-curved laminated composite shells and panels with a general higher-order equivalent single layer formulation. *Composites Part B: Engineering*, 55(0):642–659, 2013.

[128] U. Lee. *Spectral Element Method in Structural Dynamics*. John Wiley & Sons, Singapore, 2009.

[129] G. Giunta, F. Biscani, S. Belouettar, and E. Carrera. Analysis of thin-walled beams via a one-dimensional unified formulation through a Navier-type solution. *International Journal of Applied Mechanics*, 3(3):407–434, 2011.

[130] A. Catapano, G. Giunta, S. Belouettar, and E. Carrera. Static analysis of laminated beams via a unified formulation. *Composite Structures*, 94:75–83, 2011.

[131] N.J. Pagano. Exact solution for composite laminates in cylindrical bending. *Journal of Composite Materials*, 3:398–411, 1969.

[132] X. Lu and D. Liu. An interlaminar shear stress continuity theory for both thin and thick composite laminates. *Transactions of the ASME, Journal of Applied Mechanics*, 59:502–509, 1992.

[133] R.U. Vinayak, G. Prathap, and B.P. Naganarayana. Beam elements based on a high order theory. I: Forumlation and analysis of performance. *Composite Structures*, 58(4):755–789, 1996.

[134] B.S. Manjunatha and T. Kant. Different numerical techniques for the estimation of multiaxial stresses in symmetric/unsymmetric composite and sandwich beams with refined theories. *Journal of Reinforced Plastics and Composites*, 12:2–37, 1993.

[135] T. Kant and B.S. Manjunatha. Refined theories for composite and sandwich beams with C^0 finite elements. *Computers & Structures*, 33:755–764, 1989.

[136] D.K. Maiti and P.K. Sinha. Bending and free vibration analysis of shear deformable laminated composite beams by finite element method. *Composite Structures*, 29:421–31, 1994.

[137] R.P. Shimpi and Y.M. Ghugal. A layerwise trigonometric shear deformation theory for two layered cross-ply laminated beams. *Journal of Reinforced Plastics and Composites*, 18:1516–1542, 1999.

[138] R.P. Shimpi and Y.M. Ghugal. A new layerwise trigonometric shear deformation theory for two layered cross-ply laminated beams. *Composites Science and Technology*, 61:1271–1283, 2001.

[139] M. Tahani. Analysis of laminated composite beams using layerwise displacement theories. *Composite Structures*, 79:535–547, 2007.

[140] A. Catapano, G. Giunta, S. Belouettar, and E. Carrera. Analysis of thickness locking in classical, refined and mixed multilayered plate theories. *Composite Structures*, 82(4):549–562, 2008.

[141] MSC.Software Corporation. *MD Nastran 2010 Quick Reference Guide*, 2010.

[142] K. Chandrashekhara, K. Krishnamurthy, and S. Roy. Free vibration of composite beams including rotary inertia and shear deformation. *Composite Structures*, 14:269–279, 1990.

[143] W.Q. Chen, C.F. Lv, and Z.G. Bian. Free vibration analysis of generally laminated beams via state-space-based differential quadrature. *Composite Structures*, 63:417–425, 2004.

[144] K. Chandrashekhara and K. M. Bangera. Free vibration of composite beams using a refined shear flexible beam element. *Computers & Structures*, 43(4):719–727, 1992.

[145] L. Jun, L. Wanyou, S. Rongying, and H. Hongxing. Coupled bending and torsional vibration of non symmetrical axially loaded thin-walled Bernoulli-Euler beams. *Mechanics Research Communications*, 31:697—-711, 2004.

[146] L. Jun, S. Rongying, H. Hongxing, and X. Jin. Coupled bending and torsional vibration of axially loaded thin-walled Timoshenko beams. *International Journal of Mechanical Sciences*, 46:299—-320, 2004.

[147] A. N. Bercing and M. Tanaka. Coupled flexural-torsional vibrations of Timoshenko beams. *Journal of Sound and Vibration*, 207:47–59, 1997.

[148] W. H. Wittrick and F. W. Williams. A general algorithm for computing natural frequencies of elastic structures. *Quarterly Journal of Mechanics and Applied Mathematics*, 24(3):263–284, 1971.

[149] P. O. Friberg. Beam element matrices derived from Vlasov's theory of open thin-walled elastic beams. *International Journal for Numerical Methods in Engineering*, 21:1205–1228, 1985.

[150] F. de Borbón and D. Ambrosini. On free vibration analysis of thin-walled beams axially loaded. *Thin-Walled Structures*, 48(12):915–920, 2010.

[151] J. R. Banerjee. Explicit modal analysis of an axially loaded Timoshenko beam with bending-torsion coupling. *Journal of Mechanical Engineering*, 67:307–313, 2000.

[152] H. Matsunaga. Buckling instabilities of thick elastic beams subjected to axial stress. *Computers & Structures*, 59(5):859–868, 1996.

[153] S.M. Ibrahim, E. Carrera, M. Petrolo, and E. Zappino. Buckling of composite thin-walled beams by refined theory. *Composite Structures*, 94:563–570, 2012.

[154] M.-Y. Kim, N.-I. Kim, and H.-T. Yun. Exact dynamic and static stiffness matrices of shear deformable thin-walled beam-columns. *Journal of Sound and Vibration*, 267:29–55, 2003.

[155] T.P. Vo and J. Lee. Flexural–torsional coupled vibration and buckling of thin-walled open section composite beams using shear-deformable beam theory. *International Journal of Mechanical Sciences*, 51:631–641, 2009.

[156] G. Giunta, S. Belouettar, F. Biscani, and E. Carrera. Hierarchical theories for a linearized stability analysis of thin-walled beams with open and closed cross-section. *Advances in Aircraft and Spacecraft Science*, 1(3):253–271, 2014.

[157] T.P. Vo and H.-T. Thai. Vibration and buckling of composite beams using refined shear deformation theory. *International Journal of Mechanical Sciences*, 62:67–76, 2012.

[158] M. Aydogdu. Buckling analysis of cross-ply laminated beams with general boundary conditions by Ritz method. *Composites Science and Technology*, 66(10):1248–1255, 2006.

[159] T.P. Vo and H.-T. Thai. Vibration and buckling of composite beams using refined shear deformation theory. *International Journal of Mechanical Sciences*, 62:67–76, 2012.

[160] A. Chattopadhyay and A.G. Radu. Dynamic instability of composite laminates using a higher order theory. *Computers & Structures*, 77:453–460, 2000.

[161] J. N. Reddy. *Mechanics of laminated composite plates and shells. Theory and Analysis*. CRC Press, Boca Raton, 2^{nd} edition, 2004.

Index

Carrera Unified Formulation, 3, 4, 21, 26, 41, 47, 54, 77, 106
  LE models, 23, 67, 79, 106
  TE models, 22, 67, 77, 81, 84, 87, 89, 91, 96, 99–101, 103, 106
Classical lamination plate theory, 103
Components
  Displacement vector, 19
  Line loading, 30
  Strain vector, 19
  Stress vector, 19
  Surface loading, 29
Composite beams, 67, 84, 100
Composite plates, 85, 89
Constitutive laws, 20, 106, 113
Coordinate system
  Material, 20
  Physical, 9, 20
Cross-sectional functions, 21
  L16 Lagrange polynomials, 24
  L4 Lagrange polynomials, 23
  L9 Lagrange polynomials, 23
  McLaurin polynomials, 22

Dynamic Stiffness
  Matrix, 4, 54, 62, 65, 107
  Method, 4, 53, 77, 81, 84, 87, 89, 91, 96, 99–101, 103, 106

Eigenvalue problem, 45, 49, 61, 65
Euler buckling formula, 96
Euler-Bernoulli beam model, 2, 9, 69, 87, 103, 105
Exact solution for the cylindrical bending of plates, 68

Finite Element Method, 4, 53, 77, 81, 85, 89, 97, 99–101
First order shear deformation theory, 68, 87, 99, 101, 103
Fundamental Nuclei, 6, 26, 49, 55
  Algebraic stiffness matrix, 49
  Differential stiffness matrix, 26
  Expansion, 34
  Geometric stiffness matrix, 28
  L-matrix, 55, 57, 59
  Mass matrix, 31
  Natural boundary conditions, 27, 51, 57, 58
Fundamental nuclei, 44, 106

Gauss elimination, 61, 121
Generalized Beam Theory, 3, 13, 105
Geometrical relations, 20, 106
Governing algebraic equations, 42
  Free vibration analysis, 45
  Static analysis, 42
Governing differential equations, 32, 106
  Buckling analysis, 36, 58
  Free vibration analysis, 35, 47, 55

  Free vibration of beam-columns, 38, 58
  Static analysis, 33

Higher order shear deformation theory, 4, 68, 85, 87, 101, 103

Layer-wise, 68
Layer-wise trigonometric shear deformation theory, 68

Material elastic coefficients
  Monoclinic, 20, 114
  Orthotropic, 20, 113
Metallic beams, 77, 81, 91, 96, 99

Natural boundary conditions, 34
Navier-type solution, 41, 79, 85, 100
Numerical results, 67, 107
  Buckling analysis, 96
  Free vibration analysis, 77
  Free vibration of beam-columns, 91
  Static analysis, 67

Poisson locking, 21
Principle of Virtual Work, 6, 25, 106
  Buckling analysis, 36
  Free vibration analysis, 35
  Free vibration of beam-columns, 38
  Static analysis, 32
Proper Generalized Decomposition, 2, 3, 17, 105

Radial Basis Functions, 5, 47, 49, 77, 81, 84, 106
Rigid torsion, 12

Saint Venant beam model, 2, 3, 15, 16
Shape functions, 53, 77
Shape parameter, 49, 79, 81, 84
Shear correction factor, 2, 3, 11, 105
Thin-walled structures, 81, 91, 98, 99
Timoshenko beam model, 2, 10, 77, 81, 105

Variational Asymptotic
  Beam Sectional Analysis, 2, 3, 18
  Method, 2, 3, 17, 105
Virtual variation, 26
  External work, 29
  Inertial work, 31
  Strain energy, 26
  Work of axial pre-stress, 28
Vlasov-Reddy beam theory, 12, 15, 106

Warping functions, 2, 3, 15
Wittrick-Williams algorithm, 6, 54, 65, 77, 107